UNIVERSIDAD JUÁREZ DEL ESTADO DE DURANGO

PROGRAMA INSTITUCIONAL DE DOCTORADO EN CIENCIAS AGROPECUARIAS Y FORESTALES

Análisis de la biomasa aérea mediante información térmica de sensores remotos en bosques templados del estado de Durango, México

Tesis que presenta:

MARCELA ROSAS CHAVOYA

Como requisito parcial para obtener el grado de

DOCTOR EN CIENCIAS AGROPECUARIAS Y FORESTALES

Opción terminal: Manejo, aprovechamiento y conservación de recursos naturales
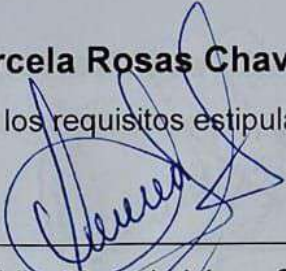
Durango, Dgo., México
Octubre 2023

Universidad Juárez del Estado de Durango

Programa Institucional de Doctorado en Ciencias Agropecuarias y Forestales

Los abajo firmantes, certifican que la tesis de doctorado **"Análisis de la biomasa aérea mediante información térmica de sensores remotos en bosques templados del estado de Durango, México"**, que se presenta como requisito parcial para la obtención del Grado de Doctor en Ciencias Agropecuarias y Forestales por parte de:

Marcela Rosas Chavoya

ha cumplido con los requisitos estipulados por la UJED
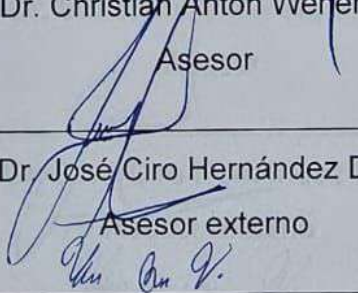
_____

Dr. Pablito Marcelo López Serrano
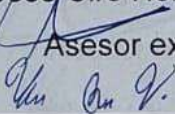
Director

_____

Dr. Daniel José Vega Nieva

Asesor

_____

Dr. Christian Anton Wehenkel

Asesor

_____

Dr. José Ciro Hernández Díaz

Asesor externo

_____

Dra. Veronica Osuna Vallejo

Asesor externo

Durango, Dgo., México.
Octubre 2023

DEDICATORIA

A mis padres Ángel y María Eugenia por ser inspiración en mi vida, por demostrarme su amor y apoyo incondicional, por estar presentes SIEMPRE.

A mi esposo José Luis por caminar a mi lado y apoyarme en todo momento, por compartir conmigo todos los retos y momentos felices.

A mi hermana Jesy por su apoyo y amor incondicional, por sus consejos y su hermoso don de escuchar.

A mis sobrinos con el profundo deseo que mi trabajo y ejemplo siembre en ellos amor hacia el mundo que nos rodea.

A mis abuelos y a mi tío Alfonso en donde quiera que se encuentren por todo su amor, base esencial para mi desarrollo.

A todos los compañeros y amigos que compartieron conmigo esta etapa de mi vida.

AGRADECIMIENTOS

ÍNDICE GENERAL

ÍNDICE DE CUADROS

ÍNDICE DE FIGURAS

RESUMEN

La temperatura superficial (TS) es una variable esencial para el monitoreo de ecosistemas forestales. Esta variable puede estimarse a partir de información satelital; un ejemplo de ello es Landsat el cual pusó en órbita diversas plataformas satelitales que han capturado información de TS de manera ininterrumpida por más de cuatro décadas. Esto constituye una fuente de información consistente, útil para el análisis térmico enfocado a ecosistemas naturales, con diversas áreas de oportunidad como en la estimación de Biomasa Aérea Arbórea (BAA) y el análisis de dinámica termal de ecosistemas forestales. Una de las aplicaciones de esta información es el análisis de procesos climáticos en ecosistemas montañosos, una de las variables más importantes en cuanto a dinámica térmica e hidrológica de ecosistemas montañosos es el gradiente térmico (GT). La información de TS permitió estimar los valores de GT para dos estaciones del año en la UMAFOR 1001, mostrando una estrecha relación con variables topográficas (pendiente y ángulo de incidencia cenital del sol) y una variable biofísica (índice de estrés hídrico). Así mismo, la información de TS mostró estar relacionada con la cantidad de BAA en bosques templados del estado de Durango, según los datos de BAA provenientes de los Sitios Permanentes de Investigación Forestal y de Suelos (SPIFyS). Dicha relación muestra variación a lo largo del año, siendo más fuerte en la primavera. Así mismo se observó que los modelos semi paramétricos permiten generar un modelo parsimonioso, con una precisión moderada. La utilidad de la información de TS de la serie Landsat se incrementa si se conjunta con la información otras fuentes, como MODIS y ECOSSTRES. Por lo tanto, en próximas investigaciones, se recomienda incorporar a estos análisis otras fuentes de información con mayor resolución espacial, como las imágenes termales capturadas con drones.

Palabras clave: Temperatura superficial, gradiente térmico, satélite, sensores remotos, Biomasa aérea arbórea.

SUMMARY

Land Surface temperature (LST) is a key variable for monitoring forest ecosystems. This variable can be estimated using satellite information; one example of this is the Landsat missions, which has deployed various satellite platforms that have continuously captured LST data for over four decades. This constitutes a consistent source of information that is valuable for thermal analysis in natural ecosystems, offering numerous opportunities for applications such as the estimation of Aboveground Arboreal Biomass (AGB) and the analysis of thermal dynamics in forest ecosystems. One of the applications of this information is the analysis of climatic processes in mountain ecosystems, with one of the most important variables concerning thermal and hydrological dynamics in mountain ecosystems being the temperature lapse rate. LST data allowed estimation of temperature lapse rate values for two seasons in UMAFOR 1001, demonstrating a close relationship with topographical variables (slope and zenith solar incidence angle) and a biophysical variable (water stress index). Furthermore, LST data were found to be related to the amount of AGB, according to data taken from Permanent Forest and Soil Research sites (SPIFyS in Spanish) in temperate forests in the state of Durango. This relationship showed variation throughout the year, being stronger during spring. Additionally, it was observed that semi-parametric models enable the generation of a parsimonious model with moderate accuracy. Finally, if LST information from the Landsat is analysed in conjunction with other data sources such as MODIS and ECOSSTRES, enhances its utility. Therefore, in future research, it is recommended to incorporate higher-resolution data sources, such as thermal images captured by drones, into these analyses.

Key words: Land Surface Temperature, Termal Lapse Rate, satellite, remote sensing, above ground biomass.

CAPÍTULO 1 INTRODUCCIÓN GENERAL

Los ecosistemas forestales son parte importante del ciclo de carbono ya que incorporan dióxido de carbono a la estructura vegetal en forma de biomasa además de exportar materia orgánica al suelo (Razo-Zárate et al., 2013). La capacidad de fijación de biomasa varía en función de la composición florística, madurez y densidad. Cuantificar la capacidad de fijación de biomasa es un tema relevante por sus implicaciones con el cambio climático (Fonseca-González, 2017).

Para contribuir en la toma de decisiones respecto a los programas de manejo y conservación de recursos forestales, es transcendental conocer los mecanismos que determinan la dinámica de la biomasa aérea arbórea (BAA) a través del tiempo en los ecosistemas forestales (Martínez-Salvador et al., 2019; Wang et al., 2019). Para ello, una estrategia ha sido establecer Sitios Permanentes de Investigación Forestal y de Suelos (SPIFyS), donde se realizan mediciones *in situ* con una periodicidad establecida (5 años). La información obtenida permite estudiar la dinámica de la biomasa a través de variables dasométricas (altura, diámetro a la altura del pecho, cobertura de copa, entre otros) (Corral-Rivas et al., 2009).

La información obtenida a través del monitoreo forestal, integrada a datos ambientales históricos, puede usarse para comprender como algunos factores ambientales intervienen en el funcionamiento de los ecosistemas forestales. Por ello, diversos estudios se han centrado en mejorar la comprensión del papel que juegan los factores climáticos, topográficos y ambientales en la dinámica de la BAA dentro de dichos ecosistemas (Wang et al., 2019a; Ali et al., 2019; Peng et al., 2019; Sun et al., 2020).

Estos estudios son muy relevantes, ya que ayudan a comprender los mecanismos que determinan la dinámica de captura e incremento de biomasa, lo cual a su vez permite dilucidar los flujos de carbono a nivel regional y global (Venter et al., 2017; Van de Perre et al., 2018).

Actualmente, son muy usadas las técnicas de percepción remota, disciplina que permite obtener información de la superficie terrestre sin entrar en contacto directo con ella, para monitorear variables ambientales, climáticas y forestales (White et al.,

1993; Chuvieco, 2010; Baumann et al., 2014). Las técnicas de obtención de información van desde el uso de fotografías aéreas, imágenes capturadas con drones, hasta información proveniente de las distintas plataformas satelitales (Ruiz et al., 2016). Entre las ventajas de estas técnicas están: la oportunidad de realizar estudios a nivel regional, datos periódicos accesibles e información de distintos tipos de sensores, lo que permite trabajar con secciones del espectro electromagnético que de otra manera escaparían a la vista del ser humano (Pal y Mather, 2004).

Los productos satelitales provenientes de sensores remotos pasivos son con frecuencia imágenes multiespectrales; esta característica permite estudiar la superficie terrestre mediante el análisis de información espectral; esto se logra usando índices de vegetación (Muñoz, 2013), los cuales son parámetros calculados a partir de información de dos o más bandas espectrales y tienen como objetivo resaltar ciertas características de la superficie, permitiendo la estimación de determinados parámetros biofísicos (Correa, 2016).

Uno de los proyectos más ambiciosos sobre observación de la superficie terrestre con fines de monitoreo ambiental ha sido el proyecto Landsat, desarrollado por la NASA en Estados Unidos, y el cual ha generado la colección más grande y consistente de imágenes satelitales desde hace más de 40 años, esta información resulta muy adecuada para realizar estudios multitemporales de las condiciones ambientales y forestales (Roy et al., 2016).

Específicamente, los sensores los satélites Landsat 5 y Landsat 8 cuentan con resolución espacial y radiométrica adecuada para realizar estudios ambientales y de monitoreo de recursos forestales (Malakar et al., 2018). Un ejemplo, es el modelo desarrollado por López-Serrano et al. (2020), en el cual se utilizaron imágenes provenientes del sensor OLI de Landsat 8 para estimar la variación de BAA dentro de algunos bosques templados de la Sierra Madre Occidental, Durango, con una R^2 de 0.80.

La información satelital también permite estimar parámetros ambientales como: la temperatura superficial, disponibilidad de humedad y características topográficas, las

cuales permiten identificar patrones de distribución de BAA a través del gradiente ambiental (Eisfelder et al., 2011; He et al., 2018). La temperatura superficial (TS) puede definirse como la cantidad de energía radiante o radiancia emitida por la superficie dentro de una longitud de onda de entre los 8 a los 13 µm, la cual proporciona información sobre la energía que un cuerpo obscuro emite de acuerdo con la temperatura en la que se encuentra. Esta información tiene la ventaja de no depender de estaciones meteorológicas establecidas, lo que hace posible obtener información termal de toda la superficie terrestre (Czajkowski et al., 2004).

Tomando en cuenta los antecedentes descritos y el conocimiento empírico, será valioso generar información sobre la dinámica de la BAA con un enfoque multitemporal y su relación con los factores ambientales; todo esto utilizando imágenes satelitales e información de BAA *in situ.* Es por ello que en este trabajo se proponen los objetivos siguientes:

1.1. Objetivos e hipótesis

1.1.1. Objetivo general

Analizar la dinámica temporal de la biomasa aérea arbórea (BAA) ante los cambios en factores ambientales y topográficos, mediante información satelital de sensores pasivos, en los bosques templados del estado de Durango.

1.1.2. Objetivos particulares

- Analizar la posible correlación de la variabilidad espacio-temporal de la temperatura superficial con respecto a las variables topográficas derivadas del modelo digital de elevación, en los bosques templados del estado de Durango.
- Analizar la posible correlación de la variabilidad espacio-temporal de la temperatura superficial con respecto a las variables climáticas y parámetros biofísicos en los bosques templados del estado de Durango.
- Analizar la dinámica espacio-temporal de la biomasa en relación con cambios en la temperatura superficial y parámetros biofísicos, en dos periodos de tiempo, en los bosques templados del estado de Durango.

1.1.3. Hipótesis

Los factores topográficos, parámetros biofísicos y la temperatura superficial tienen estrecha relación con la cantidad de biomasa en los bosques templados distribuidos en el área de estudio.

1.2. Organización de la tesis

La presente tesis doctoral se encuentra estructurada en el formato de tesis por compendio de artículos científicos. Se ha organizado en cuatro capítulos, que son la introducción y tres capítulos adicionales que consisten en un artículo científico cada uno. Los artículos se presentan en el formato original de la revista científica en que se publicaron.

En el Capítulo 1 se presenta una introducción general del tema, así como una revisión general de la literatura relacionada al tema.

El Capítulo 2 es un análisis bibliométrico sobre el uso de información de la banda infrarrojo termal del sensor Landsat 8 en el monitoreo y análisis de ecosistemas forestales.

En el Capítulo 3 se analizan los patrones de tasa de cambio térmico a través de un gradiente altitudinal en un sistema montañosos del estado de Durango.

El Capítulo 4 se centra en el desarrollo de un modelo para la estimación de biomasa a partir de información de temperatura superficial y evapotranspiración, en los bosques templados del estado de Durango.

1.3. Revisión general de literatura

1.3.1. Bosques templados

Lo bosques templados son el segundo bioma más extenso de México, después de las zonas áridas y semiáridas (Monárrez-González et al., 2018). Estos bosques son ecosistemas de alta diversidad y se distribuyen principalmente en las áreas

montañosas del país (Granados-Sánchez et al., 2007; Guzmán-Mendoza et al., 2014).

Históricamente, los bosques templados han sido afectados por actividades humanas; esto debido a que muchas de las especies de pinos y encinos que los componen son ideales para producir madera con fines comerciales. Además, en los pueblos cercanos a estos ecosistemas extraen diversos materiales maderables (material de construcción, leña) y no maderables (resinas, semillas) (Sánchez et al*.,* 2003).

La principal reserva forestal de México se ubica en el complejo montañoso de la Sierra Madre Occidental, que recorre más de 1500 km desde el norte del estado de Jalisco, pasando por Zacatecas, Nayarit, Sinaloa, Durango, Sonora, Aguascalientes y Chihuahua, hasta la frontera con Estados Unidos de América. El estado de Durango cuenta con 5.1 millones de hectáreas de estos bosques, lo que representa el 48.9 % de la superficie estatal (SEMARNAT, 2014).

Los bosques templados de Durango han recibido especial atención para su estudio, en gran parte debido a que poseen una alta diversidad y endemismo. Lo anterior explicado por la confluencia de las zonas Neártica y Neotropical, lo que permite el desarrollo de vegetación con afinidad boreal y a la vez de especies tropicales, en su mayoría de porte herbáceo (Reina y Van Devender, 2005).

Los estudios desarrollados en esta área han permitido ampliar el conocimiento sobre la composición florística (Gordon,1968; Fisher et al.1995; Reina y Van Devender, 2005; Nixon y Poole, 2003; González-Elizondo et al*.,* 2012), estructura forestal (Aguirre-Calderón, 2003; Delgado-Zamora et al*.,* 2016; Graciano-Ávila et al., 2017), monitoreo de biomasa forestal y capacidad de captura de carbono (Nájera y Hernández*,* 2009; Silva-Arredondo y Návar-Cháidez, 2010; López-Serrano et al., 2016; 2020), por mencionar algunos.

1.3.2. Biomasa aérea

Durante el siglo XX el ámbito forestal dejó de enfocarse solamente en extracción de productos maderables, reconociendo la importancia de los servicios ambientales, la conservación y la importancia de planes de manejo forestal para asegurar

sustentabilidad en el aprovechamiento de estos ecosistemas (Chadwick, 2003). En 1995, la FAO reconoce a la biomasa como una variable de estudio con alta relevancia en el monitoreo de recursos forestales. El monitoreo de BAA en un bosque, permite comprender el ciclo de carbono, el ciclo hídrico, así como los procesos de erosión y degradación del suelo (Eisfelder et al., 2012).

En México los esfuerzos en el estudio de biomasa forestal se han enfocado en variables como la concentración de carbono de acuerdo con la especie forestal y la determinación de ecuaciones alométricas, lo que ha permitido conocer el potencial de captura de biomasa de acuerdo con su composición por especie (Acosta-Mireles et al., 2009; Návar-Cháidez, 2010; Pompa-García y Yerena-Yamalliel, 2014; Cortés-Sánchez et al., 2019).

En cuanto a los bosques de Durango, Silva-Arredondeo y Návar-Cháidez (2010) realizaron un estudio en bosques de pino con el objetivo de calcular la BAA, además de modelar los factores de expansión de la biomasa. Estos autores encontraron que la biomasa total en los bosques de *Pinus* spp. estudiados fue de 73.73 Mg ha^{-1}; en cuanto a los factores de expansión se encontró que guardan relación estrecha con respecto a la altura de los árboles.

Así mismo, se estudió el potencial de captura de carbono entre especies con valor de conservación y, con base en muestras extraídas en los distintos puntos cardinales, se observó que la concentración de carbono varía entre las especies estudiadas, aunque no existieron diferencias significativas con respecto a la orientación cardinal de extracción (Hernández-Vera et al., 2017).

Un estudio realizado en los bosques de Pueblo Nuevo, Durango, mostró diferencias significativas en la cantidad de biomasa y carbono en dos periodos diferentes; esto debido a que las actividades silvícolas han contribuido a aumentar algunas variables dasométricas permitiendo que la BAA incremente a través del tiempo aun cuando existe extracción forestal (Lira-Tuero et al., 2019).

Graciano-Ávila et al. (2019) realizaron un estudio para estimar la BAA y contenido de carbono en los bosques templados del estado de Durango y encontraron que la

vegetación arbórea está compuesta principalmente por 16 especies, pertenecientes a cuatro familias. Las especies más abundantes son: *Quercus sideroxyla* Humb. & Bonpl*., Pinus durangensis* Ehren, *Quercus grisea* Liebm., y *Pinus tecocote* Schltdl. & Cham., concluyendo que estos bosques poseen un potencial elevado para fijar biomasa y capturar carbono.

1.3.3. Teledetección

La percepción remota es la ciencia que permite obtener datos de un objeto sin entrar en contacto con él (Cracknell y Hayes, 2007; Chiuveco, 2010). Para que la obtención de información a distancia de algún objeto sea posible, se requiere la interacción entre los objetos y el sensor (receptor de información); en el caso de los sensores pasivos esta interacción ocurre mediante ondas electromagnéticas (Silva et al., 2007). Dentro de cierta proporción de longitud de onda esta información la percibe el ojo humano (luz visible), sin embargo, existe una amplia porción del espectro electromagnético que escapa a nuestra visión, por lo que, otra de las ventajas de obtener datos mediante sensores remotos es la posibilidad de tener información con distinta sensibilidad espectral (Turner et al., 2003).

Se han diseñado diversos sensores, desde los más convencionales, sensibles a la longitud de onda visible, hasta cámaras multiespectrales que capturan información del espectro electromagnético en sus diversas longitudes de onda, como: microondas, infrarrojo cercano, infrarrojo termal, entre otros (Markham et al., 2004).

Los satélites Landsat, desde su misión Landsat 4 lanzada en el año 1982, han contado con una resolución temporal de 16 días, pasando en el mismo punto a una hora similar cada vez. Actualmente se encuentran operando Landsat 8 (lanzado en 2013) y Landsat 9 (lanzado en 2022). Así como Landsat 7 (lanzado en 2003), aunque los datos derivados a partir de este satélite muestran un error debido a una falla del corrector de línea del escáner. A pesar de lo anterior, las imágenes obtenidas desde el inicio de la primera misión Landsat se encuentran disponibles de forma gratuita, por medio del Servicio Geológico de los Estados Unidos (USGS) (Mueller-Warrant, 2019).

Entre la información espectral obtenida por los satélites de las misiones Landsat, destaca la banda de infrarrojo termal, en el sensor Thematic Mapper (TM) incorporado en Landsat 4 y 5, con resolución de 120 m (banda 6, 10.4-12.5µm). Posteriormente, se desarrolló el sensor Enhanced Thematic Mapper (ETM+) para Landsat 7, el cual posee datos de Infrarrojo termal con resolución espacial de 60 m (banda 6, 10.4 - 12.5 µm), y por último el sensor TIRS, montado sobre Landsat 8, el cual posee dos sensores capaces de obtener información de longitud de onda infrarrojo termal, con resolución de 100 m (banda 10 y banda 11, 10.6-12.51 µm), con reescalado a 30 m (USGS, 2017).

La banda de la porción infrarrojo termal permite estimar los valores de TS: esto de acuerdo con la ley Planck, la cual menciona que "la energía emitida por una superficie está directamente relacionada a su temperatura", por lo que es posible estimar la temperatura de cuerpos brillantes u obscuros a partir de los valores de radiancia, corrección angular y emisividad (Oguz, 2016). Estimar valores de TS permite comparar valores globales y temporales sin depender del establecimiento de estaciones meteorológicas (Mallick et al., 2012).

Los datos tomados con sensores remotos tienen las ventajas de cubrir grandes extensiones, lo que permite trabajar información a diferentes escalas (local, nacional e inclusive a nivel mundial), aunado a que la calidad de la información satelital ha mejorado sustancialmente en las últimas décadas (Voogt y Oke, 2003).

1.3.4. Factores ambientales determinantes para la biomasa aérea

La topografía de una región suele ser determinante en la composición y estructura de los bosques; con frecuencia estas variables determinan la presencia, distribución y densidad de algunas especies e inclusive, su vulnerabilidad ante los disturbios antropogénicos (Riley et al., 1999). Algunos trabajos han tenido como objetivo explicar cómo los factores topográficos locales determinan la presencia de algunas especies de importancia ecológica e inclusive, pueden relacionarse con la capacidad de recuperación de una zona perturbada (Harris y Baird, 2018).

De igual manera, se ha estudiado como la topografía se relaciona con la cantidad de biomasa y la capacidad de captura de carbono de los bosques. Un ejemplo es el trabajo realizado por McEwan et al. (2011), en el cual se observó una estrecha relación entre las zonas con mayor BAA y las zonas con pendientes menos marcadas; esto podría deberse a que estas características permiten una mayor acumulación de nutrientes en el suelo.

Wang et al. (2019) mencionan que, comprender los patrones de distribución de biomasa y su relación con la topografía, es indispensable para una mejor estimación del carbono en los ambientes forestales, así como para aumentar la exactitud de la estimación de los modelos de flujo de carbono existentes.

Al igual que los factores topográficos, algunos estudios sugieren que las características climáticas son clave en la dinámica de la biomasa y carbono a distintas escalas espaciales. Por lo que se ha propuesto estudiar el efecto de características climáticas y topográficas en la estructura de bosques con composición similar. En un trabajo realizado en bosques del sur de China, se observó que las áreas con mayor potencial de captura de carbono están relacionadas con zonas de mayor precipitación media anual y mayores temperaturas promedio (Wang et al., 2019a).

Venter et al. (2017), buscaron identificar relaciones entre los gradientes medioambientales y la BAA en bosques de Papua, Nueva Guinea. Ellos reportaron que no existe relación directa entre los factores estudiados (precipitación, temperatura, suelo, topografía) y los patrones de la BAA en dichos bosques.

Peng et al. (2019), en un trabajo realizado en bosques semiáridos en Mongolia, encontraron que los factores climáticos juegan un rol determinante en la distribución, en la dinámica y acumulación de biomasa. Siendo la radiación, temperatura y características hídricas los elementos más importantes, encontraron que el proceso de fijación de carbono puede acelerarse por un incremento de la temperatura, siempre y cuando la vegetación no presente estrés hídrico; concluyeron que los

factores climáticos y topográficos deben tomarse en cuenta para modelar la capacidad de captura de carbono de los ecosistemas forestales.

Así mismo, un estudio realizado en los Montes Apalaches en Estados Unidos, con datos históricos de BAA de 20 años, mostró que la capacidad de fijar biomasa de los ecosistemas forestales puede afectarse en forma negativa por el incremento de temperatura y la variación en el régimen de precipitaciones (Knoepp et al., 2018). En contraste, un estudio realizado en bosques templados de Canadá y España mostró que un incremento moderado de temperatura podría tener relación positiva con la productividad forestal (Paquette et al., 2018).

Así mismo, se han desarrollado modelos de estimación de biomasa aérea a partir de imágenes satelitales (Wu et al., 2016; Li et al., 2018; López-Serrano et al., 2016, 2020), lo cual conlleva un gran avance en el conocimiento de la biomasa de estos bosques, ya que permite monitorear la biomasa aérea con mayor frecuencia y con una reducción considerable de costos.

En bosques de Durango, López-Sánchez et al. (2017) evaluaron el uso de variables topográficas e información espectral obtenida a partir de imágenes satelitales del Landsat 8, para estimar variables de importancia forestal (número de árboles, diámetro a altura del pecho, diámetro a la base, altura media, diámetro de copa, volumen); concluyeron que es posible estimar variables dasométricas a partir de información satelital con precisión aceptable.

Si bien el estudio de la dinámica de biomasa dentro de los bosques de Durango, México, ha recibido atención, la comprensión de los patrones temporales y espaciales es aún un campo poco estudiado.

Por lo tanto, comprender las características ambientales que promueven un mayor almacenamiento de carbono en los ecosistemas forestales, será útil para desarrollar estrategias de manejo forestal que aumenten el potencial de captura de carbono y que por ende, promuevan la reducción del cambio climático.

1.4.   Literatura citada

Acosta-Mireles, M., Carrillo-Anzures, F., & Díaz Lavariega, M. (2009). Determinación del carbono total en bosques mixtos de *Pinus patula* Schl. et cham. *Terra Latinoamericana*, 27(2), 105-114.

Ali, A., Lin, S., He, J., Kong, F. M., Yu, J. H., & Jiang, H. S. (2019). Elucidating space, climate, edaphic and biodiversity effects on aboveground biomass in tropical forests. *Land Degradation and Development*, 30, 918-927. doi:10.1002/ldr.3278

Aguirre-Calderón, O. A., Hui, G., Gadow, K. y Jiménez-Pérez, J. (2003). Análisis estructural de bosques naturales en Durango, México. *XII World Forestry Congress, Quebec City, Canada.*

Baumann, M., Ozdogan, M., Wolter, P., Krylov, A., Vladimirova, N., & Radeloff, V. (2014). Landsat remote sensing of forest windfall disturbance. *Remote Sensing of Environment, 143*, 171-179. doi:10.1016/j.rse.2013.12.020

Chadwinck, D. O. (2003). Sustainable Forestry What Is It? How Do We Achive It? *Journal of Forestry*, 101(5):8-14

Chuvieco, E. (2010). Teledetección Ambiental. La observación de la Tierra desde el espacio. (3era edición ed.) Ed. Ariel. España.

Cracknell, A. P., & Hayes, L. (2007). Introduction to remote sensing. Ed. Taylor y Francis Group. 327 pp.

Corral-Rivas, J., Vargas, B., Wehenkel, C., Aguirre, O., Álvarez, J. y Rojo, A. (2009). Guía para el establecimiento de Sitios de Inventario Periódico Forestal y de Suelos del Estado de Durango; Facultad de Ciencias Forestales, Universidad Juárez del Estado de Durango: Durango, Mexico.

Correa, N. (2016). Índices espectrales de vegetación para la detección de áreas quemadas. *La Calera, 16*(27), 111-114. doi:10.5377/calera.v16i27.6010

Cortés-Sánchez, B. G., Ángeles-Pérez, G., Santos-Posadas, H. M. y Ramírez-Maldonado, H. (2019). Ecuaciones alométricas para estimar biomasa en

especies de encino en Guanajuato, México. *Madera y Bosques*, 25(2). doi: 10.21829/myb.2019.2521799.

Czajkoeski, K. P., Goward, S. N., Mulhern, T., Stadler, S., Prince, S. & Dubayah, E. O. (2004). Estimating environmental variables using thermal remote sensing. En: Quattrochi, D.A., & Luvall, J.C. Thermal Remote Sensing in Land Surface Processes (eds.). CRC Press. 469 pp.

Delgado-Zamora, D. A., Heynes-Silerio, S. A., Mares-Quiñones, M. D., Piedra-Leandro, N. L., Retana-Rentería, F. I., Rodríguez-Corral, K., Villanueva-Hernández, A. I., González-Elizondo, M. S. y Ruacho-González, L. (2016). Diversidad y estructura arbórea de dos rodales en Pueblo Nuevo, Durango. *Revista mexicana de ciencias forestales*, 7(33), 94-107.

Eisfelder, C., Kuenzer, C., & Dech, S. (2012). Derivation of biomass information for semi-arid areas using remote-sensing data. *International Journal of Remote Sensing, 33*(9), 2937-2984. doi:10.1080/01431161.2011.620034

Fisher, J. T., Glass, P. A., & Harrington, J. T. (1995). Temperate pines of northern Mexico: their use, abuse and regeneration. En: DeBano, L. F., Folliott, P. F., Ortega-Rubio, A. Gottfried, G. J., Hamre, R. H. y Edminster, C. B. (Coords.). Biodiversity and management of the Madrean archipelago: The sky islands of southwestern United States and northwestern Mexico. United States Department of Agriculture Forest Service, General Technical Report RM 264: 165-173.

Fonseca-González, W. (2017). Revisión de métodos para el monitoreo de biomasa y carbono vegetal en ecosistemas forestales tropicales. Revista de ciencias ambientales. *Tropical Journal of Enviromental Sciences*, 51(2):91-109. doi: 10.15359/rca.51-2.5

Graciano-Ávila, G., Aguirre-Calderón, O. A.; Alanís-Rodríguez, E. y Lujan-Soto, J. E. (2017). Composición, estructura y diversidad de especies arbóreas en un bosque templado del Noroeste de México. *Ecosistemas y recursos agropecuarios*, 4(12):535-542.

Graciano-Ávila, G., Alanís-Rodríguez, E., Aguirre-Calderón, O. A., Tagle-González, M. A., Treviño-Garza, E.J., Mora-Olivo, A. y Buendía-Rodríguez, E. (2019). Estimación de volumen, biomasa y contenido de carbono en un bosque de clima templado-frío de Durango, México. *Revista fitotecnia mexicana publ. por la Sociedad Mexicana de Fitogenética*, *42*, 119-127. doi:10.35196/rfm.2019.2.

González-Elizondo, M. S., Elizondo, M., Ruacho-González, L., y Enríquez, I. (2012). Vegetación de la Sierra Madre Occidental, México: Una síntesis. *Acta botánica mexicana, 100*, 351-403. doi:10.21829/abm100.2012.40

Gordon, A. G. 1968. Ecology of *Picea chihuahuana* Martínez. *Ecology,* 49: 880 896.

Granados-Sánchez, D., López-Rios, G. F. y Hernández-García, M. A. (2007). Ecología y silvicultura en bosques templados. *Revista Chapingo, Serie Ciencias Forestales*, 13(1):67-83.

Guzmán-Mendoza, R., Zavala-Hurtado, J. A., Castaño-Meneses, G. y León-Cortés J. L. (2014). Comparación de la mirmecofauna en un gradiente de reforestación en bosques templados del centro occidente de México. *Madera y Bosques*, 20(1):71-83

Harris, A., & Baird, A. J. (2018). Microtopographic Drivers of Vegetation Patterning in Blanket Peatlands Recovering from Erosion. *Ecosystems, 22*(5), 1035-1054. doi:10.1007/s10021-018-0321-6

He, J., Zhao, W., Li, A., Wen, F., & Yu, D. (2018). The impact of the terrain effect on land surface temperature variation based on Landsat-8 observations in mountainous areas. *International Journal of Remote Sensing*, 1-20. doi:10.1080/01431161.2018.1466082

Hernández-Vera, D., Pompa-García, M., Wehenkel, C.; Pérez-Verdín, G.; Carrillo-Parra, A. (2017). Are there any differences in carbon concentration among species of high conservation value forests in Northern Mexico? Revista de la Facultad de Ciencias Agrarias, 49(2):183-192

Knoepp, J. D., See, C. R., Vose, J. M., Miniat, C. F., & Clark, J. S. (2018). Total C and N Pools and Fluxes Vary with Time, Soil Temperature, and Moisture Along an Elevation, Precipitation, and Vegetation Gradient in Southern Appalachian Forests. *Ecosystems, 21*(8), 1623-1638. doi:10.1007/s10021-018-0244-2

Li, B., Wang, W., Bai, L., Chen, N., & Wang, W. (2018). Estimation of aboveground vegetation biomass based on Landsat-8 OLI satellite images in the Guanzhong Basin, China. *International Journal of Remote Sensing*, 40:3927-3947. doi: 10.1080/01431161.2018.1553323

Lira-Tuero, L. A., Corral-Rivas, J. J., Padilla-Martínez, J. R., López-Serrano, P. M., Pompa-García, M., & Cruz-Cobos, F. (2019). Efecto del manejo forestal en biomasa y carbono en bosques de Durango. *Revista Mexicana de Agroecosistemas*. 6(1):89-97

López-Sánchez, C., García-Ramírez, P., Resl, R., Hernández-Díaz, J. C., López Serrano, P. M., & Wehenkel, C. (2017). Modelling dasometric attributes of mixed and uneven-aged forests using Landsat-8 OLI spectral data in the Sierra Madre Occidental, Mexico. *iForest* - Biogeosciences and Forestry. 10. 1-8. 10.3832/ifor1891-009.

López-Serrano, P., Corral-Rivas, J. J., Díaz-Varela, R., Álvarez-González, J. G., & López-Sánchez, C. (2016). Evaluation of Radiometric and Atmospheric Correction Algorithms for Aboveground Forest Biomass Estimation Using Landsat 5 TM Data. *Remote Sensing*, 369. doi:10.3390/rs8050369

López-Serrano, P., Domínguez, P., Corral-Rivas, J. J., Jiménez, E., López-Sánchez, C., & Vega-Nieva, D. (2020). Modeling of Aboveground Biomass with Landsat 8 OLI and Machine Learning in Temperate Forests. *Forests*, 11. doi:10.3390/f11010011

Malakar, N., Hulley, G., Hook, S., Laraby, K., Cook, M., & Schott, J. (2018). An Operational Land Surface Temperature Product for Landsat Thermal Data:

Methodology and Validation. *IEEE Transactions on Geoscience and Remote Sensing,* 1-19. doi:10.1109/TGRS.2018.2824828

Mallick, J., Kumar, C., Shashtri, S., Rahman, A., & Mukherje, S. (2012). Land surface emissivity retrieval based on moisture index from LANDSAT TM satellite data over heterogeneous surfaces of Delhi city. *International Journal of Applied Earth Observation and Geoinformation,* 19, 348–358. doi: 10.1016/j.jag.2012.06.002

Markham, B. L., Storey, J. C., Williams, D. L., & Irons, J. R. (2004). Landsat sensor performance: history and current status. *IEEE Transactions on Geoscience and Remote Sensing*, 42(12), 2691–2694. doi:10.1109/TGRS.2004.840720

Martínez-Salvador, M., Sosa, G., Chacón, J., Pinedo, A., Guerrero, F., y Prieto-Amparán, J. (2019). El monitoreo forestal por medio de Sitios Permanentes de Investigación Silvícola en Chihuahua, México. *Revista Mexicana de Ciencias Forestales, 10*. doi:10.29298/rmcf.v10i55.511

McEwan, R., Lin, Y., Sun, I. F., Hsieh, C. F., Su, S. H., Chang, L. W., Song, G. M., Wang, H. H., Hwong, J. L., Lin, K. C., Yang, K. C., & Chiang, J. M. (2011). Topographic and biotic regulation of aboveground carbon storage in subtropical broad-leaved forests of Taiwan. *Forest Ecology and Management, 262*, 1817-1825. doi:10.1016/j.foreco.2011.07.028

Mueller-Warrant, G. (2019). Multistep block mapping on principal component uniformity repairs Landsat 7 defects. *International Journal of Applied Earth Observation and Geoinformation*, 79:12-23. doi: 10.1016/j.jag.2019.02.005

Monárrez-González, J. C., Pérez-Verdín G., López-González, C., Márquez-Linares, M. A. y González-Elizondo, M. S. (2018). Efecto del manejo forestal sobre algunos servicios ecosistémicos en los bosques templados de México. *Madera y Bosques*, 24(2):e2421569. doi: 10.21829/myb.2018.2421569

Muñoz, P. (2013). Apuntes de Teledetección: Índices de vegetación. Centro de Información de Recuros Naturales. 13 pp.

Nájera L., J. A. y Hernández H., E. (2009). Acumulación de biomasa aérea en un bosque coetáneo de la región de El Salto, Durango. *Ra Ximhai*, 5(2):225-230.

Návar-Cháidez, J. J. (2010). Biomass allometry for tree species of Northwestern Mexico. . *Tropical and Subtropical Agroecosystems, 12*, 507-519.

Nixon, K. & Poole J. M. (2003). Revision of the Mexican and Guatemalan species of Platanus (Platanaceae). *Lundellia*, 6: 103-137.

Oguz, H. (2016). Automated Land Surface Temperature Retrieval from Landsat 8 Satellite Imagery: A Case Study of Kahramanmaraş – Turkey. En: Environmental Sustainability and Landscape Management. Efe, R., Cürebal, I., Gad, A. y Tóth, B. (Eds.) 598-605 p.

Pal, M., & Mather, P. (2004). Assessment of the effectiveness of support vector machines for hyperspectral data. *Future Generation Computer Systems, 20*, 1215-1225. doi:10.1016/j.future.2003.11.011

Paquette, A., Vayreda, J., Coll, L., Messier, C., & Retana, J. (2018). Climate Change Could Negate Positive Tree Diversity Effects on Forest Productivity: A Study Across Five Climate Types in Spain and Canada. *Ecosystems, 21*(5), 960-970. doi:10.1007/s10021-017-0196-y

Peng, D., Zhang, H., Liu, L., Huang, W., Huete, A., Zhang, X., Wang, F., Yu, L., Xie, Q., Wang, C., Luo, S., Li, C., & Zhang, B. (2019). Estimating the Aboveground Biomass for Planted Forests Based on Stand Age and Environmental Variables. *Remote Sensing, 11*, 2270. doi:10.3390/rs11192270

Pompa-García, M. y Yerena-Yamalliel, J. I. (2014). Concentración de carbono en *Pinus cembroides* Zucc: Fuente potencial de mitigación del calentamiento

global. *Revista Chapingo serie ciencias forestales y del ambiente*, 20(3):169-175.

Razo-Zárate, R., Gordillo-Martínez, A. J., Rodríguez-Laguna, R., Maycotte-Morales, C. C. y Acevedo-Sandoval, O. A. (2013). Estimación de biomasa y carbono almacenado en árboles de oyamel afectados por el fuego en el Parque nacional "El Chico", Hidalgo, México. *Madera y bosques*, 19(2):73-86.

Reina-G., A. L., & Van Devender, T. (2005). Floristic comparison of an Arizona Sky Island and the Sierra Madre Occidental in eastern Sonora: the Huachuca Mountains and the Yécora Area. En: Gottfried, G. J., B. S. Gebow, L. G. Eskew y C. B. Edminster. (coords.). Biodiversity and management of the Madrean Archipelago II: Connecting mountain islands and desert seas. United States Department of Agriculture Forest Service, General Technical Report RMRS-P-36: 154-157.

Riley, S., Degloria, S., & Elliot, S. D. (1999). A Terrain Ruggedness Index that Quantifies Topographic Heterogeneity. *Internation Journal of Science, 5*, 23-27.

Roy, D. P., Kovalskyy, V., Zhang, H. K., Vermote, E. F., Yan, L., Kumar, S. S., & Egorov, A. (2016). Characterization of Landsat-7 to Landsat-8 reflective wavelength and normalized difference vegetation index continuity. *Remote Sensing of Environment, 185*, 57-70. doi:https://doi.org/10.1016/j.rse.2015.12.024

Ruiz, L. A., Estornell, J., & Erena, M. (Eds.). (2016). Teledetección: Nuevas plataformas y sensores. Asociación Española de teledetección. Valencia, España.

SEMARNAT. (2014). Inventario Estatal Forestal y de Suelos - Durango. Secretaría de Medio Ambiente y Recursos Naturales.

Sánchez, O., Vega E. y Peters, E. (2003) Conservación de Ecosistemas Templados de Montala en México. *Instituto Nacional de Ecología*. Ciudad de México, México. 314 pp.

Silva, T. S. F., Costa, M. P. F., Melack, J. M., & Novo, E. M. L. M. (2007). Remote sensing of aquatic vegetation: theory and applications. *Environmental Monitoring and Assessment*, 140(1-3):131–145. doi: 10.1007/s10661-007-9855-3

Silva-Arredondeo, F. M. y Návar-Cháidez. J. J. (2010). Factores de expansión de biomasa en comunidades forestales templadas del norte de Durango, México. *Revista Mexicana de ciencias forestales.* 1(1):55-62.

Sun, L., Wang, M., & Fan, X. (2020). Spatial pattern and driving factors of biomass carbon density for natural and planted coniferous forests in mountainous terrain, eastern Loess Plateau of China. *Forest Ecosystems, 7*(1), 9. doi:10.1186/s40663-020-0218-7

Turner, W., Spector, S., Gardiner, N., Fladeland, M., Sterling, E., & Steininger, M. (2003). Remote sensing for biodiversity science and conservation. *Trends in Ecology y Evolution*, 18(6):306–314. DOI: 10.1016/S0169-5347(03)00070-3

USGS (2017) Landsat Missions. Recuperdo de: https://earthexplorer.usgs.gov/

Van de Perre, F., Willig, M. R., Presley, S. J., Bapeamoni Andemwana, F., Beeckman, H., Boeckx, P., Cooleman, S., Haan, M. De Kesel, A., Dessein, S., Grootaert, P., Huygens, D., Janssens, S.B., Kearsley, E., Kabeya, P., Leponce, M., Van den Broeck, D., Verbeeck, H., Würsten, B., Leirs, H, & Verheyen, E. (2018). Reconciling biodiversity and carbon stock conservation in an Afrotropical forest landscape. *Science Advances, 4*(3). doi:10.1126/sciadv.aar6603

Venter, M., Dwyer, J., Dieleman, W., Ramachandra, A., Gillieson, D., Laurance, S., Cernusak, L. A., Beehler, B., Jensen, R., & Bird, M. I. (2017). Optimal climate for large trees at high elevations drives patterns of biomass in

remote forests of Papua New Guinea. *Global Change Biology, 23*(11), 4873-4883. doi:10.1111/gcb.13741

Voogt, J., & Oke, T. (2003). Thermal remote sensing of urban climates*. Remote Sensing of Environment,* 86(3): 370–384. doi: 10.1016/S0034-4257(03)00079-8

Wang, G., Guan, D. S., Xiao, L., & Peart, M. R. (2019). Forest biomass-carbon variation affected by the climatic and topographic factors in Pearl River Delta, South China. *Journal of Environmental Management, 232*, 781–788. doi:10.1016/j.jenvman.2018.11.130

Wang, S., Qi, G., & Knapp, B. (2019). Topography Affects Tree Species Distribution and Biomass Variation in a Warm Temperate, Secondary Forest. *Forests, 10*, 895. doi:10.3390/f10100895

White, K., Cracknell, A., & Hayes, L. (1993). Introduction to Remote Sensing. *The Geographical Journal, 159*, 89. doi:10.2307/3451502

Wu, C., Shen, H., Wang, K., Shen, A., Deng, J., & Gan, M. (2016). Landsat Imagery-Based Above Ground Biomass Estimation and Change Investigation Related to Human Activities. *Sustainability*, 8:159. doi: 10.3390/su8020159

CAPÍTULO 2   APPLICATION OF LAND SURFACE TEMPERATURE FROM LANDSAT SERIES TO MONITOR AND ANALYZE FOREST ECOSYSTEMS: A BIBLIOMETRIC ANALYSIS

Marcela Rosas-Chavoya, Pablito Marcelo López-Serrano, Daniel José Vega-Nieva, Christian A. Wehenkel, José Ciro Hernández-Díaz

Abstract

Aim of study: Land surface temperature (LST) is an essential variable to monitor and characterize forest ecosystems. This variable has been consistently captured for almost four decades by the Landsat program. The current study aimed at identifying trends, knowledge gaps and opportunity areas in the use of Landsat derived LST for the monitoring and analysis of forest ecosystems.

Materials and methods: A bibliometric analysis of scientific articles indexed in Scopus in the period 1995 – 2020 was conducted.

Main results: Annual increase rate in the number of publications on the topic analyzed was 22.58%. The journal with more publications on the topic was Proceedings of SPIE, followed by Remote Sensing. The authors with the highest productivity on this topic are Quintano C, Vorovencii I, Yakubailik OE and Zoran MA. Regarding productivity by country, 38 countries with publications on this topic were identified, with the highest productivity located in China, USA and India. This group of countries also represented the most solid network of cooperation between countries. Forest ecosystems more frequently analyzed were temperate forests, followed by tropical forests. The analysis of keywords highlighted topics such as remote sensing, NDVI, MODIS and evapotranspiration. The analysis of thematic evolution indicated that areas of research and interpretation of LST data has evolved in parallel with remote sensing areas.

Research highlights: Landsat LST analysis is an evolving topic with potential to contribute to improve ecosystem knowledge and to support diverse challenges in forest resources decision-making.

Keywords: Thematic Mapper; Enhanced Thematic Mapper; Thermal Infrared sensor; Thermal infrared; LST

Abbreviations used: LST (land surface temperature); NDVI (normalized difference vegetation index); MODIS (moderate resolution imaging spectroradiometer); TM (thematic mapper); ETM+ (enhanced thematic mapper plus); TIRS (thermal infrared sensor); LIDAR (light detection and ranging o laser imaging detection and ranging); JCR (journal citation report); LAI (leaf area index).

2.1. Introduction

Land surface temperature (LST) is an important parameter to characterize the energy exchange between the land surface and the atmosphere (Amalyahya, 2015; Quispe-Reymundo & Révolo-Acevedo, 2020). It is considered an essential climate variable to analyze land surface processes by the Global Climate Observing System (GCOS, 2016). LST data allows analyzing evapotranspiration, climate change, hydrological cycles, fire monitoring, and other phenomena influencing the functioning of forest ecosystems (Li et al., 2013; Vlassova & Pérez-Cabello, 2016; Bendib et al., 2017). LST can be estimated from satellite information, allowing an opportunity to study the thermal dynamics in forest ecosystems at regional to global scales (Bendib et al., 2017).

The Landsat program has captured land surface information in the thermal infrared spectrum consistently for almost four decades (Table S1[suppl]), since the launch of Landsat 4 TM (Thematic Mapper), followed by Landsat 5 TM, Landsat 7 ETM+ (enhanced thematic mapper plus) and Landsat 8 TIRS (Thermal Infrared Sensor), making possible LST estimation (Wang et al., 2015). Thermal information from Landsat satellites has represented an opportunity for the analysis of various aspects of forests ecosystems (Banskota et al., 2014). For example, Landsat LST has been used to quantify the impact of climate change on forest ecosystems (Arekhi et al., 2018; Ghazaryan et al., 2018; Savastru et al., 2020), to analyze land use change in forest areas (Sabajo et al., 2017; Del Mundo & Tiburan Jr, 2019; Herrero et al., 2019), to evaluate forest evapotranspiration processes (Zhu et al., 2010; Yang et al., 2017) or to monitor urban forests (Huang et al., 2015; Jana et al., 2020).

While there are several studies that have used LST to monitor and analyze forest ecosystems, to our best knowledge, there is no previous study that has analyzed the scientific publications on this topic, which could allow identifying trends and areas of opportunity in the use of thermal information for the analysis of forest ecosystems. Bibliometric analyses are tools that allow to characterize publications with common topics, quantifying annual publication growth rate, analyzing citation, or identifying collaboration networks, among other bibliometric indicators. For example, Zhuang et al. (2013) conducted a bibliometric analysis on the trends in research using remote sensing in the 1991-2010 period. They concluded that topics more frequently analyzed were land use change, vegetation analysis and climate change and identified USA as the country with the highest scientific publication on this topic. Duan et al. (2020) analyzed the use of remote sensing to monitor natural protected areas; they concluded that most utilized information was satellite data from Landsat and MODIS, together with LIDAR sensors and they identified international collaboration networks.

A bibliometric analysis on the scientific contributions utilizing Landsat LST to monitor and analyze forest ecosystems, could allow gaining a general perspective on the evolution of the main topics and applications of this research area. The current study aimed at identifying trends, challenges, and areas of opportunity in the use of Landsat LST on forest ecosystems, with the following goals: 1) to characterize scientific contributions on the topic; 2) to identify scientific networks between authors and countries in this research area; 3) to identify trends in research using LST to study forest ecosystems.

2.2. Materials and Methods

The scientific repository Scopus (https://www.scopus.com) was used for the literature search. Scopus is one of the most important scientific repositories, with more than 20,000 scientific journals registered, representing an adequate source to gather information for a bibliometric analysis (Joshi, 2017). Our search focused on words

within the title, summary and keywords. One of the areas of knowledge more analyzed with LST is urban areas characterization (Rasul et al., 2017). The present study focused on investigations using LST to study forest ecosystems, therefore studies on urban climate and urban heat islands characterization were excluded from the analysis. The search period analyzed was from 1982, the year at which Landsat 4 TM was launched (Arvidson et al., 2013). The search equation used was: TITLE-ABS-KEY = ("land surface temperature" AND Landsat AND forests OR "forest ecosystem" OR forestry OR silviculture OR "natural forest" OR "forest plantations " AND NOT "urban heat island" AND NOT "urban heat") AND PUBYEAR > 1981 AND (EXCLUDE (PUBYEAR, 2021).

The search resulted in 195 initial registers. Some scientific documents such as reviews, notes, correction letters and editorial material were excluded, resulting in a total of 155 filtered documents. The database was downloaded in CSV format for analysis. The database was analyzed with the package Bibliometrix and the tool Biblioshiny (http://www.bibliometrix.org) that belong to RStudio (Aria & Cuccurullo, 2017; RStudio Team, 2020). Biblioshiny is a web interface that contains the central code of Bibliometrix. It allows for bibliometric analyses, including tools to visualize the annual scientific productivity rate, journals and authors with the highest number of publications on the topic, most utilized keywords analysis or thematic evolution and collaboration network analysis, among others (Xie et al., 2020a). In particular, the following analyses were performed:

Wordtreemap: It identifies the frequency of keywords within the analyzed publications. The analysis consisted in identifying the 13 most frequent keywords in the articles from the database. The analysis of keywords frequency allows identifying the most studied topics in an area of research (Xie et al., 2020b).

Multidimensional scaling analysis: It is a correspondence analysis that summarizes the main variables of the articles analyzed and allows classifying the relationships between categorical variables (Ayele et al., 2014). This analysis considers the frequency of the keywords appearing together. Keywords are represented as dots

and their position within the graph represent the coincidences between them. Groups are formed with keywords that appear together more frequently (Ayele et al., 2014; Aria & Cuccurullo, 2017).

Thematic evolution analysis: This analysis allows visualizing the development and relative increase or decrease of some topics, identifying thematic evolution through time, represented by a Sankey diagram. Inside the Sankey diagram, each node represents one topic, the size of the node represents the number of keywords associated to that topic, the lines joining the nodes represent the direction of the topic evolution and the thickness of the line shows the strength of the relationships between topics (Xie et al., 2020b). Continuous lines between nodes of different years indicate that the topic has prevailed through time.

Finally, studies were classified by their main topic, out of 15 identified topics defined after careful review of all analyzed publications. Main topics were Classification land cover, Forest monitoring, Evapotranspiration/Dryness, Thermal analysis, Urban forests analysis, Wildfire, Deforestation, Vegetation indexes, Environmental quality analysis, Mountain ecology/Snow monitoring, Climatic change analysis, Phenological analysis, Desertification, Mining and Above-ground biomass estimation.

2.3. Results

2.3.1. General information

Search period started in 1982; nevertheless, the earliest identified publication was from 1995, resulting in a period of analysis from 1995 to 2020. 554 authors, with an average of 0.29 articles by author, were identified, with only four articles (3.1%) by one single author. The increase in the annual publication rate was 22.6% (Table S2, [suppl]),. An increase in the number of publications can be observed after 2007. The year with the highest number of publications was 2019 with 33 articles, followed by 2020 with 26 articles.

Annual average citations were almost null in the period 1995-2006; nevertheless, an increase was observed after the year 2007, fluctuating in the subsequent period

(2007-2020), peaking with a maximum in 2016, and later diminishing (Figure 1). 33.3% of 2016 articles focused on LST dynamics related to vegetation and land use change, as well as on the characterization of LST between different vegetation types (Ara et al., 2016; Fu & Weng, 2016; Kayet et al., 2016; Sahana et al., 2016; Wang et al., 2016).
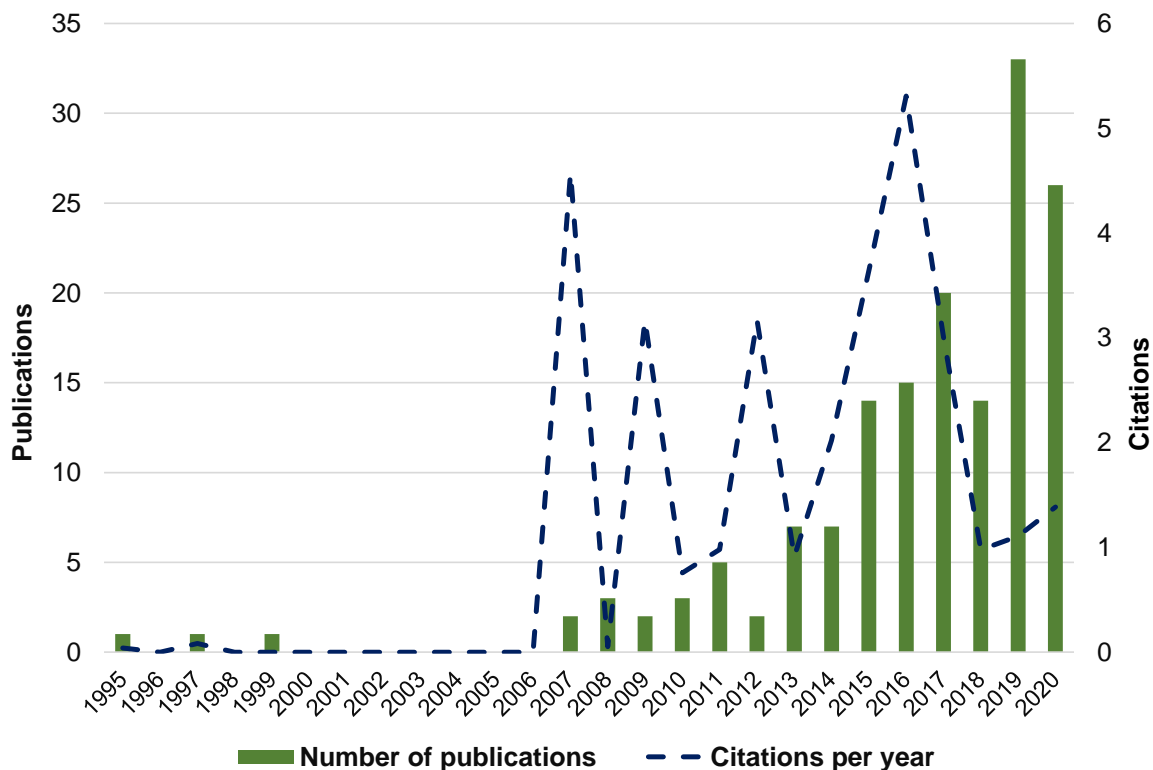
Figure 1. Number of publications and average citations

The scientific journals with a highest number of publications are show in Table 3. The journal with the highest number of publications in the topic is Proceedings of SPIE, which results from an annual congress specialized in spatial analysis. An example is the study by Ramdhani et al. (2019), who used Landsat 8 TIRS thermal images to evaluate post-mining forest remediation activities, comparing remediated areas with different forest species and years of plantation. Their results showed that all species used for forest remediation had a similar capacity to decrease LST; the reduction in LST was observed in a relatively short period of time.

The second journal with the highest number of articles in the topic was Remote Sensing, a scientific journal specialized in remote sensing techniques. This journal has a high impact factor (4.509, 2019) and is listed in the first quartile of the Journal Citation Report (JCR) index. Remote Sensing has an annual rate of 1.5 articles published on LST since the start of the publication of the journal (Table S3, [suppl]). As an example of studies published in this journal, Sánchez et al. (2015) evaluated the energy balance in a forest area after a wildfire in a mediterranean forest in Almodóvar del Pinar, Spain. The authors used Landsat 5 TM and Landsat 7 ETM+ to estimate LST and the energy balance; their results showed the potential of LST to evaluate changes in thermal balances through time in areas with previous disturbances.

The most cited article on the topic is the study of Fu & Weng (2016), published in the journal Remote Sensing of Environment. It focuses on a multi-temporal analysis of LST increase with regards to the decrease in perennial forests and their substitution by urban areas. The second most cited study is the article of Xiao & Weng (2007), which evaluated land use change in a province at the Southeast of China; the study found that reforestation activities decreased LST in the region of study (Table S4, [suppl]).

2.3.2. Main authors and collaborative networks

The productivity by author can be evaluated using Lotka´s law (Lotka 1926). This criterion quantifies how often authors publish about a specific topic. Based on Lotka´s law, 86.7 % of authors who have published about LST have only published one article, while only one author has participated in 5 studies on the topic. Figure 2 shows the authors with the highest scientific publication and the year of publication; the size of the circles represents the number of articles; the circle shading density represents the amount of citations.
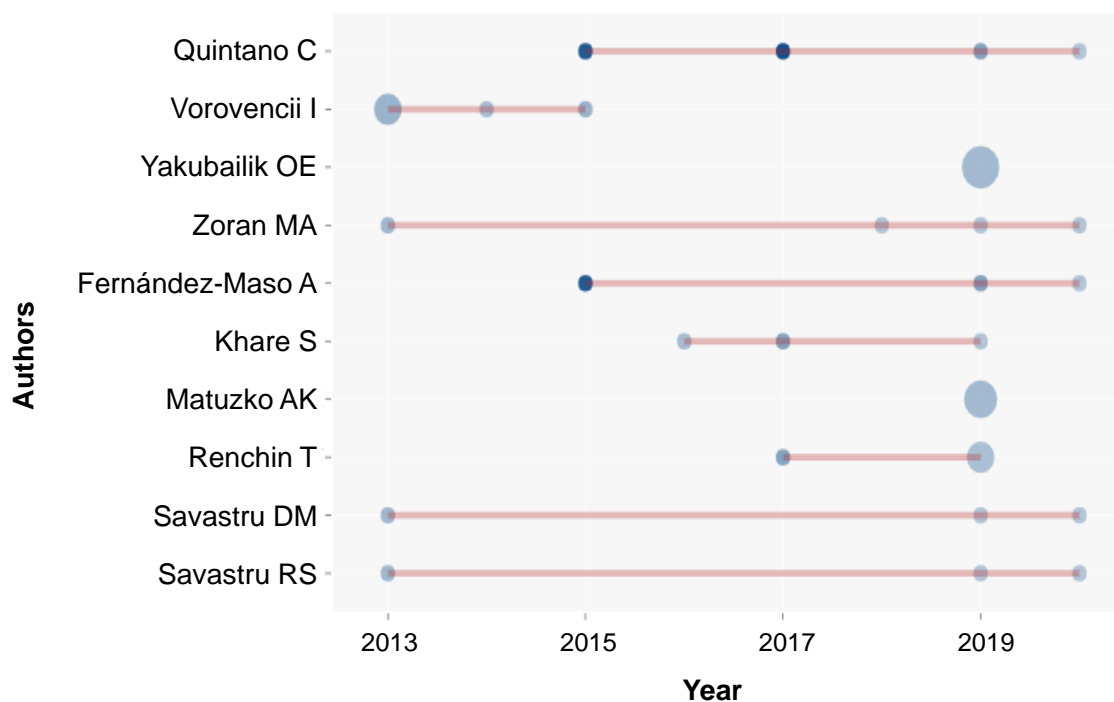
Figure 2. Authors' production over time in the field of land surface temperature derived from Landsat missions

The four authors with the highest amount of publications on the topic in the last years are: Quintano C, Vorovencii I, Yakubailik OE and Zoran MA, with four articles each. Quintano C started publishing on the topic in 2015; this author works on topics related to the evaluation of forest fires from LST information. The most cited article from this author (57 citations, 2020) is a study published in International Journal of Applied Earth Observation and Geoinformation about fire severity evaluation from LST, estimated from Landsat 7 ETM+ images. A coefficient of determination > 0.85 was observed in this study between LST and a field fire severity index (composite burn index) (Quintano et al., 2015). In a latter study, Quintano et al. (2017) combined MESMA fraction images with Landsat 7 ETM+ LST to analyze fire severity in a forest fire in Spain.

On the other hand, Vorovencii (2015) used thermal information from Landsat series to analyze land use change and desertification risk in Romania. This author evaluated and monitored desertification risk thorugh vegetation indices and Landsat 5 TM LST

data, observing that areas with highest desertification risk had high LST; areas with extensive vegetation loss has higher temperatures and higher desertification risk.

The analysis of scientific productivity by country reveals that is a topic under development, since there are publications from 38 countries only, 7 from America, 10 from Europe, 5 from Africa, 15 from Asia and Australia (Figure 3). The five countries with the highest scientific productivity are China, India, USA, Spain and Indonesia. The countries with the highest number of corresponding authors are China, India and Spain. In the case of China, 64% of the articles have conational authors. In contrast, all the articles with corresponding authors from India were conducted by authors from the same country. Regarding type of ecosystems analyzed, temperate forests are the most analyzed ecosystems with Landsat LST, followed by tropical forests and urban forests (Figure 4).
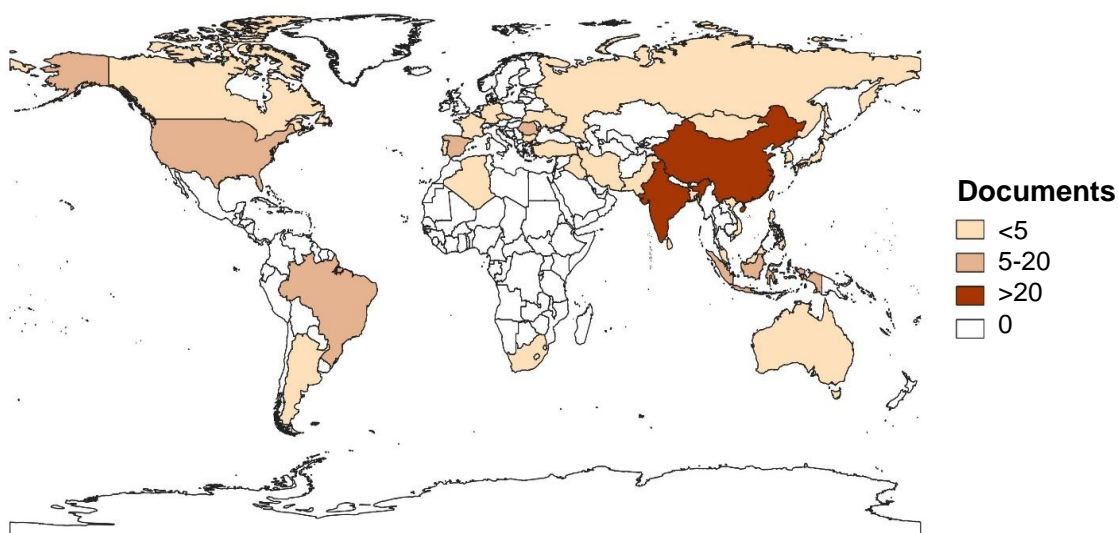
Figure 3. Country scientific production in the field of land surface temperature derived from Landsat missions
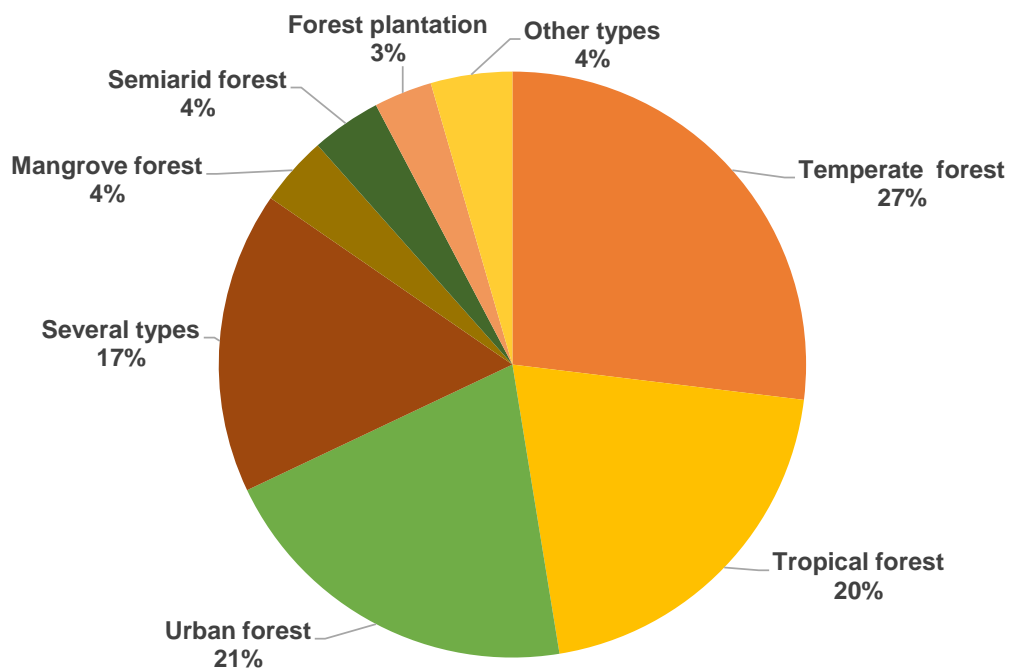
Figure 4. Forest types analyzed in the field of land surface temperature information from the Landsat missions

The collaboration network analysis is shown in Figure 5. Nodes represent countries, lines show the collaboration between countries; the size of the nodes represent the relative amount of publications for each country. Four main groups of collaboration can be distinguished, one of them integrated by China, USA and Spain; another network is integrated by Iran and Canada; a third one by Australia, China and Netherlands and another collaboration group can be distinguished between Germany and India. The most notable collaboration network is composed by China, USA and Spain. On the other hand, countries such as Brazil, Indonesia and Romania also have scientific production on LST but only with authors from the same country.
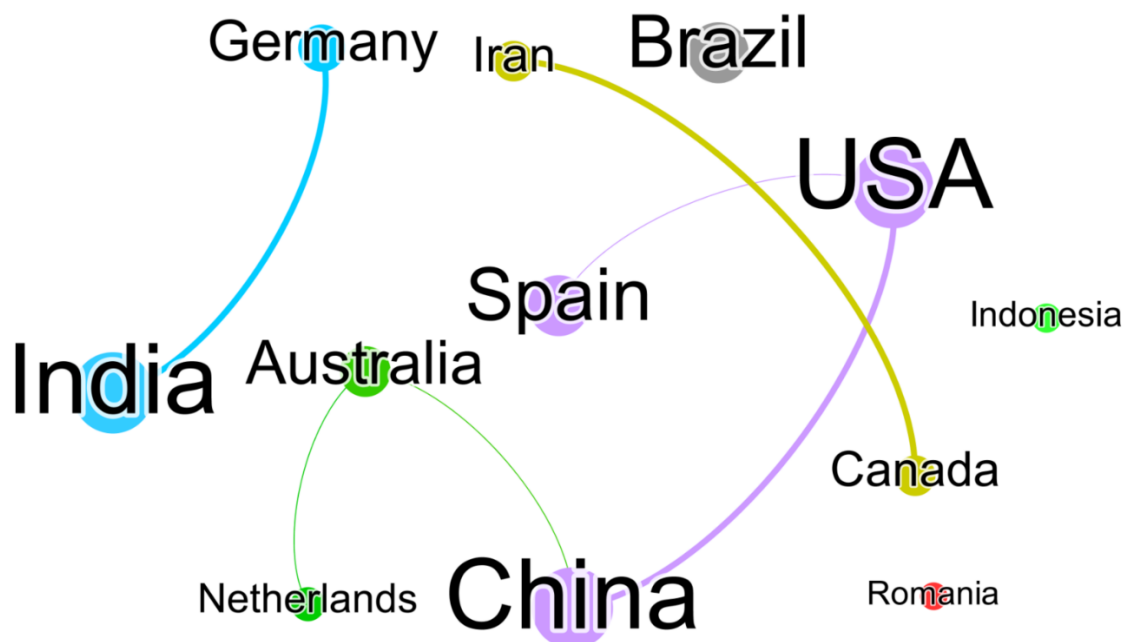
Figure 5. Country collaboration map of the 12 highest producing countries in the field of land surface temperature

2.3.3. Keyword analysis and thematic evolution

Keyword analysis allowed for identifying the main topic of the articles in a systematic and intuitive manner. A WorldTreeMap was generated from the Biblioshyni interface to represent the most frequently used keywords (Figure 6). Most used keywords (in addition to those used as criteria for the initial search i.e. "land surface temperature" and "Landsat") were: remote sensing (21%), NDVI (17%), MODIS (9%), Landsat 8 (8%), evapotranspiration (6%), land cover (6%), followed by burn severity, deforestation and soil moisture (each with 4%). Likewise, our analysis revealed that 40.4% of analyzed studies used Landsat 8 TIRS to estimate LST; 33.8% of studies used Landsat 4 and 5 TM; while Landsat 7 ETM+ was only used in 25.8% of studies.
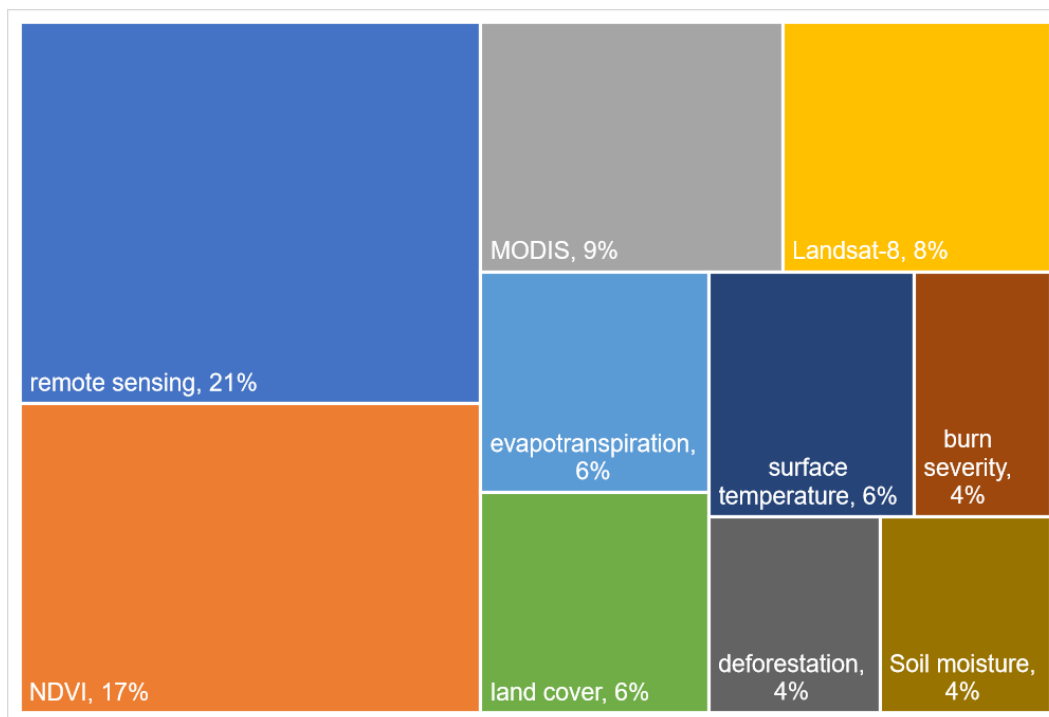
Figure 6. WordTreeMap of high-frequency keywords in the field of land surface temperature information from the Landsat missions

Multidimensional analysis allows identifying main keywords and the frequency of the relationships between them. Three groups can be distinguishd (Figure 7): the first group includes topics related to characterization of terrestrial surface, including surface mesurement, evapotranspiration and regression analysis. A second group is integrated by the keywords land cover, deforestation and eviromental monitoring in relation to urbanization. Finally, another group is formed only by three terms, artificial neural network, surface temperatures and climate change; this last group might represent an area of opportunity for the use of Landsat LST. One example is the study by Neinavaz et al. (2019) published in the journal Remote Sensing, where Landsat 8 short wave infrared and thermal infrared data were analyzed with neuronal networks to improve Left Area Index (LAI) characterization in a forest ecosystem.
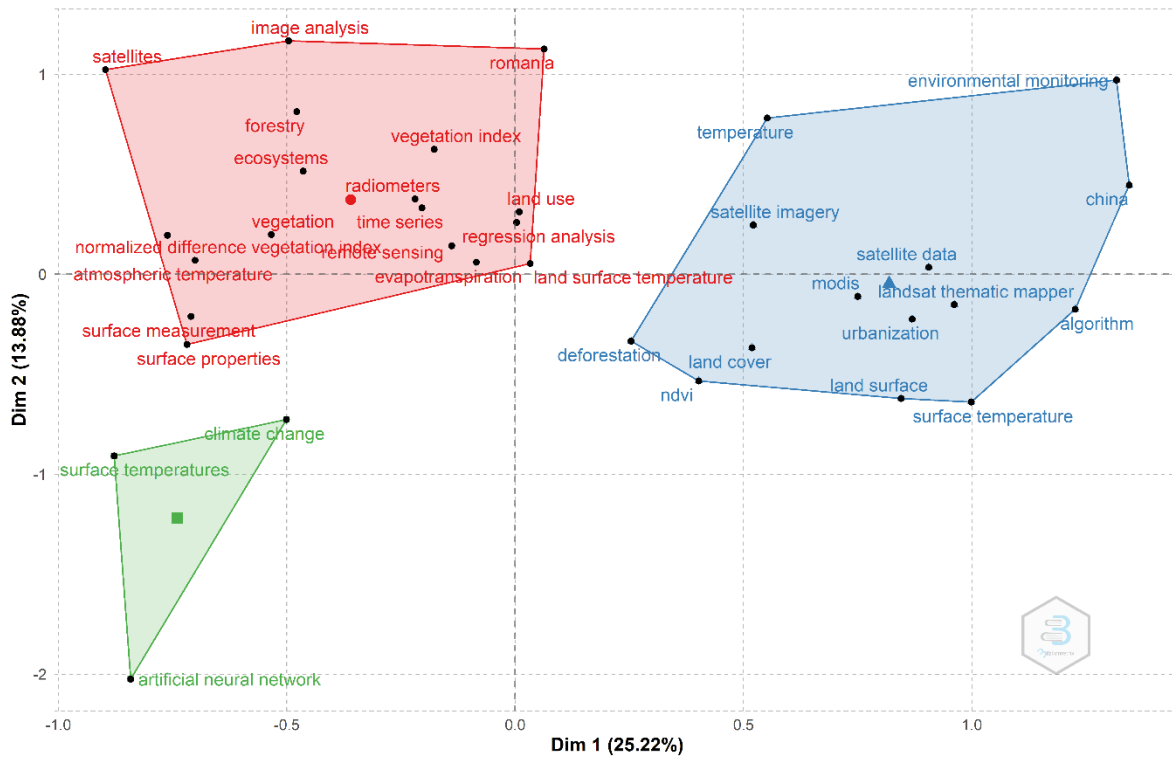
Figure 7. Multidimensional scaling analysis of high-frequency keywords in the field of land surface temperature information from the Landsat missions

A gradual change was found in the topics of the analyzed articles using LST to characterize forest ecosystems (Figure 8). In a first period (1995-2012), the most recurrent topics were: geology, vegetation and evapotranspiration. Topics related to keywords landforms and meteorology were frequent in years 2010 and 2012. Finally, in the most recent period keywords such as time series analysis and climate change were the most frequent.
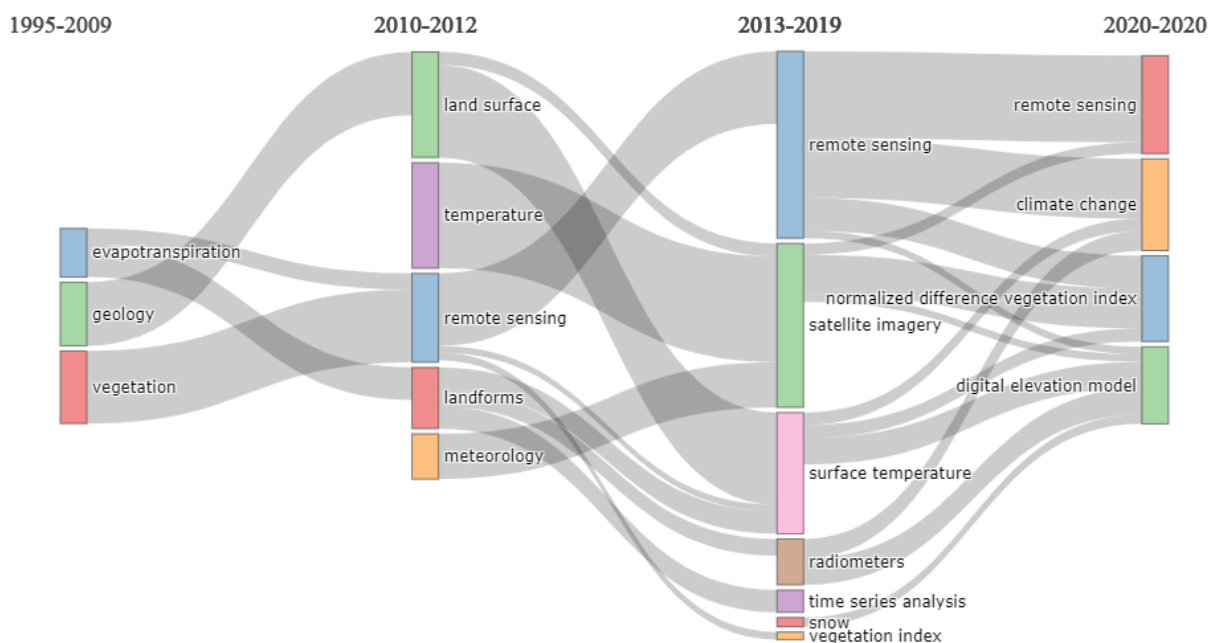
Figure 8. Thematic evolution of the field of land surface temperature information from the Landsat missions

2.3.4. Research topic analysis

The classification of the 155 analyzed studies by main research topic is shown in (Table S5,[suppl]). The most frequent research topic (51 publications) was Classification of land cover. LST data can reflect changes in the temperature fluxes of land surfaces associated to land surface composition changes, which results in a widespread use to analyze land use and vegetation type changes (Tan et al., 2020).

With regards to the documents centered on Forest monitoring, they focus on topics such as evaluating the dynamics of the cover and structure of forests (Siyal et al., 2017), monitoring natural protected areas (Gillespie et al., 2014), forest degradation analysis (Barros Santiago et al., 2019), forest cover change monitoring (van Leeuwen et al., 2011), and forest pests detection (Sprintsin et al., 2011).

2.4.   Discussion

Bibliometric analyses have been widely used to understand and define the paths of scientific development in different areas of knowledge (Bonilla et al., 2015; Ahmad et al., 2020; Moral-Muñoz et al., 2020; Mora et al., 2017). This type of analysis helps to know the volume and characteristics of scientific research on a particular topic, as well as the topic evolution over time (Ramanan et al., 2020).

The results of this analysis showed that the use of thermal information from the Landsat time-series in forest ecosystems started to gain importance in 1995, even though the first Landsat satellite capable of capturing thermal infrared information was launched in 1985. This might be explained by a more extensive use of satellite platforms to analyze urban areas and agricultural lands, with a comparative delay in the thermal analysis of forest areas. The interest in thermal dynamics on the earth's surface became relevant after climate change was acknowledged as a global issue by the United Nations Framework Convention on Climate Change. There, 197 countries signed a treaty with 10 commitments to reduce human interference with the global climate system. Notable aspects of this agreement include the following:

"Promote and cooperate in scientific, technological, technical, socio-economic and other research, systematic observation and development of data archives related to the climate system and intended to further the understanding and to reduce or eliminate the remaining uncertainties regarding the causes, effects, magnitude and timing of climate change." (UN, 1992).

This shift in policy may have resulted in a growing interest among the scientific community in the use of thermal information to analyze the Earth's surface, at times with a multi-temporal approach (Arif et al., 2019; Boike et al., 2016; Gosteva et al., 2019 a,b; Kayet et al., 2016). For instance, Kayet et al. (2016) analyzed for three years (1994, 2004 and 2014) the LST for different land uses and vegetation in an African forest. They found that the rapid growth of the industrial zone and the loss of vegetation favor a significant increase in LST.

Some of the journals with the greatest number of articles published on the matter notably include Proceedings of SPIE and Remote Sensing. Both are journals with prestige and a high impact factor. Proceedings of SPIE is a pioneering journal in research on remote sensing, as it started publications in 1995, and publishes proceedings of 350 SPIE conferences. Some of these are focused on research in remote sensing. As such, it is a journal with high visibility among the scientific community. On the other hand, Remote Sensing is a specialized journal that publishes the most cutting-edge breakthroughs on remote sensing (Gallardo-Salazar et al., 2020). High visibility and impact are often characteristics of journals that matter most to members of the scientific community.

Regarding the type of ecosystems analyzed, temperate forests are the most analyzed ecosystems with Landsat LST, followed by tropical forests and urban forests. The FAO reports that the world's largest forests are tropical forests, followed by temperate and boreal forests (FAO, 2020). Therefore, the prevalence of these forests in studies related to surface temperature may be closely related to the surface they represent worldwide (Peters et al., 2013). In addition, countries with the highest production on the matter have temperate forests, which can be reflected in the type of vegetation studied under this approach.

China has the highest scientific production on the subject, which can be explained mainly by two conditions: (1) China is a developed country with an important investment in science and technology. In addition, the Chinese scientific community has expressed a commitment to obtain information to characterize and restore the environment (Xie et al., 2020a). (2) Since the previous decade, several Chinese researchers started to publish their contributions in English, which has strengthened collaboration networks between China and English-speaking countries such as the USA and Australia (Pan & Block, 2011; Ramanan et al., 2020). This is undoubtedly a positive dynamic for research on the matter, as the development of collaboration networks results in an increase in the quality of scientific contributions (Ramanan et al., 2020).

Articles elaborated by Chinese institutions cover a variety of topics such as land use and vegetation type change detection (Tan et al., 2020), impact of deforestation on LST (Shen et al., 2020), relationships between environmental degradation and LST (Hou et al., 2020), algorithms to identify snow (Wang et al., 2020), impact of green areas in decreasing LST (Yin et al., 2019), evaluation of ecological indices and their relationship with LST (Zhu et al., 2019), factors influencing forest canopy LST (Zuo et al., 2018), multi-temporal evaluation of forest burned area (Wang et al., 2017), among others.

Among articles analyzed, the most used sensors were TIRS (Landsat 8) and TM (Landsat 4 and 5). The latter might be related to the failure suffered in 2003 by the scanner line of the Landsat 7 ETM+ sensor, resulting in incomplete image capture that reduced its use in the scientific community (Yin et al., 2017).

Similarly, widely used spectral indices such as NDVI are analyzed jointly with LST data to understand physiological processes such as water stress and forest decline. NDVI is deemed as the most widely used spectral index, given its simplicity and dependence on spectral bands (NIR and red) that are easy to obtain (Huang et al., 2021). The wide use of NDVI can be explained by the influence on thermal processes of the condition and amount of vegetation cover, which can be inferred from NDVI, a proxy of vegetation density and vegetative vigor. For example, Wan Mohd Jaafar et al. (2020) analyzed the influence of deforestation on LST, using NDVI to determine the conditions of the forest cover.

In addition to this, MODIS and Landsat products are often used jointly, which allows benefitting from Landsat's higher spatial resolution and from MODIS' temporal resolution (Guan et al., 2021). For example, in the study by Herrero et al. (2019), Landsat 8 LST was integrated with MODIS data to classify savanna forest types in Zambia. The authors concluded that using both data sources allowed to develop multi-temporal land use change analysis in African savannas.

Regarding the multidimensional scaling analysis, a link was observed between the terms evapotranspiration, vegetation index and vegetation. This finding can be related

to the development of spectral indices, which use information from the thermal infrared band. For example: Temperature Dryness Vegetation Index (TDVI) and the Vegetation Temperature Condition Index (VTCI), which are based on the theoretical relationship between NDVI and LST, allowing to predict areas with greater potential evapotranspiration than humidity availability (Xu et al., 2011).

Similarly, the topics urbanization, deforestation and land cover were grouped together, emphasizing the growing interest in understanding the processes of land use change and analysis of urban environments under a thermal approach (Wang & Zhang, 2015; Arif et al., 2019; Hua & Ping, 2018). For example, Jana et al. (2020) analyzed the impact of urban forests and green areas in the thermal dynamics of a city in Doon Valley, India and concluded that the expansion of areas with urban land use in replacement of forests and green areas influenced an observed increase in LST of up to 8.6°C.

The thematic evolution plot indicates that the use of thermal information from the Landsat series in the analysis of forest ecosystems has been a matter that has changed over time. It was initially used for the analysis of processes, such as evapotranspiration in the vegetation cover. Subsequently, a trend was observed in the use of this information for climatic and meteorological analysis and the development of vegetation indices. In recent years, it has been used for the analysis of processes associated with climate change. This suggests that the topics of application and techniques of analysis have evolved in lockstep with remote sensing trends, also related to topics of global importance such as climate change. Other emerging topics such as phenomenological analysis, desertification, mining or above-ground biomass estimation can represent areas of opportunity for the use of LST from Landsat series.

The paper herein has certain limitations, especially regarding the use of a single database (Scopus), which does not include all indexed journals and focuses on documentation only in English; therefore, this analysis could be excluding relevant documentation. In future studies, the search could be extended to other scientific

databases such as Web of Science and Google Scholar. Lastly, it is worth noting that a few months ago, the Landsat 9 satellite was successfully launched. This satellite shares an orbit with Landsat 8, which increases the temporal resolution of images and reduces the risk of interrupted information (USGS, 2020). Without a doubt, Landsat 9 represents the commitment and interest in ensuring the continuity of the Landsat series' data collection.

2.5. Conclusions

The use of land surface temperature (LST) data from Landsat series to monitor and characterize forest ecosystems is a topic in evolution, with applications in vegetation cover classification, forest monitoring, and drought and evapotranspiration analysis, among others. There are several countries with scientific productivity on the topic, with other regions such as Africa, Central America or Mexico showing potential for expanding its application. Thermal analysis of forest ecosystems has mainly focused on temperate forests, tropical forests, and urban forests. There is consequently an area of opportunity for the analysis of other types of vegetation with LST data.

The analysis of collaboration between countries showed a limited cooperation between countries, centered on a relatively small amount of collaboration networks. Increasing the collaboration between countries in this topic will allow improving the knowledge of thermal dynamics of forest ecosystems and its application to improve forest decision making in diverse regions of the world. The use of Landsat LST in forest ecosystems has evolved in pair with the trends and methodologies of remote sensing, with some emerging topics such as climate change monitoring in the last years.

The current bibliometric analysis allowed understanding the characteristics and evolution of this research topic. Future bibliometric research could focus on further comparing the thermal information from Landsat with those of other satellite platforms i.e. MODIS, Sentinel-3, NOAA-AVHRR, to obtain a multi-sensor perspective on the use of remote sensing for thermal characterization of forest ecosystems.

2.6. References

Ahmad P, Asif, JA, Alam, MK, Slots, J, 2020. A bibliometric analysis of Periodontology 2000. Periodontol 2000 82: 286- 297.

Amalyahya A, 2015. Vegetation Cover Density and Land Surface Temperature Interrelationship Using Satellite Data, Case Study of Wadi Bisha, South KSA. ARS 4:248-262.

Ara S, Islam MA, Showkat S, 2016. Effect of land-use intensity on surface temperature: A study on Chittagong city corporation área. In: 5th International Conference on Informatics, Electronics and Vision (ICIEV), 72-77.

Arekhi M, Yesil A, Ozkan UY, Sanli FB, 2018. Detecting treeline dynamics in response to climate warming using forest stand maps and Landsat data in a temperate forest. For Ecosyst 5:23.

Aria M, Cuccurullo C, 2017. Bibliometrix: An R-tool for comprehensive science mapping analysis. J Informetr 11:959-975.

Arif N, Khasanah AN, Jaya R, Gozan M, Hendrawan B, 2019. The Effect of Land Surface Temperature and Land Use on Energy System Development in Gorontalo City. J Phys Conf Ser 1179:012103.

Arvidson T, Barsi J, Jhabvala M,Reuter D, 2013. Landsat and Thermal Infrared Imaging. In: Kuenzer C, Dech S (eds) Thermal Infrared Remote Sensing: Sensors, Methods, Applications. Springer Netherlands, Dordrecht pp 177-196.

Ayele D, Zewotir T, Mwambi H, 2014. Multiple correspondence analysis as a tool for analysis of large health surveys in African settings. Afr. Health Sci 14.

Banskota A, Kayastha N, Falkowski MJ, Wulder MA, Froese RE, White JC, 2014. Forest Monitoring Using Landsat Time Series Data: A Review. Can J Remote Sens 40:362-384.

Barros Santiago D, Correia Filho WLF, de Oliveira-Júnior JF Silva-Junior CA, 2019. Mathematical modeling and use of orbital products in the environmental

degradation of the Araripe Forest in the Brazilian Northeast. Model Earth Syst Environ 5:1429-1441.

Bendib A, Dridi H, Kalla MI, 2017. Contribution of Landsat 8 data for the estimation of land surface temperature in Batna city, Eastern Algeria. Geocarto Int 32:503-513.

Boike J, Grau T, Heim B, Günther F, Langer M, Muster S, Gouttevin I, Lange, S, 2016. Satellite-derived changes in the permafrost landscape of central Yakutia, 2000-2011: Wetting, drying, and fires. Glob. Planet. Change 139:116-127.

Bonilla CA, Merigó JM, Torres-Abad C, 2015. Economics in Latin America: a bibliometric analysis. Scientometrics 105:1239-1252.

Del Mundo VKM, Tiburan Jr CL, 2019. Analyzing the effects of land cover change on surface temperature in Mount Makiling Forest Reserve (MMFR) and its neighboring municipalities using Landsat data. ISPRS Archives XLII-4/W19:165-172.

Duan P, Wang Y, Yin P, 2020. Remote Sensing Applications in Monitoring of Protected Areas: A Bibliometric Analysis. Remote Sens 12(5) 10.3390/rs12050772.

FAO, 2020. Global Forest Resources Assessment 2020: Main report. Rome. https://www.fao.org/documents/card/en/c/ca8753en/. [20 September 2021].

Fu P, 2016. A time series analysis of urbanization induced land use and land cover change and its impact on land surface temperature with Landsat imagery. Remote Sens Environ 175:205–214.

Gallardo-Salazar JL, Pompa-García M, Aguirre-Salado CA, López-Serrano PM, y Meléndez-Soto A, 2020. Drones: Tecnología Con Futuro Promisorio En La gestión Forestal. Revista Mexicana De Ciencias Forestales 11 (61).

GCOS, 2016. Essential Climate Variables. Global Climate Observing System. https://gcos.wmo.int/en/essential-climate-variables. [20 September 2021].

Ghazaryan G, Dubovyk O, Graw V, Schellberg J, 2018. Vegetation monitoring with satellite time series: an integrated approach for user-oriented knowledge extraction.

Proc of SPIE 10783, Remote Sensing for Agriculture, Ecosystems, and Hydrology XX, October 10.

Gillespie TW, Willis KS, Ostermann-Kelm S, 2014. Spaceborne remote sensing of the world's protected areas. Prog Phys Geogr: Earth and Environment 39:388-404.

Gosteva A, Matuzko A, Yakubailik O, 2019a. Detection of changes in urban environment based on infrared satellite data. IOP Conf Ser: Mater Sci Eng 537:062051.

Gosteva A, Matuzko A, Yakubailik O, 2019b. Identification of changes in urban environment on the basis of the satellite data of the infrared range (on the example of Krasnoyarsk). InterCarto InterGIS 25:90-100.

Guan X, Shen H, Wang Y, Chu D, Li X, Yue L, Liu X, Zhang L, 2021. Fusing MODIS and AVHRR products to generate a global 1-km continuous NDVI time series covering four decades. Earth Syst Sci Data

Herrero HV, Southworth J, Bunting E, Kohlhaas RR, Chil B, 2019. Integrating Surface-Based Temperature and Vegetation Abundance Estimates into Land Cover Classifications for Conservation Efforts in Savanna Landscapes. Sensors 19(16):3456.

Hou CH, Li FP, He BJ, Gu H, Song W, 2020. Study on surface thermal environment differentiation effect in mining intensive area through developing remote sensing assessment model. J Infrared Millim Terahertz Waves 39:635-649.

Hua AK, Ping OW, 2018. The influence of land-use/land-cover changes on land surface temperature: a case study of Kuala Lumpur metropolitan city. Eur J Remote Sens 51:1049-1069.

Huang H, Xie W, Sun H, 2015. Simulating 3D urban surface temperature distribution using ENVI-MET model: Case study on a forest park. Proc IEEE International Geoscience and Remote Sensing Symposium (IGARSS). pp: 1642-1645.

Huang S, Tang L, Hupy JP, Wang Y, Shao G, 2021. A commentary review on the use of normalized difference vegetation index (NDVI) in the era of popular remote sensing. J For Res 32:1-6

Jana C, Mandal D, Shrimali SS, Alam NM, Kumar R, Sena DR, Kaushal R, 2020. Assessment of urban growth effects on green space and surface temperature in Doon Valley, Uttarakhand, India. Environ Monit Assess 192:257.

Joshi A, 2017. Comparison between Scopus & ISI Web of science. J Glob Values 7:2016

Kayet N, Pathak K, Chakrabarty A, Sahoo S, 2016. Spatial impact of land use/land cover change on surface temperature distribution in Saranda Forest, Jharkhand. Model Earth Syst Environ 2:127.

Li ZL, Tang BH, Wu H, Ren H, Yan G, Wan Z, Trigo IF, Sobrino JA, 2013. Satellite-derived land surface temperature: Current status and perspectives. Remote Sens Environ 131:14-37.

Lotka AJ, 1926. The frequency distribution of scientific productivity. J Wash Acad Sci 16:317-323

Mora L, Bolici R, Deakin M, 2017. The First Two Decades of Smart-City Research: A Bibliometric Analysis. Journal of Urban Technology 24(1):3-27.

Moral-Muñoz JA, Herrera-Viedma E, Santisteban-Espejo A, Cobo M J, 2020. Software tools for conducting bibliometric analysis in science: An up-to-date review. Profesional de la Información 29(1).

Neinavaz E, Darvishzadeh R, Skidmore AK, Abdullah H, 2019. Integration of Landsat-8 Thermal and Visible-Short Wave Infrared Data for Improving Prediction Accuracy of Forest Leaf Area Index. Remote Sens 11(4):390.

Pan L, Block, D, 2011. English as a "global language" in China: An investigation into learners' and teachers' language beliefs. System 39(3):391-402.

Peters EB, Wythers KR, Zhang S, Bradford JB, Reich PB, 2013. Potential climate change impacts on temperate forest ecosystem processes. Can J For Res 43(10).

Quintano C, Fernández-Manso A, Calvo L, Marcos R, Valbuena L, 2015. Land surface temperature as potential indicator of burn severity in forest Mediterranean ecosystems. Int J Appl Earth Obs Geoinf 36:1-12.

Quintano C, Fernández-Manso A, Roberts DA, 2017. Burn severity mapping from Landsat MESMA fraction images and Land Surface Temperature. Remote Sens Environ 190:83-95.

Quispe-Reymundo BJ, Révolo-Acevedo RH, 2020. Surface temperature and states of the vegetation of the forest of Polylepis spp, district of San Marcos de Rocchac, Huancavelica – Peru. Enfoque UTE 11:69 - 86.

Rahaman S, Kumar P, Chen R, Meadows ME, Singh RB, 2020. Remote Sensing Assessment of the Impact of Land Use and Land Cover Change on the Environment of Barddhaman District, West Bengal, India. Front environ sci 8:127.

Ramdhani NF, Sulistyawati E, Sutrisno, 2019. Land surface temperature analysis of post-mining area using Landsat 8 imagery. Proc of SPIE 11372, Sixth International Symposium on LAPAN-IPB Satellite 113720P, December 24.

Rasul A, Balzter H, Smith C, Remedios J, Adam B, Sobrino JA, Srivanit M, Weng Q, 2017. A Review on Remote Sensing of Urban Heat and Cool Islands. Land 6(2):38.

RStudio Team, 2020. RStudio: Integrated Development for R. RStudio, PBC, Boston, MA. http://www.rstudio.com/. [20 September 2021].

Sabajo CR, le Maire G, June T, Meijide A, Roupsard O, Knohl A, 2017. Expansion of oil palm and other cash crops causes an increase of the land surface temperature in the Jambi province in Indonesia. Biogeosciences 14(20):4619-4635.

Sahana M, Ahmed R, Sajjad H, 2016. Analyzing land surface temperature distribution in response to land use/land cover change using split window algorithm and

spectral radiance model in Sundarban Biosphere Reserve, India. Model Earth Syst Environ 2:81.

Sánchez JM, Bisquert M, Rubio E, Caselles V, 2015. Impact of Land Cover Change Induced by a Fire Event on the Surface Energy Fluxes Derived from Remote Sensing. Remote Sens 7(11): 14899-14915.

Savastru DM, Zoran MA, Savastru RS, 2019. Satellite remote sensing detection of forest vegetation land cover changes and their potential drivers. Proc SPIE, Remote Sensing for Agriculture, Ecosystems, and Hydrology XXI; 1114926.

Shen W, He J, Huang C, Li M, 2020. Quantifying the Actual Impacts of Forest Cover Change on Surface Temperature in Guangdong, China. Remote Sens 12(15):2354.

Siyal AA, Siyal AG, Mahar RB, 2017. Spatial and temporal dynamics of Pai forest vegetation in Pakistan assessed by RS and GIS. J For Res 28:593-603.

Sprintsin M, Chen JM, Czurylowicz P, 2011. Combining land surface temperature and shortwave infrared reflectance for early detection of mountain pine beetle infestations in western Canada. J Appl Remote Sens 5:1-14.

Tan J, Yu D, Li Q, Tan X, Zhou W, 2020. Spatial relationship between land-use/land-cover change and land surface temperature in the Dongting Lake area, China. Sci Rep 10:9245.

UN, 1992. United Nations framework convention on climate change. https://unfccc.int/files/essential_background/background_publications_htmlpdf/appli cation/pdf/conveng.pdf [10 November 2021].

USGS, 2020. Landsat—Earth observation satellites. https://pubs.er.usgs.gov/publication/fs20153081. [15 October 2021].

van Leeuwen TT, Frank AJ, Jin Y, Smyth P, Goulden M, vab der Werf GR, Randerson JT, 2011. Optimal use of land surface temperature data to detect changes in tropical forest cover. J Geophys Res Biogeosci 116.

Vlassova L, Pérez-Cabello F, 2016. Effects of post-fire wood management strategies on vegetation recovery and land surface temperature (LST) estimated from Landsat images. Int J Appl Earth Obs Geoinf 44:171-183.

Vorovencii I, 2015. Assessing and monitoring the risk of desertification in Dobrogea, Romania, using Landsat data and decision tree classifier. Environ Monit Assess 187:204.

Wan Mohd Jaafar WS, Abdul Maulud KN, Muhmad Kamarulzaman AM, Raihan A, Md Sah S, Ahmad A, Saad SNM, Mohd Azmi AT, Jusoh Syukri NKA, Razzaq Khan W, 2020. The Influence of Deforestation on Land Surface Temperature—A Case Study of Perak and Kedah, Malaysia. Forests 11(6):670.

Wang L, Zhang S, 2015. Analysis on the relationship be-tween the pattern of green spaces and land surface tem-perature based on normalized difference vegetation in-dex: A case study in Changchun city, China. Fresenius Environ Bull 24: 2444-2451.

Wang F, Qin Z, Song C, Tu L, Karnieli A, Zhao S, 2015. An Improved Mono-Window Algorithm for Land Surface Temperature Retrieval from Landsat 8 Thermal Infrared Sensor Data. Remote Sens 7(4):4268-4289.

Wang J, Qian YG, Han LJ, Zhou WQ, 2016. Relationship between land surface temperature and land cover types based on GWR model: A case of Beijing-Tianjin-Tangshan urban agglomeration, China. Chi J Appl Ecol 27:2128-2136

Wang Q, Yu X, Shu Q, 2017. Forest burned scars area extraction using time series remote sensing data. J Nat Disaster Sci 26:1-10.

Wang X, Chen S, Wang J, 2020. An Adaptive Snow Identification Algorithm in the Forests of Northeast China. IEEE J Sel Top Appl Earth Obs Remote Sens 13:5211-5222.

Xiao H, Weng Q, 2007. The impact of land use and land cover changes on land surface temperature in a karst area of China. J Environ Manage 85:245-257.

Xie H, Zhang Y, Wu Z, Lv T, 2020a. A Bibliometric Analysis on Land Degradation: Current Status, Development, and Future Directions. Land 9(1):28.

Xie H, Zhang Y, Zeng X, He Y, 2020b. Sustainable land use and management research: a scientometric review. Landsc Ecol 35:2381-2411.

Xu L, Niu R, Li J, Dong Y, 2011. Soil moisture status estimation over Three Gorges area with Landsat TM data based on temperature vegetation dryness index. Proc of SPIE 8006, MIPPR 2011: Remote Sensing Image Processing, Geographic Information Systems, and Other Applications, 80061F, November 23.

Yang Y, Anderson MC, Gao F, Hain CR, Semmens KA, Kustas WP, Noormets A, Wynne RH, Thomas VA, Sun G, 2017. Daily Landsat-scale evapotranspiration estimation over a forested landscape in North Carolina, USA, using multi-satellite data fusion. Hydrol Earth Syst Sci Discuss 21:1017-1037.

Yin G, Mariethoz G, McCabe MF, 2017. Gap-Filling of Landsat 7 Imagery Using the Direct Sampling Method. Remote Sens 9(1):12.

Yin J, Wu X-x, Shen M, Zhang X, Zhu C, Xiang H, Shi C, Guo Z, Li C, 2019. Impact of urban greenspace spatial pattern on land surface temperature: a case study in Beijing metropolitan area, China. Landsc Ecol 34:2949 – 2961.

Zhu J, Ju W, Ren Y, 2010. Effects of land cover types and forest age on evapotranspiration detected by remote sensing in Xiamen City, China. Proc 18th International Conference on Geoinformatics, June 18-20. pp:1-5.

Zhu X, Wang X, Yan D, Liu Z, Zhou Y, 2019. Analysis of remotely-sensed ecological indexes' influence on urban thermal environment dynamic using an integrated ecological index: a case study of Xi'an, China. Int J Remote Sens 40:3421-3447.

Zhuang Y, Liu X, Nguyen T, He Q, Hong S, 2013. Global remote sensing research trends during 1991–2010: a bibliometric analysis. Scientometrics 96:203-219.

Zuhro A, Tambunan M, Marko K, 2020. Application of vegetation health index (VHI) to identify distribution of agricultural drought in Indramayu Regency, West Java Province. IOP Conference Series: Earth and Environmental Science 500:012047.

Zuo S, Dai S, Song X, Xu C, Liao Y, Chang W, Chen Q, Yaying L, Tang J, Man W, et al., 2018. Determining the Mechanisms that Influence the Surface Temperature of Urban Forest Canopies by Combining Remote Sensing Methods, Ground Observations, and Spatial Statistical Models. Remote Sens 10(11):1814.

Suplementary material

Table 1. Landsat satellite missions with thermal infrared spectral band

Satellite	Sensor	Operational period	Band	Wavelength
Landsat 4	TM	1982 - 1993	B6	10.40 - 12.50 µm
Landsat 5	TM	1984 - 2013	B6	10.40 - 12.50 µm
Landsat 7	ETM+	1999 – present	B6	10.40 - 12.50 µm
Landsat 8	TIRS	2013 - present	B10	10.6 - 11.19 µm
			B11	11.5 - 12.51 µm

Source: USGS 2016

Table 2. Summary of the literature database

General Information	
Search period	1995 - 2020
Total number of documents	155
Annual growth percent	22.58
Average documents per year	4.76
Average citations per document	10.24
Annual average citation per document	1.65
Type of documents	
Article	101
Book chapter	1
Proceedings papers	53
Authors	
Total number of authors	554
Authors of single-authored document	4
Authors of multi-authored document	550
Documents per author	0.29
Authors per document	3.51
Collaboration index	3.59

Table 3. The ten journals with the most publications about land surface temperature derived from Landsat missions.

Scientific sources	Start of publication	Total publications	Publications per year
Proceedings of SPIE - The International Society for Optical Engineering	1995	14	0.6
Remote Sensing	2014	9	1.5
IOP Conference Series: Earth and Environmental Science	2014	7	1.2
International Journal of Applied Earth Observation and Geoinformation	2015	6	1.2
International Geoscience and Remote Sensing Symposium (IGARSS)	2008	5	0.4
Environmental Monitoring and Assessment	2015	4	0.8
International Archives of the Photogrammetry Remote Sensing and Spatial Information Sciences - ISPRS Archives	2008	4	0.3
International Multidisciplinary Scientific Geoconference Surveying Geology and Mining Ecology Management SGEM	2013	4	0.6
Remote Sensing of Environment	2016	4	1
International Journal of Remote Sensing	2017	3	1

Table 4. The ten most cited publications about surface temperature derived from Landsat missions.

Article	DOI	Total cites	Cites per year
Fu P, 2016, Remote Sens Environ	10.1016/j.rse.2015.12.040	174	43.5
Xiao H and Weng Q., 2007, J Environ Manage	10.1016/j.jenvman.2006.07.016	127	9.7
Srivastava Pk, 2009, Adv Space Res	10.1016/j.asr.2009.01.023	66	6
Rodriguez-Galiano V, 2012, Appl Geogr	10.1016/j.apgeog.2012.06.014	53	6.6
Li Y, 2016, J Geophy Res	10.1002/2016JD024969	49	12.3
Eisavi V, 2015, Environ Monit Assess	10.1007/s10661-015-4489-3	49	9.8
Kayet N, 2016, Model Earth Syst Environ	10.1007/s40808-016-0159-x	47	11.7
Sinha S, 2015, Egypt J Remote Sens Space Sci	10.1016/j.ejrs.2015.09.005	44	8.8
Quintano C, 2015, Int J Appl Earth Obs Geoinformation	10.1016/j.jag.2014.10.015	44	8.8
Vlassova L, 2014, Remote Sens	10.3390/rs6076136	40	6.6

Table 5: Classification by main research topic of the 155 documents analyzed.

Research topic	No. of papers	References
Land cover classification	51	Xiao and Weng (2007); Srivastava *et al.* (2009); Sousa and Laerte (2012); Rodriguez-Galiano and Chica-Olmo (2012); Robbany *et al.* (2013); Vorovencii (2013b); Vorovencii (2013a); Vorovencii (2014); Eisavi *et al.*, (2015); Li *et al.* (2015); Park and Um (2015); Sheikhi *et al.* (2015); Sinha *et al.* (2015); Trinh *et al.* (2015); Fu (2016); Ilayaraja *et al.* (2017); Kayet *et al.* (2016); Sahana *et al.* (2016); Wang *et al.* (2016); Al-Hamdan *et al.* (2017); Faqe Ibrahim (2017); Kumari and Sarma (2017); Mushore *et al.* (2018); Thakur *et al.* (2017); Ghosh and Porchelvan (2018); Hua and Ping (2018); Zoran *et al.* (2018); Gosteva *et al.* (2019a); Gosteva *et al.* (2019b); Hao *et al.* (2019); Madakarah *et al.* (2019); Nguyen and Henebry (2019); Norovsuren *et al.* (2019); Ranagalage *et al.* (2019); Rangzan *et al.* (2019); Savastru *et al.* (2019); Shumilo *et al.* (2019b); Shumilo *et al.* (2019a); Al-Doski *et al.* (2020); Carrasco *et al.* (2020); Fathololoumi *et al.* (2020); Rahaman *et al.* (2020); Sarker *et al.* (2020); Sayão *et al.* (2020); Shidiq *et al.* (2020); Singh and Mishra (2020); Tan *et al.* (2020); Thakur *et al.* (2020); Yee *et al.* (2016); Dash and Revi (2017); Satriawan *et al.* (2020).
Forest monitoring	25	Sprintsin *et al.* (2011); van Leeuwen *et al.* (2011); Bright *et al.* (2013); Gillespie *et al.* (2014); Yang *et al.* (2014); Zhao *et al.* (2014); Dutta *et al.* (2015); Zhang *et al.* (2015); Cristóbal *et al.* (2016); Godinho *et al.* (2016); Siyal *et al.* (2017); Cao and Sanchez-Azofeifa (2017); Sabajo *et al.* (2017); Arekhi *et al.* (2018); Ghazaryan *et al.* (2018); Barros Santiago *et al.* (2019); Herrero *et al.* (2019); Sholihah and Shibata (2019); Khorrami *et al.* (2019); Shen *et al.* (2020); Inanaga *et al.* (1997); Boike

et al. (2016); Crabbe *et al.* (2019); Dergunov *et al.* (2019).

Evapotranspiration/Dryness	12	Lahoche *et al.* (1999); Xu *et al.* (2008); Zhu *et al.* (2010); Cristóbal *et al.* (2011); Natsagdorj *et al.* (2017); Yagci *et al.* (2017); Yang *et al.* (2017); Gustin *et al.* (2019); Natsagdorj *et al.* (2019); Xu *et al.* (2011); Gao and Gao (2011).

Table 5. Continued

Thermal analysis	12	Yang *et al.* (2008); Srivastava *et al.* (2010); Silva *et al.* (2015); Bendib *et al.* (2017); Geletič *et al.* (2017); Marques *et al.* (2017); Arif *et al.* (2019); Firoozy Nejad and Zoratipour (2019); Zhang and Zhang (2019); Sharma *et al.* (2020); Winanti *et al.* (2020); Li *et al.* (2015).
Urban forests analysis	12	Yang *et al.* (2010); Wang and Zhang (2015); Huang *et al.* (2015); Ahmad and Goparaju (2017); Ara *et al.* (2016); Urmambetova (2017); Gage and Cooper (2017); Zuo *et al.* (2018); Yin *et al.* (2019); Jana *et al.* (2020); Matuzko and Yakubailik (2019); Zhang *et al.* (2014).
Wildfire	10	Vlassova *et al.* (2014); Sánchez *et al.* (2015); Vlassova and Pérez-Cabello (2016); Wang *et al.* (2017); Guindos-Rojas *et al.* (2018); Çolak and Sunar (2020); Fernández-Manso *et al.* (2020); García-Llamas *et al.* (2019); Quintano *et al.* (2017); Quintano *et al.* (2015).
Deforestation	8	Zoran *et al.* (2013a); Huang and Anderegg (2014); Li *et al.*,(2016); Liou *et al.* (2017); Roitberg *et al.* (2018); Tarawally *et al.* (2018); Wan Mohd Jaafar *et al.* (2020); Silva *et al.* (2020).
Vegetation indexes	5	Zoran *et al.* (2013b); Ning *et al.* (2017); Malik and Shukla (2018); Neinavaz *et al.* (2019); Neinavaz *et al.* (2020).

Environmental quality analysis	4	Zheng and Ren (2013); Liu *et al.* (2018); Zhu *et al.* (2019); Zuhro *et al.* (2020).
Mountain ecology /Snow monitoring	4	Park *et al.* (2016); Firozjaei *et al.* (2020); Wang *et al.* (2020); Lv and Pomeroy (2019).
Climate change analysis	3	Mukherjee and Siddique (2018); Savastru *et al.* (2020); Oh (2017)
Phenological analysis	3	Khare *et al.* (2016); Khare *et al.* (2017); Khare and Rossi (2019).
Mining	3	Trinh and Zablotskii (2017); Ramdhani *et al.* (2019); Hou *et al.* (2020).
Desertification	2	Roozekrans (1995); Vorovencii (2015).
Above-ground biomass estimation	1	Gunawardena and Fernando (2016).

CAPÍTULO 3   ANALYSIS OF NEAR-SURFACE TEMPERATURE LAPSE RATES IN MOUNTAIN ECOSYSTEMS OF NORTHERN MEXICO USING LANDSAT-8 SATELLITE IMAGES AND ECOSTRESS

Marcela Rosas-Chavoya, Pablito Marcelo López-Serrano, José Ciro Hernández-Díaz, Christian Wehenkel, Daniel José Vega-Nieva

3.1. Abstract

Mountain ecosystems provide environmental goods, which can be threatened by climate change. Near-Surface Temperature Lapse Rate (NSTLR) is an essential factor used for thermal and hydrological analysis in mountain ecosystems. The aims of the present study were to estimate NSTLR and to identify its relationship with aspect, Local solar zenith angle (LSZA) and Evaporative Stress Index (ESI) for two seasons of the year in a mountain ecosystem at the North of Mexico. Normalized Land Surface Temperature (NLST) was estimated using environmental and topographical variables. LSZA was calculated from slope to consider the effect of solar position. NSTLR was estimated through simple linear models. Observed NSTLR was 9.4 °C km^{-1} for the winter and 14.3 °C km^{-1} for the summer. Our results showed variation in NSTLR by season. In addition, aspect, LSZA and ESI also influenced NSTLR regulation. In addition, Northwest and West aspects exhibited the highest NSTLR. LSZA angles closest to 90° were related with a decrease in NSTLR for both seasons. Finally, ESI values associated with less evaporative stress were related to lower NSTLR. These results suggest potential of Landsat-8 LST and ECOSTRESS ESI to capture interactions of temperature, topography, and water stress in complex ecosystems.

Keywords: evaporative stress index; land surface temperature; Landsat-8; ECOSTRESS; evapotranspiration

3.2. Introduction

Mountain ecosystems are characterized by being located at high elevations and showing environmental heterogeneity within their altitudinal gradient [1,2]. Mountain ecosystems provide a large quantity of ecosystem services [3,4]. One of most

important ecosystem services is water supply, it is estimated more than half of water resources for human consumption are directly or indirectly from these areas [5,6,7]. In addition, forested areas and grasslands within the altitudinal gradient of mountain ecosystems are important for the processes of climatic regulation, net primary productivity, and soil conservation [5,7,8,9,10].

These ecosystems and the environmental processes occurring within them are very sensitive to climate change and other impacts from human activities, such as deforestation and overgrazing [8,11]. Globally, mountain ecosystems are threatened by human activities, including land use change degradation and human-caused climate change, which is affecting forests distribution [12,13]. For examples, changes in forest and glacier distribution related to climate change have been documented in Himalayan ecosystems [13,14]. These processes modify the humidity, precipitation and temperature patterns throughout the altitudinal gradient and affect water availability, endangering water reserves for human population, and affecting fauna and flora [14,15]. In spite of the importance and fragility of these ecosystems, research on climatic processes in mountain areas has been limited by accessibility constraints [11,16].

The analysis of mountain ecosystems trough a thermal approach could provide information about environmental dynamics of these ecosystems. An essential variable to studied thermal and climatic conditions in mountainous area is near-surface temperature lapse rate (NSTLR), defined as the rate of change in temperature by elevation [17]. NSTLR is defined as inverse relationship between elevation and temperature [17,18,19]. It is generally assumed to have a value of 6.5 °C km−1, inferred from the NSTLR of the atmospheric column within the troposphere [20,21], and is generally the constant value of NSTLR in mountain areas. Nevertheless, several studies have concluded that the NSTLR is locally variable, depending on the region and season, with varying results of the thermal gradient value and the factors affecting it [18,22,23,24]. There is consequently a need to further analyze the factors influencing the seasonal and spatial variability in NSTLR.

NSTLR can be affected by topographic variables, such as aspect and slope and other variables such as evapotranspiration (ET) [1,25], although many questions remain regarding the environmental drivers of NSTLR. The characterization of NSTLR in mountain ecosystems is limited by the availability and spatial distribution of weather stations, often limiting a spatially detailed characterization of climatic data [24,26,27].

Higher resolution DEM and satellite climate information offers a new opportunity to better analyze thermal and hydric processes in mountain ecosystems [13,28]. Remote sensing techniques utilizing satellite images from passive remote sensors can be a useful alternative to study mountain ecosystems, since they can provide information in areas without water stations data and areas under low accessibility conditions, providing historical data at regional and global scales [29]. The thermal dynamics can be monitored from land surface temperature (LST) data estimated from satellite images, which provide spectral information about the processes of energy exchange between solar radiation and the terrestrial surface [30].

Several studies have been utilized satellite information to estimate and analyze the NSTLR in mountain ecosystems, using the relationship between LST and a digital elevation model (DEM) [8,18,26,31,32,33]. Nevertheless, it has been observed that some environmental variables (i.e., solar incidence, moisture, land cover characteristics) cause interference of NSTLR estimated from LST data [18,34]. Therefore, it has been suggested normalizing LST data with respect to environmental variables, potentially improving the accuracy of estimation of NSTLR from satellite information [8,35]. This approach has been less explored and requires further evaluation, particularly for the relatively less utilized medium resolution sensors. In particular, studies using Landsat Land Surface Temperature product to analyze factors driving thermal gradients in forest ecosystems are still relatively scarce [18,26,36]. In the present study, we used LST derived from Landsat-8 TIRS, which was normalized using random forests to obtain NSTLR information. This information allowed us to analyze the variability of NSTLR with respect to biophysical parameters, such as evapotranspiration (ET) and topographic characteristics.

The knowledge about NSTLR and the factors influencing it at a regional scale can allow to improve the understanding the thermal and hydric dynamics of mountain ecosystems [18] and could be used to develop climatic models, hydrological models and analysis of soil moisture [37]. For example, the effect of slope which depends on solar radiation flux incidence on the terrestrial surface; it can be quantified through the Local Solar Zenith Angle (LSZA). This parameter is calculated considering the interaction of the slope relative to sun position at time of satellite pass [38].

In addition to the previously documented contrasting effects of vegetation and topography on NSTLR [18,26], other parameters potentially affecting thermal gradients have received less attention. For example, very few studies have analysed the variation of thermal gradients with respect to remotely sensed evapotranspiration (ET) indices, particularly from medium resolution sensors.

ET is a key hydrologic component for the energy balance of terrestrial surface, influencing water availability [39]. Until recently, there remained a large gap in our ability to monitor ET concurrently at both fine spatial and fine temporal scales globally [40]. The relatively recently launched (June 2018) ECOSTRESS sensor provides a good opportunity for monitoring daily ET at medium (70 m) resolution globally [40,41]. There remains a need to evaluate ECOSTRESS mission performance, particularly the ET estimates in humid, temperate, mountainous areas [41]. In addition, to our best knowledge, no previous study has analyzed the variations Landsat-derived NSTLR against ECOSTRESS ET indices such as the Evaporative Stress Index (ESI).

Therefore, the aim of current study was to examine the variability of NSTLR for two contrasting year seasons (winter-summer) in a forest management area at the Sierra Madre Occidental (SMO) in Durango State, Mexico and to analyze the influence of topography and other biophysical factors such as evaporative stress, through Landsat-8 and ECOSTRESS images. The study had following hypotheses: (1) NSTLR in the study area is different than the constant value (6.5 °C km−1), (2) NSTLR is influenced by different topographic and biophysical characteristics (LSZA, aspect and ESI). Improved NSTLR characterization could contribute to ecological

modeling and water management planning, including water balances assessment [31,42]. Furthermore, understanding the effects of topography on temperature gradients could contribute to ongoing fire risk analysis e.g., [43,44].

3.3. Materials and Methods

3.3.1. Study Area

The area of study was the management unit UMAFOR 1001, in the central part of the SMO, at the North of Durango State, Mexico (Figure 1). The SMO is the highest mountain range in México, it has a one of the main forest reserves in Mexico, which gives it great economic and ecological relevance given the wide variety of environmental services it provides [45,46,47]. UMAFOR 1001 is bounded between 25.57° and 26.84°N latitude and 105.05° and 106.55°W longitude with an approximate 11,336 km2 of area. The average elevation of study area is 2131 m above the mean sea level. The vegetation includes more than 75 species of pine and oak forests in the upper and middle elevations [48]. Among these species, Quercus sideroxyla Humb and Bonpl, Pinus durangensis Martínez, Quercus grisea Liebm and Pinus teocote Humb and Bonpl stand out [49], while mid-slopes and flat terrains are characterized by semiarid vegetation, such as shrublands, chaparral, natural grasslands and induced pasturelands [47]. Climate ranges from subhumid to semiarid, with an annual precipitation average of 664 mm and mean temperatures ranging from 8.7 (average of coldest month) to 16.1 °C (average of the warmest month), with an annual average of 11.1 °C [48,50]. UMAFOR 1001 has a variable topography ranging from undulating to rugged topography and altitudinal characteristics that make it valuable to analyze regional thermal processes.
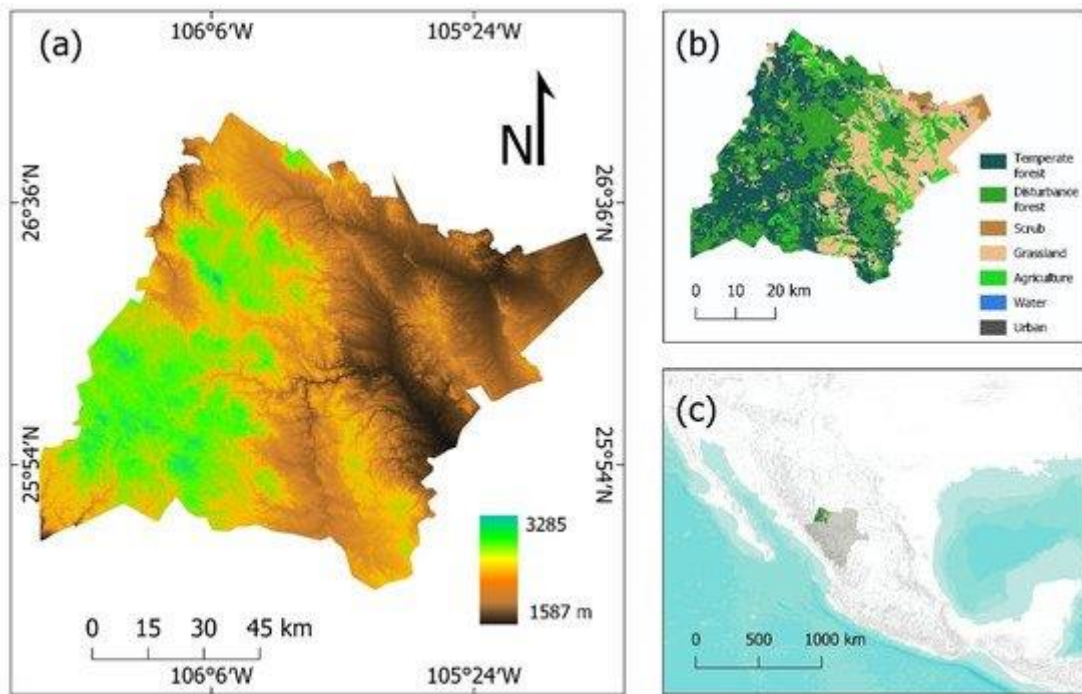
Figure 1. Study area. (a) Elevation; (b) Vegetation. The data on land use and vegetation were taken from information from the National Institute of Statistics and Geography of Mexico [50]. Temperate forests include pine forests, oak forests, and mixed forests. The disturbance forest classification corresponds to forests that suffered some alteration and are under a natural regeneration process; (c) Location of study area.

3.3.2. Images Acquisition

The Digital Elevation Model (DEM) from the Shuttle Radar Topography Mission (SRTM), with a resolution of 30 m, was downloaded from the US Geological Service webpage (https://earthexplorer.usgs.gov) (accessed on 25 July 2020). Slope and aspect were obtained from the DEM, using QGIS 3.14 [51].

Google Earth Engine (GEE) platform was used to visualize, process, and download Landsat-8 OLI/TIRS (with a 30 m resolution) [52]. The GEE allows processing large datasets in a cloud-based platform, accessing satellite data such as Landsat collections. The images correspond to LANDSAT/LC08/C01/T1_SR collection from winter and summer of 2019 (Table 1). In addition, a cloud and cloud shadow mask from Quality assessment band (BQA) band was applied to remove pixels where attributes might be altered by climatic conditions; this process is a

prerequisite to perform a more trustable thermal analysis; this process that must be considered every time that satellite images are processed [53,54].

Table 1. Path/Row and acquisition dates of Landsat-8 images.

Path/Row	Acquisition Date		Path/Row	Acquisition Date	
	Winter	**Summer**		**Winter**	**Summer**
31/42	31 December 2018	05 June 2019	32/41	22 December 2018	02 June 2019
	16 January 2019	11 July 2019		07 January 2019	18 June 2019
	01 February 2019	27 July 2019		23 January 2019	03 August 2019
	17 February 2019	12 August 2019		08 February 2019	19 August 2019
	05 March 2019	28 August 2019		24 February 2019	04 September 2019
				12 March 2019	20 September 2019
31/43	31 December 2018	25 June 2019	32/42	22 December 2018	02 July 2019
	16 January 2019	11 July 2019		07 January 2019	18 July 2019
	01 February 2019	27 July 2019		23 January 2019	03 August 2019
	17 February 2019	12 August 2019		08 February 2019	19 August 2019
	05 March 2019	28 August 2019		24 February 2019	04 September 2019
				12 March 2019	20 September 2019

3.3.3. Spectral Indices Estimation

The spectral indices had estimated employing Landsat-8 bands. These indices were estimated using the Equations (1)–(3) in the GEE platform and was used for the normalization LST.

$$NDVI = \frac{B5 - B4}{B5 + B4} \tag{1}$$

$$NDBI = \frac{B6 - B5}{B6 + B5} \tag{2}$$

$$NDWI = \frac{B3 - B5}{B3 + B5} \tag{3}$$

where NDVI is the Normalized difference vegetation index developed by Rouse, et al. [55], which is used for analyzing the photosynthetic activity in the terrestrial surface. NDVI was estimated using red band (B4) and Near infrared band (B5). Whereas NDBI is the Normalized difference built-up index (NDBI), this index allows

emphasizing the impervious surfaces such as bare and built-up land [56]. NDBI was calculated with the Equation (2), using the Shortwave-infrared band (B6) and Near infrared (B5) data of Landsat-8. Finally, the Normalized difference water index (NDWI) provides wetness information, as soil moisture, vegetation, and built-up land [57]. The NSWI was calculated using B3 (green band) and B5 (Near infrared band).

3.3.4. Land Surface Temperature Estimation

LST was estimated using the inversion of Planck's function (Equation (4)). Where, TB is brightness temperature, defined as the temperature of blackbody. TB values come from band 10 coming from Google Earth Engine Landsat collection, λ is wavelength in radiance values, and ρ is a constant value of 14,380.

$$LST = \frac{T_B}{1+\left(\lambda \cdot \frac{T_B}{\rho}\right)\ln\varepsilon} \tag{4}$$

Land surface emissivity (ε) was calculated using the methodology of Sobrino and Raissouni [58], as shown in Equation (5), using the constants predefined according to the sensor (0.986 and 0.0004) and NDVI, NDVImin, NDVImax calculated in previously step.

$$\varepsilon = 0.986 + 0.0004 \cdot \left(\frac{NDVI-NDVImin}{NDVImax-NDVImin}\right)^2 \tag{5}$$

The LST obtained was in Kelvin and it was converted to Celsius by subtracting 273.15. LST images was processed in the GEE platform using the code developed by Ermida, et al. [59] applying the methodology previously described.

3.3.5. Local Solar Zenith Angle

In order to analyze the effect of slope relative to sun position at the moment of satellite pass, LSZA, the angle between the zenith vertical and solar radiation (ranging from 0° to 90°) was calculated. The local LSZA was calculated utilizing Equation (6), which was developed by Dozier and Frew [60].

$$cos\theta = cosZs\ cosS + sinZs\ sinS\ cos(As - A) \tag{6}$$

where Ө is LSZA, Zs and As are the solar zenith angle and azimuth angle, respectively, and A and S are the aspect and slope of terrain, in degrees, obtained from the DEM.

3.3.6. Evaporative Stress Index

Evaporative stress index (ESI) is an ECOSTRESS product, which is a useful tool to analyze drought processes in areas where precipitation data are limited. It is based on evapotranspiration and potential evapotranspiration obtained from satellite thermal bands and some auxiliary products, i.e., vapor pressure data and relative humidity [61]. ESI can range between 0 and 1, where 0 is an area with high hydric stress, while 1 represents an area without hydric stress [39]. Likewise, ECOSTRESS products have a spatial resolution of 70 × 70 m [40] and its products include information for geometric correction and cloud detection [62]. Raster data was downloaded from the LP DAAC platform from US Geological Service (https://lpdaac.usgs.gov) (accessed on 19 August 2020). Images were downloaded for the UMAFOR 1001 polygon; the selected images were those which had the highest number of quality pixels for winter (24 February 2019) and summer (21 June 2019).

3.3.7. Near-Surface Temperature Lapse Rate Estimation

The NSTLR estimation trough the LST-DEM linear regression has a well-known error, which is due of effect of surface characteristics [8,63,64]. To solve this effect the LST obtained from Landsat-8 was normalized relative to biophysical characteristics and solar incidence angle. We used the approach developed for Firozjaei, Fathololoumi, Alavipanah, Kiavarz, Vaezi and Biswas [8], through a normalization of LST relative to the surface biophysical characteristics and the solar incidence angle (Equation (7)).

$$NLST = \mathfrak{f}(NDVI, NDBI, NDWI, LSZA) \tag{7}$$

where NLST is LST modeled based on the surface biophysical characteristics and solar incidence angle, f is non-linear linking model. Random Forest regression method was used to build the non-linear linking model between LST obtained and the

predictors (NDVI, NDBI, NDWI and LSZA). Finally, NSTLR was calculated by a simple linear regression between NLST (dependent variable) and DEM (independent variable), where regression slope represents the NSTLR value [8,33].

The raster layers (NLST, Aspect, LSZA and ESI) were aligned and aggregated to the same spatial context; this process was made with Bicubic interpolation raster algorithm. A database was constructed extracting information for every pixel, these processes were performed using QGIS 3.14 [51]. The NSTLR was analyzed separately to each aspect (i.e., N, NE, E, SE, S, SW, W, NW), while for LSZA, values were divided in different ranges with an interval of 15° (i.e., 0–15°, 15–30°, 30–45°, 45–60°, 60–75°, 75–90°). Likewise, the ESI values were divided into five ranges (i.e., 0–0.2, 0.2–0.4, 0.4–0.6, 0.6–0.8, 0.8–1). We applied linear regressions of NLST against elevation to determine the NSTLR (Equation (8)) for each one of the data ranges analyzed for aspect, slope and ESI (Table 2). The goodness of fit of the 19 fitted linear models was evaluated by the coefficient of determination (R2) and root square mean error (RMSE).

$$NLST = b + m(DEM) \tag{8}$$

where b and m are coefficients of the linear regression between NLST and elevation (DEM); m is the slope value of linear regression, which represents the NSTLR.
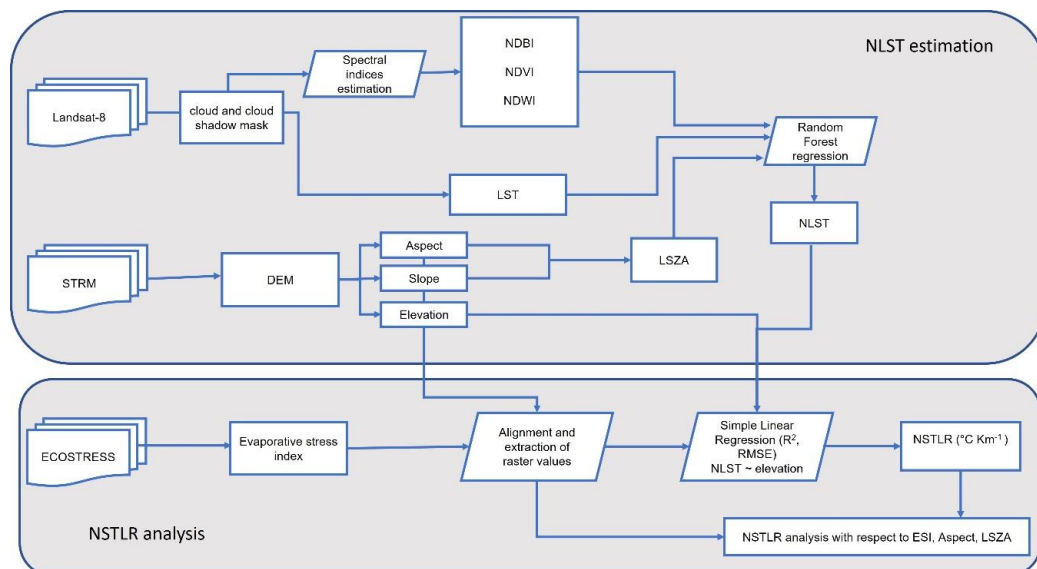
Figure 2. Flow diagram of data analysis.

The accuracy of Random Forest model to normalization LST data were to winter and summer were 0.71 R2 and 0.86 R2, respectively. Meanwhile, the mean winter NLST of the study area ranged between 5.8 and 26.7 °C, with an average value of 17.4 °C. Mean summer LST ranged in the study area between 18.1 and 47.8°C, with an average value of 34.3 °C. ESI values ranged for the study area between 0.03 and 0.7 in winter and be-tween 0.3 and 0.9 in summer (Table 2).

Table 2. Descriptive data of normalized surface temperature in winter and summer (NLSTw and NLSTs), and of evaporative stress index in winter and summer (ESIw and ESIs). Q1 and Q3 are quartiles of the data series.

Parameter	Min	Q1	Mean	Q3	Max
NLSTw (°C)	5.8	14.5	17.4	20.3	26.7
NLSTs (°C)	18.1	29.9	34.3	39.57	47.8
ESIw	0.03	0.2	0.3	0.4	0.7
ESIs	0.3	0.6	0.7	0.8	0.9
Elevation (m)	1587	1897	2,31	2492	3285

NLST maps for winter and summer show the LST distribution in the study area, where the LST decreasing in the zones with highest elevation, while in the lower areas was found higher temperature (Figure 3). Linear regression between LST and elevation for winter had an R2 of 0.74, with a RMSE of 1.9°C; for summer, R2 was 0.81 and RMSE 2.4°C. Linear models showed that elevation influenced LST more in summer. The ob-served dispersion of data from the linear regression in both seasons (Figure 4) suggests that there is a complex relationship where interacting multiple factors, in addition to elevation. The complementary factors which affect the NSTLR can be related to land cover, wetness of soil and amount of solar radiation, caused by slope and angle.
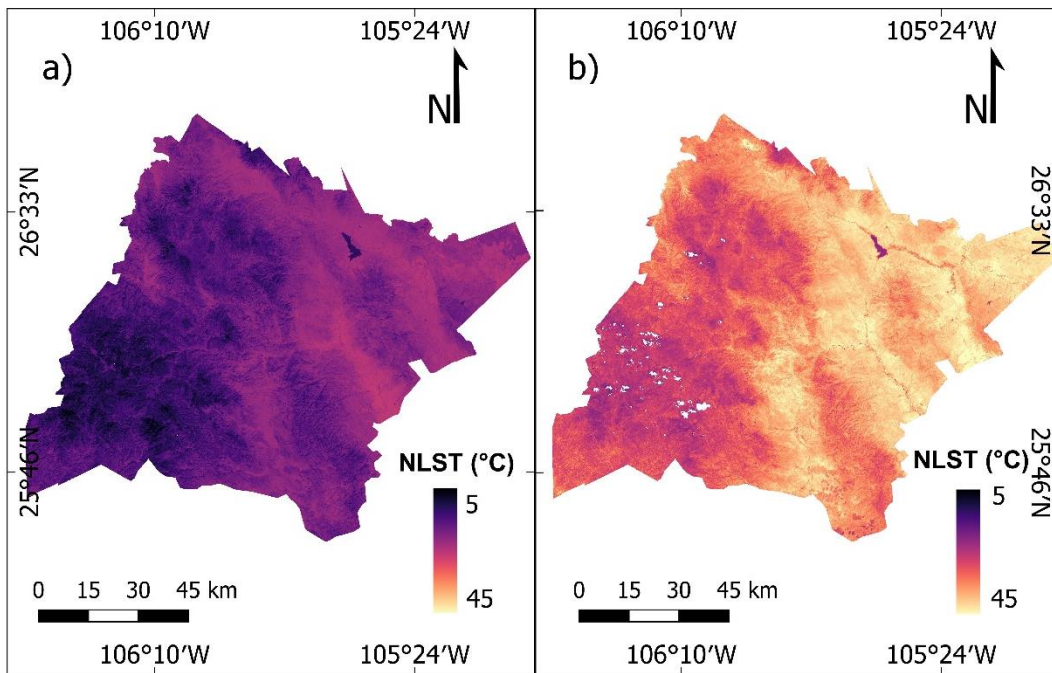
Figure 3. NLST estimated for two seasons of year. a) winter; b) summer
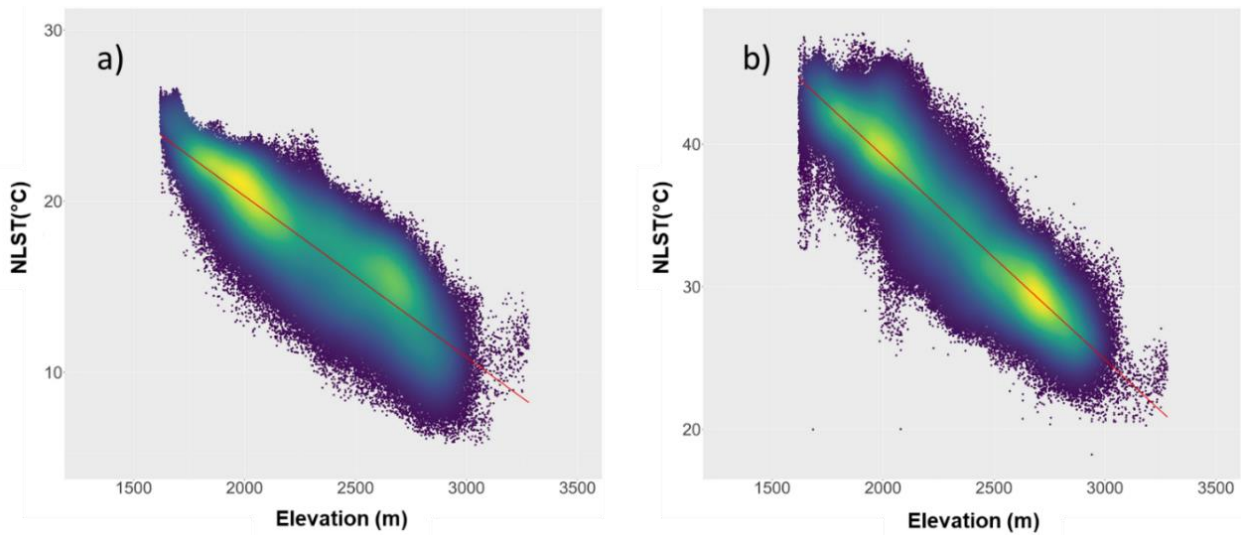
Figure 4. Point density plots of elevation (meters above sea level) against Normalized Land Surface Temperature at two seasons a) winter and b) summer. The red line is the linearly fitted line.

The NSTLR in the areas with different features of aspect, LSZA and ESI, was calculated the DEM-NLST lineal regression model separately and the results is showed in Table 3. The goodness of fit of the 19 fitted linear models shown R2 above 0.5 in almost all variables. However, the differences in R2 values suggest that ESI condition strongly affects the DEM-NLST relationship.

Table 3. Metrics of simple regression models. R^2: coefficient of determination; RMSE: root mean square error; LSZA: Local solar zenith angle; ESI: Evaporative Stress Index. The gaps in the ESI data (-) are shown where there are not data of these ranges in this season of year.

		R^2		RMSE	
		Summer	Winter	Summer	Winter
Aspect	**North**	0.79	0.72	2.47	2.05
	Northeast	0.82	0.76	2.33	1.83
	East	0.81	0.78	2.26	1.64
	Southeast	0.83	0.80	2.26	1.53
	South	0.82	0.82	2.31	1.51
	Southwest	0.83	0.81	2.36	1.63
	West	0.81	0.77	2.42	1.91
	Northwest	0.78	0.71	2.55	2.13
LSZA	**0-15°**	0.80	0.71	2.23	1.48
	15-30°	0.69	0.77	2.55	1.52
	30-45°	0.75	0.81	2.30	1.68
	45-60°	0.81	0.73	2.27	1.81
	60-75°	0.82	0.66	2.44	1.69
	75-90°	0.77	0.63	2.40	1.62
ESI	**0-0.2**	-	0.61	-	1.08
	0.2-0.4	0.35	0.63	2.92	1.66
	0.4-0.6	0.51	0.48	1.63	1.96
	0.6-0.8	0.77	0.59	2.54	1.63
	0.8-1	0.25	-	3.87	-

3.3.8. Temperature Lapse Rate

In our study area, observed NSTLR was 9.4 °C km-1 for winter and 14.3 °C km-1 for summer. Likewise, the NSTLR values was different in the different aspects, in summer range between 14.2 to 15.1 while summer shows NSTLR range between 9.2 to 10.8. The highest NSTLR was found for Northweast aspect and the lowest for Southeast aspect at both seasons of the year (Figure 5).
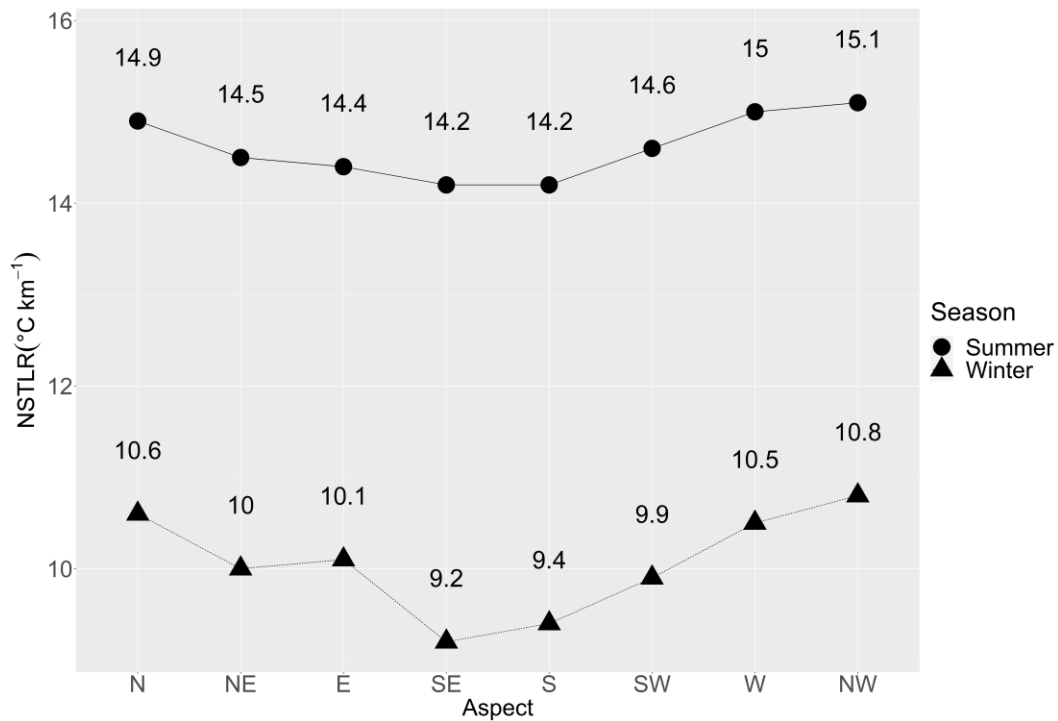
Figure 5. Temperature lapse rate of the two seasons against aspect

We utilized the LSZA equation to quantify the effect of solar position on the terrain slope at acquisition time, since the solar position changes the angle and intensity of the solar energy above the terrain [65,66]. NSTLR decreased with increasing LSZA for both seasons, possibly caused by a less direct impact of sunlight at higher LSZA, with a difference between seasons of more than 5 °C km-1 (Figure 6).
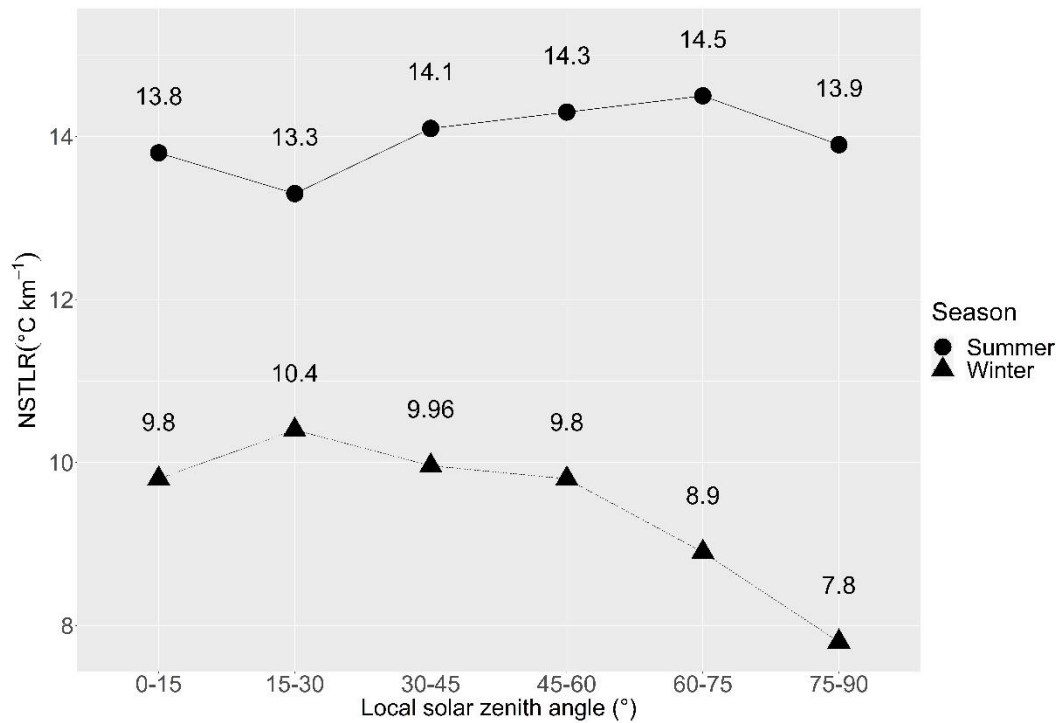
Figure 6. Temperature lapse rate of the two seasons at different Local solar zenith angle

NSTLR against ESI ranges are shown in Figure 7. Observed ESI ranges were 0.2-1 for summer and 0-0.8 for winter (Figure 7). Observed NSTLR in our study was lower in areas with higher ESI for both seasons. These results suggest that areas with the higher water availability have lower thermal gradients and this effect is stronger in summer season.
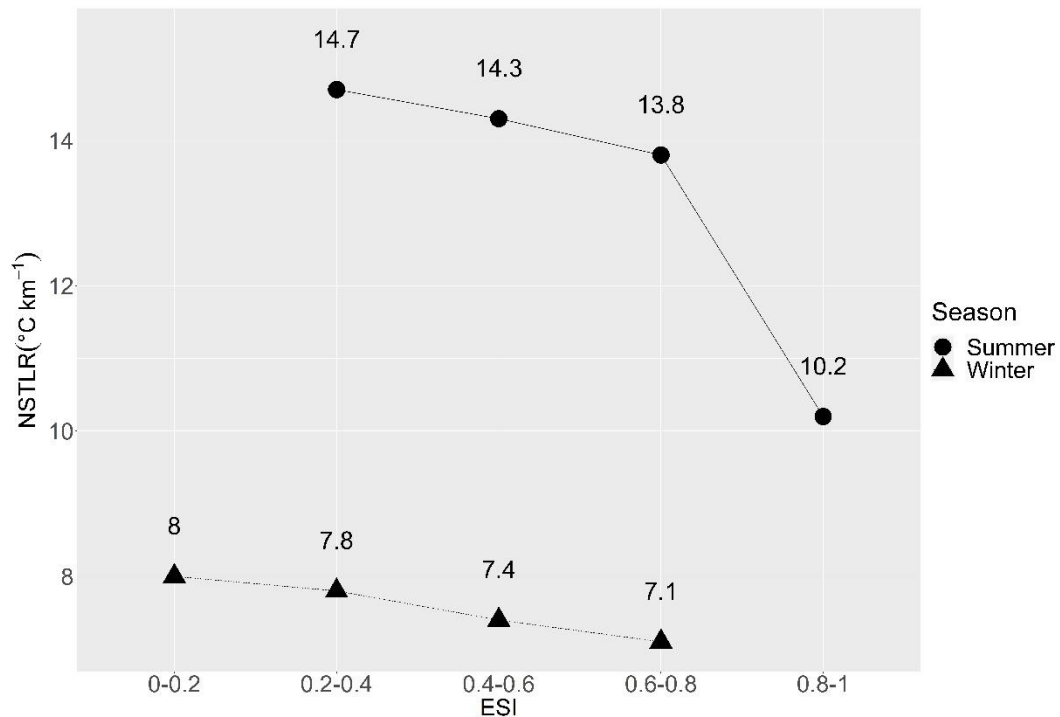
Figure 7. Temperature lapse rate of the two seasons at different ESI ranges.

3.4. Discussion

In areas with a low availability of field weather stations, satellite data can provide an alternative information, capturing a higher degree of variability caused by interactions of climate with topography or evaporative processes, the latter influenced by land cover properties. NSTLR have been shown to have a middle uncertainty when estimated from satellite data, nevertheless the methodology developed by Firozjaei et al. [8] allows estimating NSTLR with more accuracy.

There is a clear difference of NLST between both seasons of year (winter and summer) explained by amount of energy received in summer, that is two times more than in winter [67]. In addition, biophysical and topographical features were key factors to NLST distribution, the effect of these variables seems to be stronger in winter. He at al. [18] noted that NLST was also influenced by aspect, slope, and solar radiation. On the order hand, the relative fine resolution scale of thermal satellite information might be evincing the topographic influences more accurately and cause the dispersion data observed in density plots of elevation-NLST.

The most widely accepted altitudinal NSTLR value is 6.5 °C km−1. This value is given as a function of temperature in a vertical atmospheric column of wet air is frequently accepted as a NSTLR constant in mountainous environments [20,24,68]. This general value does not address the particularities of every study area and might be inexact in some specific locations [69]. For example, Soto Molina and Delgado Granados [70] found NSTLR to vary between locations in their analysis in Nevado de Toluca, Mexico, and consequently suggested that it should be quantified at each location. The seasonal and spatial variation observed in our study supports the importance to analyze NSTLR at a regional and season level. Our observed NSTLR were higher than the values previously reported by several studies [32,42,71]; this could be related to the influence of the land use types analysed on the thermal characteristics of the land Surface. Future studies could focus on analysing NSTLR variations against land use categories [72].

In the present study, the NSTLR was higher in summer, this agrees with higher NSTLR observed in summer in previous studies, such as Tang and Fang [27] study in a mountainous location in China or Navarro-Serrano, López-Moreno, Azorin-Molina, Alonso-González, Tomás-Burguera, Sanmiguel-Vallelado, Revuelto and Vicente-Serrano [71] analysis in the main mountain ranges in Spain. In contrast, Li et al. [73] observed a more marked NSTLR in winter season in Northern China mountain areas. This discrepancy could be related to our study area being dominated by semiarid ecosystems, with pasturelands in the lower slopes. It could also possibly be explained by the precipitation regimes characteristic of the area of study, receiving precipitation in summer season [74], therefore having lower evaporative stress in spite of the high temperatures. On the other hand, lower precipitation in winter resulted in lower water availability for evapotranspiration and a higher hydric stress. Conversely, studies reporting higher NSTLR in winter than in summer are generally associated with mountain ecosystems with higher humidity conditions [24,27,73,75]. These results confirm the utility of accounting for evaporative stress in understanding the seasonal and spatial variations of the thermal gradient.

More specifically, our study reveals the potential of the relatively recent ECOSTRESS sensor to characterize the impact of vegetation evaporative stress on thermal gradients from the Landsat sensor at relatively fine spatial scales. The high variation observed in summer NSTLR across ESI intervals, with a range from wetter areas with lower NSTLR, to areas with higher water stress and with higher NSTLR values, might be related to contrasting interactions of vegetation cover and water stress conditions. Areas with high vegetation cover limit sunlight incidence on terrain surface, cooling surfaces through evapotranspiration, while bare ground areas are associated to high surface temperatures; this might result in high NSTLR, mainly in summer season, where the solar radiation has higher effects [18,26]. While our findings agree with previous studies reporting effects of water availability on LST in environments with altitudinal variability (e.g., [1,27]), such previous analyses were conducted utilizing other water availability variables such as NDVI [1], unlike the ECOSTRESS ESI data utilized here.

The aspect was an important characteristic for the NSTLR values, it had higher values in the Northwest aspect of the two seasons studied (winter and summer). In the north hemisphere, southern and eastern aspects generally present a more homogeneous temperature through the altitudinal gradient. That agrees with, Liu and Li [76] in a study in China mountains where observed a higher NSTLR in North and West aspects, which are opposite to solar radiation direction. Aspect plays a key role in thermal processes in mountain areas; the higher NSTLR observed for N and NW aspects for both seasons might be related to a non-homogeneous heating process in aspects opposed to solar radiation, as opposed to a more homogeneous heating in aspects oriented towards solar radiation (i.e., S and SE) [18]. In the north hemisphere, southern and eastern aspects generally present a more homogeneous temperature through the altitudinal gradient.

Meanwhile, higher NSTLR in the 0–15° LSZA range are very possibly a consequence of a higher solar radiation, which in turns affects moisture conditions [75], which also affects NSTLR (i.e., higher NSTLR under water stress conditions)

(e.g., [77]). This supports the effect of solar angle and slope interactions on the thermal conditions in mountain ecosystems observed by several authors [18,24,69].

These results suggest sensitivity of NLST derived of Landsat-8 thermal information. Besides, ECOSTRESS product, ESI allows to analyze dynamics of vegetation water stress and temperature in our study area across an altitudinal gradient, possibly capturing variations between vegetation types and tree cover characteristics, a point that deserves further analysis. NSTLR analysis can help to understand the altitudinal migration of forest species that has been reported in several locations globally as a consequence of climate change [78,79,80,81]. Detailed NSTLR and ESI maps might aid in identifying fire-prone areas [82,83]. Future studies might explore the inclusion of local relationships of topographic effects on temperature (e.g., [84]) to refine ongoing research of fire risk (e.g., [43,44,85,86,87]) or biomass or tree growth modeling (e.g., [88,89]) in these diverse and complex ecosystems.

3.5. Conclusions

Near-surface temperature lapse rate (NSTLR) is one of the main features to understand climatic dynamics in mountain environments. Our results showed variation in NSTLR, quantified from NLST derived of Landsat-8 surface temperature and environmental variables, by season. Winter and summer NSTLR were different than the global average constant value widely utilized (6.5 °C km−1). NSTLR also varied widely between aspects, with the highest value observed for Northwest aspect in both seasons. In addition, Local solar zenith angle (LSZA) and evapotranspiration also influenced NSTLR regulation. The areas with greater LSZA showed lower NSTLR in both seasons. Evaporative Stress Index (ESI) showed a negative relation with NSTLR values, suggesting a role of water stress in increasing the NSTLR, this being more marked in summer season.

The results from the current study suggest potential of Landsat-8 LST and ECOSTRESS ESI to capture the interactions of topographic factors and vegetative stress on NSTLR gradients at relatively fine spatial scales, which can aid in water

management planning and conservation planning. Further factors, such as vegetation types and tree cover are possibly influencing these water stress-topography-temperature gradient interactions, a point that should be further analyzed in future studies. Furthermore, future studies might focus on a multitemporal analysis of thermal gradients, including further quantifying topography and water stress interactions with vegetation and fuel characteristics, which might be beneficial for enhancing fire risk or tree growth predictions in these complex ecosystems.

3.6. References

1. Bindajam, A.A.; Mallick, J.; AlQadhi, S.; Singh, C.K.; Hang, H.T. Impacts of Vegetation and Topography on Land Surface Temperature Variability over the Semi-Arid Mountain Cities of Saudi Arabia. Atmosphere 2020, 11, 762.
2. Naud, L.; Måsviken, J.; Freire, S.; Angerbjörn, A.; Dalén, L.; Dalerum, F. Altitude effects on spatial components of vascular plant diversity in a subarctic mountain tundra. Ecol. Evol. 2019, 9, 4783–4795.
3. Daw, T.M.; Hicks, C.C.; Brown, K.; Chaigneau, T.; Januchowski-Hartley, F.A.; Cheung, W.W.L.; Rosendo, S.; Crona, B.; Coulthard, S.; Sandbrook, C.; et al. Elasticity in ecosystem services: Exploring the variable relationship between ecosystems and human well-being. Ecol. Soc. 2016, 21.
4. Pastur, G.J.M.; Perera, A.H.; Peterson, U.; Iverson, L.R. Ecosystem Services from Forest Landscapes: An Overview. In Ecosystem Services from Forest Landscapes; Springer: Singapore, 2018; pp. 1–10.
5. Liu, L.; Wang, Z.; Wang, Y.; Zhang, Y.; Shen, J.; Qin, D.; Li, S. Trade-off analyses of multiple mountain ecosystem services along elevation, vegetation cover and precipitation gradients: A case study in the Taihang Mountains. Ecol. Indic. 2019, 103, 94–104.
6. Mengist, W.; Soromessa, T.; Legese, G. Ecosystem services research in mountainous regions: A systematic literature review on current knowledge and research gaps. Sci. Total Environ. 2020, 702, 134581.
7. Spehn, E.M.; Rudmann-Maurer, K.; Körner, C. Mountain biodiversity. Plant Ecol. Divers. 2011, 4, 301–302.
8. Firozjaei, M.K.; Fathololoumi, S.; Alavipanah, S.K.; Kiavarz, M.; Vaezi, A.R.; Biswas, A. A new approach for modeling near surface temperature lapse rate based on normalized land surface temperature data. Remote Sens. Environ. 2020, 242, 111746.
9. Grêt-Regamey, A.; Brunner, S.H.; Kienast, F. Mountain Ecosystem Services: Who Cares? Mt. Res. Dev. 2012, 32, S23–S34.
10. Hagedorn, F.; Mulder, J.; Jandl, R. Mountain soils under a changing climate and land-use. Biogeochemistry 2009, 97, 1–5.
11. Beniston, M. Climatic Change in Mountain Regions: A Review of Possible Impacts. Clim. Chang. 2003, 59, 5–31.

12. Sigdel, S.R.; Zhang, H.; Zhu, H.; Muhammad, S.; Liang, E. Retreating Glacier and Advancing Forest Over the Past 200 Years in the Central Himalayas. J. Geophys. Res. Biogeosci. 2020, 125, 005751.
13. Zeng, Z.; Wang, D.; Yang, L.; Wu, J.; Ziegler, A.D.; Liu, M.; Ciais, P.; Searchinger, T.D.; Yang, Z.-L.; Chen, D.; et al. Deforestation-induced warming over tropical mountain regions regulated by elevation. Nat. Geosci. 2021, 14, 23–29.
14. Sakai, A.; Fujita, K. Contrasting glacier responses to recent climate change in high-mountain Asia. Sci. Rep. 2017, 7, 1–8.
15. Tuladhar, D.; Dewan, A.; Kuhn, M.; Corner, R.J. Spatio-temporal rainfall variability in the Himalayan mountain catchment of the Bagmati River in Nepal. Theor. Appl. Clim. 2019, 139, 599–614.
16. Li, Y.; Zeng, Z.; Zhao, L.; Piao, S. Spatial patterns of climatological temperature lapse rate in mainland China: A multi-time scale investigation. J. Geophys. Res. Atmos. 2015, 120, 2661–2675.
17. Fang, J.-Y.; Yoda, K. Climate and vegetation in China (I). Changes in the altitudinal lapse rate of temperature and distribution of sea level temperature. Ecol. Res. 1988, 3, 37–51.
18. He, J.; Zhao, W.; Li, A.; Wen, F.; Yu, D. The impact of the terrain effect on land surface temperature variation based on Landsat-8 observations in mountainous areas. Int. J. Remote Sens. 2019, 40, 1808–1827.
19. Vuille, M.; Bradley, R.S. Mean annual temperature trends and their vertical structure in the tropical Andes. Geophys. Res. Lett. 2000, 27, 3885–3888.
20. Barry, R.G.; Richard, J.C. Atmosphere, Weather and Climate, 1st ed.; Taylor & Francis Group: London, UK, 2009.
21. Kattel, D.B.; Yao, T.; Panday, P.K. Near-surface air temperature lapse rate in a humid mountainous terrain on the southern slopes of the eastern Himalayas. Theor. Appl. Clim. 2018, 132, 1129–1141.
22. Guo, X.; Wang, L.; Tian, L. Spatio-temporal variability of vertical gradients of major meteorological observations around the Tibetan Plateau. Int. J. Clim. 2016, 36, 1901–1916.
23. Harlow, R.C.; Burke, E.J.; Scott, R.; Shuttleworth, W.J.; Brown, C.M.; Petti, J.R. Research Note:Derivation of temperature lapse rates in semi-arid south-eastern Arizona. Hydrol. Earth Syst. Sci. 2004, 8, 1179–1185.
24. Minder, J.R.; Mote, P.W.; Lundquist, J.D. Surface temperature lapse rates over complex terrain: Lessons from the Cascade Mountains. J. Geophys. Res. Space Phys. 2010, 115, 115.
25. Hais, M.; Kučera, T. The influence of topography on the forest surface temperature retrieved from Landsat TM, ETM+ and ASTER thermal channels. ISPRS J. Photogramm. Remote Sens. 2009, 64, 585–591.
26. Firozjaei, M.K.; Fathololuomi, S.; Alavipanah, S.K.; Kiavarz, M.; Vaezi, A.; Biswas, A.; Ghorbani, A. Modeling the impact of surface characteristics on the near surface temperature lapse rate. Int. Arch. Photogramm. Remote Sens. Spat. Inf. Sci. 2019, XLII-4/W18, 395–399.

27. Tang, Z.; Fang, J. Temperature variation along the northern and southern slopes of Mt. Taibai, China. Agric. For. Meteorol. 2006, 139, 200–207. [Google Scholar] [CrossRef]
28. Veh, G.; Korup, O.; Walz, A. Hazard from Himalayan glacier lake outburst floods. Proc. Natl. Acad. Sci. USA 2020, 117, 907–912.
29. Muradyan, V.; Tepanosyan, G.; Asmaryan, S.; Saghatelyan, A.; Dell'Acqua, F. Relationships between NDVI and climatic factors in mountain ecosystems: A case study of Armenia. Remote Sens. Appl. Soc. Environ. 2019, 14, 158–169.
30. García-Santos, V.; Cuxart, J.; Martínez-Villagrasa, D.; Jiménez, M.A.; Simó, G. Comparison of Three Methods for Estimating Land Surface Temperature from Landsat 8-TIRS Sensor Data. Remote Sens. 2018, 10, 1450.
31. Jain, S.K.; Goswami, A.; Saraf, A.K. Determination of land surface temperature and its lapse rate in the Satluj River basin using NOAA data. Int. J. Remote Sens. 2008, 29, 3091–3103.
32. Wang, Y.; Wang, L.; Li, X.; Chen, D. Temporal and spatial changes in estimated near-surface air temperature lapse rates on Tibetan Plateau. Int. J. Clim. 2018, 38, 2907–2921.
33. Zhang, H.; Zhang, F.; Zhang, G.; Che, T.; Yan, W. How Accurately Can the Air Temperature Lapse Rate Over the Tibetan Plateau Be Estimated from MODIS LSTs? J. Geophys. Res. Atmos. 2018, 123, 3943–3960.
34. Peters, J.; Van Doninck, J.; Verhoest, N.E.C.; De Baets, B.; De Clercq, E.M.; Ducheyne, E. Influence of topographic normalization on the vegetation index–surface temperature relationship. J. Appl. Remote Sens. 2012, 6, 063518.
35. Qin, Y.; Ren, G.; Zhai, T.; Zhang, P.; Wen, K. A New Methodology for Estimating the Surface Temperature Lapse Rate Based on Grid Data and Its Application in China. Remote Sens. 2018, 10, 1617.
36. Penton, D.J.; Neumann, L.E.; Karki, R.; Nepal, S. Verifying Temperature Lapse Rates in the Eastern Himalayas using Landsat 7 and 8. In Proceedings of the 21st International Congress on Modelling and Simulation, Gold Coast, Australia, 29 Novembe–4 December 2015.
37. Zhuang, Y.; Liu, X.; Nguyen, T.; He, Q.; Hong, S. Global remote sensing research trends during 1991–2010: A bibliometric analysis. Science 2013, 96, 203–219.
38. Martinez-Gracia, A.; Arauzo, I.; Uche, J. Chapter 5-Solar energy availability. In Solar Hydrogen Production; Calise, F., D'Accadia, M.D., Santarelli, M., Lanzini, A., Ferrero, D., Eds.; Elsevier: Amsterdam, The Netherlands, 2019; pp. 113–149.
39. Anderson, M.C.; Hain, C.R.; Wardlow, B.; Pimstein, A.; Mecikalski, J.R.; Kustas, W.P. Evaluation of Drought Indices Based on Thermal Remote Sensing of Evapotranspiration over the Continental United States. J. Clim. 2011, 24, 2025–2044.
40. Fisher, J.B.; Lee, B.; Purdy, A.J.; Halverson, G.H.; Dohlen, M.B.; Cawse-Nicholson, K.; Wang, A.; Anderson, R.G.; Aragon, B.; Arain, M.A.; et al. ECOSTRESS: NASA's Next Generation Mission to Measure Evapotranspiration From the International Space Station. Water Resour. Res. 2020, 56, e2019WR026058.

41. Liu, N.; Oishi, A.C.; Miniat, C.F.; Bolstad, P. An evaluation of ECOSTRESS products of a temperate montane humid forest in a complex terrain environment. Remote Sens. Environ. 2021, 265, 112662.
42. Moradi, M.; Salahi, B.; Masoodian, S.A. On the relationship between MODIS Land Surface Temperature and topography in Iran. Phys. Geogr. 2018, 39, 354–367.
43. Briones-Herrera, C.I.; Vega-Nieva, D.J.; Monjarás-Vega, N.A.; Flores-Medina, F.; Lopez-Serrano, P.M.; Corral-Rivas, J.J.; Carrillo-Parra, A.; Pulgarin-Gámiz, M.Á.; Alvarado-Celestino, E.; González-Cabán, A.; et al. Modeling and Mapping Forest Fire Occurrence from Aboveground Carbon Density in Mexico. Forests 2019, 10, 402.
44. Monjarás-Vega, N.A.; Briones-Herrera, C.I.; Vega-Nieva, D.J.; Calleros-Flores, E.; Corral-Rivas, J.J.; López-Serrano, P.M.; Pompa-García, M.; Rodríguez-Trejo, D.A.; Carrillo-Parra, A.; González-Cabán, A.; et al. Predicting forest fire kernel density at multiple scales with geographically weighted regression in Mexico. Sci. Total Environ. 2020, 718, 137313.
45. Aragón-Piña, E.E.; Garza-Herrera, A.; González-Elizondo, M.S.; Luna-Vega, I. Composición y estructura de las comunidades vegetales del rancho El Durangueño, en la Sierra Madre Occidental, Durango, México. Rev. Mex. Biodivers. 2010, 81, 771–787.
46. González-Elizondo, M.S.; González-Elizondo, M.; Tena-Flores, J.A.; Ruacho-González, L.; López-Enríquez, I.L. Vegetación de la Sierra Madre Occidental, México: Una síntesis. Acta Botánica Mex. 2012, 100, 351–403.
47. Hernandez-Díaz, J.C.; Prieto-Ruiz, J.A. Estudio Regional Forestal Caso UMAFOR 1001; Secretaría de Medio Ambiente y Recursos Naturales (SEMARNAT): Durango, Mexico, 2007.
48. Wehenkel, C.; Reyes-Martínez, A.; Martínez-Guerrero, J.H.; Pinedo-Alvarez, C.; Lopez-Sanchez, C.A. The bird species diversity in the wintering season is negatively associated with precipitation, tree species diversity and stand density in the Sierra Madre Occidental, Durango, Mexico. Community Ecol. 2017, 18, 63–71.
49. Silva-Flores, R.; Pérez-Verdín, G.; Wehenkel, C. Patterns of Tree Species Diversity in Relation to Climatic Factors on the Sierra Madre Occidental, Mexico. PLoS ONE 2014, 9, e105034.
50. INEGI. Conjunto de Datos Vectoriales de Uso del Suelo y Vegetación Escala 1:250,000, Series VI. Available online: http://www.conabio.gob.mx/informacion/metadata/gis/usv250s6gw.xml?_httpcache=yes&_xsl=/db/metadata/xsl/fgdc_html.xsl&_indent=no (accessed on 5 October 2021).
51. QGIS Development Team. QGIS Geographic Information System. Open Source Geospatial Foundation Project. 2016. Available online: http://qgis.osgeo.org (accessed on 22 November 2020).
52. Gorelick, N.; Hancher, M.; Dixon, M.; Ilyushchenko, S.; Thau, D.; Moore, R. Google Earth Engine: Planetary-scale geospatial analysis for everyone. Remote Sens. Environ. 2017, 202, 18–27.

53. Parastatidis, D.; Mitraka, Z.; Chrysoulakis, N.; Abrams, M. Online Global Land Surface Temperature Estimation from Landsat. Remote Sens. 2017, 9, 1208.
54. Dewan, A.; Kiselev, G.; Botje, D. Diurnal and seasonal trends and associated determinants of surface urban heat islands in large Bangladesh cities. Appl. Geogr. 2021, 135, 102533.
55. Rouse, J.W.; Haas, R.H.; Schell, J.A.; Deering, D.W. Monitoring vegetation systems in the great plains with ERTS. NASA Spec. Publ. 1973, 351, 309–317. [Google Scholar]
56. Zha, Y.; Gao, J.; Ni, S. Use of normalized difference built-up index in automatically mapping urban areas from TM imagery. Int. J. Remote Sens. 2003, 24, 583–594.
57. Gao, B.-C. NDWI—A normalized difference water index for remote sensing of vegetation liquid water from space. Remote Sens. Environ. 1996, 58, 257–266.
58. Sobrino, J.A.; Raissouni, N. Toward remote sensing methods for land cover dynamic monitoring: Application to Morocco. Int. J. Remote Sens. 2000, 21, 353–366.
59. Ermida, S.L.; Soares, P.; Mantas, V.; Göttsche, F.-M.; Trigo, I.F. Google Earth Engine Open-Source Code for Land Surface Temperature Estimation from the Landsat Series. Remote Sens. 2020, 12, 1471.
60. Dozier, J.; Frew, J. Rapid calculation of terrain parameters for radiation modeling from digital elevation data. IEEE Trans. Geosci. Remote Sens. 1990, 28, 963–969.
61. Nguyen, H.; Wheeler, M.C.; A Otkin, J.; Cowan, T.; Frost, A.J.; Stone, R.C. Using the evaporative stress index to monitor flash drought in Australia. Environ. Res. Lett. 2019, 14, 064016.
62. Fisher, J.B. Level-4 Evaporative Stress Index L4(ESI_PT-JPL) Algorithm Theoretical Basis Document; JPL: Pasadena, CA, USA, 2018; p. 13.
63. Hutengs, C.; Vohland, M. Downscaling land surface temperatures at regional scales with random forest regression. Remote Sens. Environ. 2016, 178, 127–141.
64. Sismanidis, P.; Keramitsoglou, I.; Bechtel, B.; Kiranoudis, C.T. Improving the Downscaling of Diurnal Land Surface Temperatures Using the Annual Cycle Parameters as Disaggregation Kernels. Remote Sens. 2016, 9, 23.
65. Bennie, J.; Hill, M.O.; Baxter, R.; Huntley, B. Influence of slope and aspect on long-term vegetation change in British chalk grasslands. J. Ecol. 2006, 94, 355–368.
66. Weiss, D.J.; Walsh, S.J. Remote Sensing of Mountain Environments. Geogr. Compass 2008, 3, 1–21.
67. Fu, P.; Rich, P.M. A geometric solar radiation model with applications in agriculture and forestry. Comput. Electron. Agric. 2002, 37, 25–35.
68. Maurer, E.P.; Wood, A.W.; Adam, J.C.; Lettenmaier, D.P.; Nijssen, B. A Long-Term Hydrologically Based Dataset of Land Surface Fluxes and States for the Conterminous United States. J. Clim. 2002, 15, 3237–3251.
69. Córdova, M.; Célleri, R.; Shellito, C.J.; Orellana-Alvear, J.; Abril, A.; Carrillo-Rojas, G. Near-Surface Air Temperature Lapse Rate Over Complex Terrain in

the Southern Ecuadorian Andes: Implications for Temperature Mapping. Arct. Antarct. Alp. Res. 2016, 48, 673–684.

70. Molina, V.H.S.; Granados, H.D. Estimación de la temperatura del aire en la alta montaña mexicana mediante un modelo de elevación del terreno: Caso del volcán Nevado de Toluca (México)/Estimation of the air temperature in the Mexican high mountain environment by means of a model of elevation of the terrain, case of the Nevado de Toluca volcano (Mexico). Ería 2020, 2, 167–182.

71. Navarro-Serrano, F.; Lopez-Moreno, I.; Azorin-Molina, C.; González, E.A.; Tomás-Burguera, M.; Sanmiguel-Vallelado, A.; Revuelto, J.; Vicente-Serrano, S.M. Estimation of near-surface air temperature lapse rates over continental Spain and its mountain areas. Int. J. Clim. 2018, 38, 3233–3249.

72. Rolland, C. Spatial and Seasonal Variations of Air Temperature Lapse Rates in Alpine Regions. J. Clim. 2003, 16, 1032–1046.

73. Li, X.; Wang, L.; Chen, D.; Yang, K.; Xue, B.; Sun, L. Near-surface air temperature lapse rates in the mainland China during 1962–2011. J. Geophys. Res. Atmos. 2013, 118, 7505–7515.

74. Echeverría, C.; Huber, A.; Taberlet, F. Estudio comparativo de los componentes del balance hídrico en un bosque nativo y una pradera en el sur de Chile. Bosque (Valdivia) 2007, 28, 271–280.

75. Blandford, T.R.; Humes, K.S.; Harshburger, B.J.; Moore, B.C.; Walden, V.P.; Ye, H. Seasonal and Synoptic Variations in Near-Surface Air Temperature Lapse Rates in a Mountainous Basin. J. Appl. Meteorol. Clim. 2008, 47, 249–261.

76. Liu, Y.; Li, F. A preliminary approach on the land surface temperature (LST) lapse rate of mountain area using MODIS data. In Proceedings of the Remote Sensing and Space Technology for Multidisciplinary Research and Applications, Beijing, China, 19 May 2006; Volume 6199, p. 619907.

77. Kattel, D.B.; Yao, T.; Yang, K.; Tian, L.; Yang, G.; Joswiak, D. Temperature lapse rate in complex mountain terrain on the southern slope of the central Himalayas. Theor. Appl. Clim. 2013, 113, 671–682

78. Joshi, R.; Sambhav, K. Near Surface Temperature Lapse Rate for Treeline Environment in Western Himalaya and Possible Impacts on Ecotone Vegetation; ResearchGate: Berlin, Germany, 2018.

79. Lute, A.C.; Abatzoglou, J.T. Best practices for estimating near-surface air temperature lapse rates. Int. J. Clim. 2021, 41, E110–E125.

80. Gheyret, G.; Mohammat, A.; Tang, Z.-Y. Elevational patterns of temperature and humidity in the middle Tianshan Mountain area in Central Asia. J. Mt. Sci. 2020, 17, 397–409.

81. Kidane, Y.O.; Steinbauer, M.J.; Beierkuhnlein, C. Dead end for endemic plant species? A biodiversity hotspot under pressure. Glob. Ecol. Conserv. 2019, 19, e00670.

82. Holden, Z.A.; Jolly, W.M.; Swanson, A.; Warren, D.A.; Jencso, K.; Maneta, M.; Burgard, M.; Gibson, C.; Hoylman, Z.; Landguth, E.L. TOPOFIRE: A Topographically Resolved Wildfire Danger and Drought Monitoring System for

the Conterminous United States. Bull. Am. Meteorol. Soc. 2019, 100, 1607–1613.

83. Havel, A.; Tasdighi, A.; Arabi, M. Assessing the hydrologic response to wildfires in mountainous regions. Hydrol. Earth Syst. Sci. 2018, 22, 2527–2550.

84. Holden, Z.A.; Jolly, W.M. Modeling topographic influences on fuel moisture and fire danger in complex terrain to improve wildland fire management decision support. For. Ecol. Manag. 2011, 262, 2133–2141.

85. Flores-Medina, F.; Vega Nieva, D.J.; Monjarás-Vega, N.; Briones-Herrera, C.I.; Corral-Rivas, J.J. Mapping fuel loads and fire behavior from Sentinel in Durango, NW Mexico. In Proceedings of the 6th International Fire Behavior and Fuels Conference, Albuquerque, NM, USA, 29 April–3 May 2019.

86. Vega-Nieva, D.J.; Briseño-Reyes, J.; Nava-Miranda, M.G.; Calleros-Flores, E.; López-Serrano, P.M.; Corral-Rivas, J.J.; Montiel-Antuna, E.; Cruz-López, M.I.; Cuahutle, M.; Ressl, R.; et al. Developing Models to Predict the Number of Fire Hotspots from an Accumulated Fuel Dryness Index by Vegetation Type and Region in Mexico. Forests 2018, 9, 190.

87. Vega-Nieva, D.J.; Nava-Miranda, M.G.; Calleros-Flores, E.; López-Serrano, P.M.; Briseño-Reyes, J.; López-Sánchez, C.; Corral-Rivas, J.J.; Montiel-Antuna, E.; Cruz-Lopez, M.I.; Ressl, R.; et al. Temporal patterns of active fire density and its relationship with a satellite fuel greenness index by vegetation type and region in Mexico during 2003–2014. Fire Ecol. 2019, 15, 28.

88. Briseño-Reyes, J.; Corral-Rivas, J.J.; Solis-Moreno, R.; Padilla-Martínez, J.R.; Vega-Nieva, D.J.; López-Serrano, P.M.; Vargas-Larreta, B.; Diéguez-Aranda, U.; Quiñonez-Barraza, G.; López-Sánchez, C.A. Individual Tree Diameter and Height Growth Models for 30 Tree Species in Mixed-Species and Uneven-Aged Forests of Mexico. Forests 2020, 11, 429.

89. López-Serrano, P.M.; Cárdenas-Domínguez, J.L.; Corral-Rivas, J.J.; Jiménez, E.; López-Sánchez, C.A.; Vega-Nieva, D.J. Modeling of Aboveground Biomass with Landsat 8 OLI and Machine Learning in Temperate Forests. Forests 2019, 11, 11.

CAPÍTULO 4 ESTIMATING ABOVE-GROUND BIOMASS FROM LAND SURFACE TEMPERA-TURE AND EVAPOTRANSPIRATION DATA AT THE TEMPERATE FORESTS OF DURANGO, MEXICO

Marcela Rosas-Chavoya, Pablito Marcelo López-Serrano, Daniel José Vega-Nieva, José Ciro Hernández-Díaz, Christian Wehenkel, José Javier Corral-Rivas.

4.1. Abstract

The study of above-ground biomass (AGB) is important for monitoring the dynamics of the carbon cycle in forest ecosystems. The emergence of remote sensing has made it possible to analyze vegetation using land surface temperature (LST), Vegetation Temperature Condition Index (VTCI) and evapotranspiration (ET) information. However, relatively few studies have evaluated the ability of these variables to estimate AGB in temperate forests. The aim of the present study was to evaluate the relationship of LST, VTCI and ET with AGB in temperate forests of Durango, Mexico, regarding each season of the year and to develop a AGB estimation model using as predictors LST, VCTI and ET, together with topographic, reflectance and Gray-Level Co-Occurrence Matrix (GLCM) texture variables. A semi-parametric model was generated to analyze the linear and non-linear responses of the predictive variables of AGB using a generalized linear model (GAM). The results show that the best predictors of AGB were longitude, latitude, spring LST, ET, elevation VTCI, NDVI (Normalized Difference Vegetation Index), slope and GLCM mean (R^2 = 0.61; RMSE = 28.33 Mg ha^{-1}). The developed GAM model was evaluated with an independent dataset (R^2 = 0.58; RMSE = 31.21 Mg ha^{-1}), suggesting the potential of this modeling approach to predict AGB for the analyzed temperate forest ecosystems.

Keywords: AGB; surface temperature; Vegetation Temperature Condition Index; evapotranspiration

4.2. Introduction

The study of forest biomass is crucial for monitoring the carbon dynamics of terrestrial ecosystems, which are relevant data in the climate change context [1]. Biomass estimation and monitoring allow the reserves and carbon capture rates of

forest ecosystems to be quantified [2]. According to the Intergovernmental Panel on Climate Change (IPCC) United Nation Programme, carbon reserves in forest ecosystems are mainly found in the following places: above-ground biomass (AGB), below ground biomass, forest litter layer, woody debris and organic matter in soil [3,4].

AGB accounts for about 70% of the forest biomass and constitutes 30% of the carbon reserves in terrestrial ecosystems [5]. AGB is a central criterion for programs seeking climate change solutions, such as Reducing Emissions from Reforestation and Forest Degradation (REDD+) United Nations Programme, and carbon trading [5,6,7]. Direct methods to estimate AGB are based on field measurements, sometimes requiring destructive methods to determine the biomass of each subject, as well as the amount of carbon in a sample of trees, and lastly, generating mathematical models or allometric equations, which allow indirect estimation, i.e., from dasometric measurements [8]. These data are fundamental for monitoring forest resources; however, they are highly expensive and require significant human effort.

Given this problem, the use of satellite technologies has been proposed, specifically remote sensors for AGB's indirect estimation. These have several benefits, including: (1) cost reduction, (2) data generation in difficult access areas, (3) data capture on a regional scale, (4) availability of historical data with consistent characteristics (i.e., periodic sampling, same schedule, same area) and (5) data capture from spectral bands beyond the visible spectrum [9]. Combining in situ measurement data with satellite data allows spatial and temporal expansion of AGB in forest ecosystems [10].

Multispectral data allow for the estimation of vegetation indices, important variables for analyzing photosynthetic activity and forest canopy structure [11,12]. Several studies have tried to estimate AGB from this type of data [6,9,10,13,14,15]. For example, López-Serrano et al. [10] used Normalized difference vegetation index (NDVI), Soil-adjusted vegetation index (SAVI), texture metrics of Gray-Level Co-

Occurrence Matrix (GLCM) and topographic and climatic data to estimate AGB with SVM in temperate forests.

In addition, the land surface temperature (LST) is a variable that can be estimated from satellite images, with thermal infrared band data, which provides spectral information on the energy exchange between solar radiation and the surface [16,17]. For example, Leeuwen et al. [17] evaluated the use of LST data to monitor deforestation processes in tropical forests in Brazil and concluded that LST data allow distinguishing between wooded and deforested areas, as well as quantifying deforestation.

One of the most important aspects of the LST-vegetation relationship are the seasonal changes [17]. Pongratz et al. [18] observed that the LST increases in areas with less forest cover, especially in dry seasons, compared to denser forests. A few studies have evaluated the use of LST for estimating AGB [19]. For example, Jiang et al. [1] evaluated the LST potential to improve AGB predictions in Chinese coniferous forests. They concluded that incorporating LST data into nonlinear models improves the AGB estimation efficiency. These studies are, nevertheless, still relatively scarce. For example, in the literature review of landsat LST applications for forest resources monitoring by Rosas-Chavoya et al. [19], only one out the 155 reviewed studies in the period 1995–2020 used LST to map forest biomass.

On the other hand, evapotranspiration (ET) is deemed as a variable closely related to carbon fluxes and biomass incorporation into forest ecosystems [20,21,22]. The Moderate Resolution Imaging Spectroradiometer (MODIS) instrument delivers the ET-8 day product, which provides data on 8-day accumulated evapotranspiration (kg m−2). In addition, one factor faced by forest ecosystems is drought stress, which occurs when potential evapotranspiration is greater than actual evapotranspiration [23]. The Vegetation Temperature Condition Index (VTCI) has been used as an indicator of drought and vegetation water stress [24]. Although these environmental factors are determining criteria for forest ecosystems, an evaluation of their efficiency for AGB estimation is required.

The relationship between environmental variables and AGB is usually complex, so an algorithm that captures these non-linear relationships between the dependent variable (AGB) and the predictor variables is required. Generalized Additive Models (GAMs) can describe complex relationships between AGB and environmental predictor variables. That is why they are deemed suitable for research in forest areas [25,26].

The aim of this paper herein was to evaluate the relationship of satellite information (LST, VTCI and ET, at different seasons) with AGB in temperate forests of Durango, Mexico. It is also aimed at generating a model in which LST and some associated variables, such as LST, VCTI and ET, together with topographic, reflectance and texture variables, for the estimation of observed AGB from field data from Permanent Forest and Soil Research Sites (SPIFyS) in temperate forests of Durango, Mexico. This was based on the following hypotheses: (1) The AGB relationship is different according to climatic conditions of each season of the year: (2) LST, VCTI and ET, together with topographic, reflectance and texture variables, could potentially be used as AGB predictors.

4.3. Materials and Methods

This study was conducted in temperate forests of the state of Durango, Mexico (Figure 1), which covers approximately 4.9 million hectares. These forests grow in the region named Sierra Madre Occidental; they show a wide tree diversity, predominating the Pinus and Quercus. Their elevation gradient goes from 363 and 3190 m. The climate is temperate humid with summer rains; average annual temperature ranges from 8.2 to 26.2 °C, while the average annual precipitation ranges from 443 to 1452 mm [27].
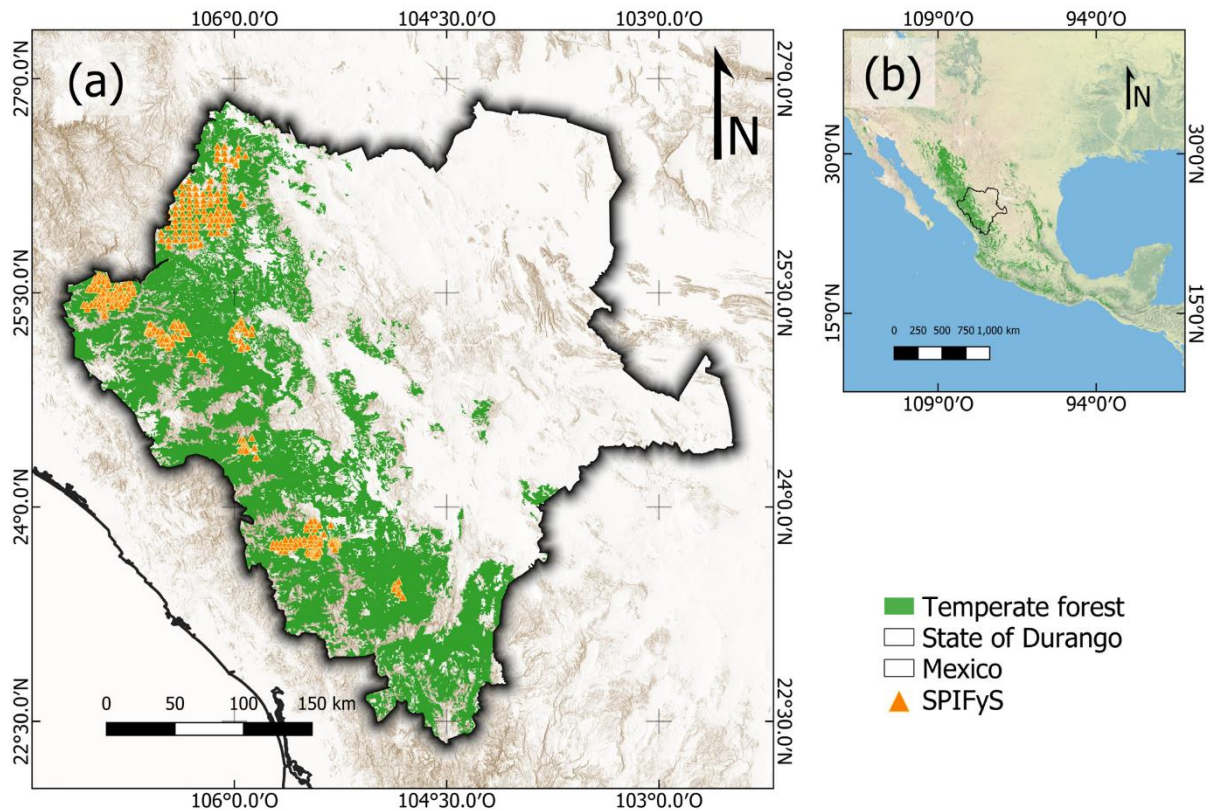
Figure 1. Study area. Permanent forest and soil research sites (SPIFyS in Spanish). Temperate forest polygon taken from Land-Used Map Series VI, which was developed by the Instituto Nacional de Estadística y Geografía (INEGI).

4.3.1. Field data

The AGB field data correspond to 318 SPIFyS, which were settled in 2011 and have been sampled periodically (every 5 years). These are part of one of the most consistent databases on growth, production and evolution of forest stands in Mexico [28]. SPIFyS have a dimension of 50 × 50 m. At each plot, direct dasometric measurements were made, i.e., diameter at breast height, height and wood density. AGB (Mg ha−1) was subsequently calculated using allometric formulas previously developed by Vargas-Larreta et al. [29]. Data used in this study resulted from a sampling in winter 2017 (Table 1).

Table 1. Descriptive statistics of AGB field data from Durango temperate forests.

Plot number	Range (Mg ha^{-1})	Range (Mg ha^{-1})	Range (Mg ha^{-1})	Coefficient of Variation (%)
318	2.05–92.34	31.03	18.14	0.58

4.3.2. Image Acquisition

Landsat 8 satellite (OLI-TIRS) data were downloaded from the USGS Earth Resources Observation and Science (EROS) Center Science Processing Architecture (ESPA) platform, which allows requests for satellite products with different characteristics (i.e., radiometric correction, reference system, pixel size, file format) [30]. Bands 5 and 4 with SR correction were requested, and band 10 with brightness temperature data. Images from scenes 30/43, 30/44, 31/42, 31/43, 31/44, 32/42, 32/43 were selected for the four seasons of the year (Table 2). The selection criterion was the presence of less than 20% cloud cover.

Table 2. Path/Row and acquisition dates of utilized images for Landsat 8

Row/Path	Acquisition date			
	Winter	Spring	Summer	Autumn
30/43	04/Feb/2017	27/May/2017	30/Jul/2017	19/Nov/2017
30/44	04/Feb/2017	11/May/2017	30/Jul/2017	19/Nov/2017
31/42	11/Feb/2017	02/May/2017	22/Aug/2017	26/Nov/2017
31/43	11/Feb/2017	02/May/2017	22/Aug/2017	26/Nov/2017
31/44	11/Feb/2017	02/May/2017	06/Aug/2017	26/Nov/2017
32/42	02/Feb/2017	09/May/2017	29/Aug/2017	17/Nov/2017
32/43	02/Feb/2017	09/May/2017	29/Aug/2017	17/Nov/2017

Similarly, evapotranspiration data was obtained from the MODIS product "MODIS/Terra Net Evapotranspiration 8-Day V.6" [30], which has a resolution of 500 m and provides data on 8-day accumulated evapotranspiration (kg m^{-2}) (Table 3).

Table 3. Path/Row and acquisition dates of utilized images for Evapotranspiration of MODIS

	Acquisition start and end dates			
Row/Path	Winter	Spring	Summer	Autumn
MYD16A2 8/6	10/02/2017-17/02/2017	2017/05/17-2017/05/24	2017/08/21-2017/08/28	17/11/2017-24/11/2017

Lastly, a cloud and cloud shadow masking approach with Landsat and MODIS quality bands was used in order to remove pixels that could be affected by weather conditions. This is a necessary process to ensure reliability of satellite products [31,32].

4.3.3. Estimation of Land Surface Temperature (LST)

LST was estimated using Planck's formula (Equation 1), where TB is the brightness temperature of Landsat 8 TIRS band 10; λ is the wavelength of radiance values, ρ is a constant value of 14,380 for this sensor and Ɛ is the surface emissivity of each pixel. Lastly, LST values obtained in the Kelvin scale were converted to Celsius, subtracting 273.15. The process was conducted in the QGIS 3.16.15 raster calculator [33,34].

$$TS = (\frac{T_B}{1+\left(\lambda \text{ x} \frac{T_B}{\rho}\right)ln\varepsilon} - 273.15)$$ (1)

Surface emissivity (Ɛ) was calculated with the equation developed by Sobrino et al. [35] (Equation 2), which uses the predefined constants for the sensor of 0.986 and 0.0004, as well as the NDVI per pixel, NDVImin and NDVImax (maximum and minimum NDVI present within the study area).

$$\varepsilon=0.986 + 0.0004 \ x \ \left(\frac{NDVI-NDVImin}{NDVImax-NDVImin}\right)^2$$ (2)

4.3.4. Spectral indices

The Soil-Adjusted Vegetation Index (SAVI) is used to identify areas where vegetation cover is low. The SAVI is calculated as a ratio between the red band (R),

near-infrared band (NIR) values with a soil brightness correction factor (L). For the Landsat 8, this factor is a constant value of 0.5 (Equation 3).

$$SAVI = \left(\frac{NIR-R}{NIR+R+L}\right) * (1+L) \qquad (3)$$

The Normalized Difference Vegetation Index (NDVI) developed by Rouse et al. [36] is a measure of photosynthetic activity and vegetation vigor. It was estimated using the red band (R) and near-infrared band (NIR) of the Landsat 8 OLI sensor (Equation 4).

$$NDVI = \frac{R-NIR}{R+NIR} \qquad (4)$$

The Vegetation Temperature Condition Index (VTCI) was subsequently estimated. This index has been used to monitor the spatial distribution of drought conditions. It was developed by Wang et al. [24]. VTCI is calculated based on equations 5 – 7, where LSTmax and LSTmin are the maximum and minimum LST values for pixels with the same NDVI value; a, b, a' and b' are the coefficients of a linear regression between the maximum and minimum NDVI values with respect to LST.

$$VTCI = \frac{LST_{max}(NDVI_i)-LST(NDVI_i)}{LST_{max}(NDVI_i)-LST_{min}(NDVI_i)} \qquad (5)$$

$$LST_{max}(NDVI_i) = a + b(NDVI_i) \qquad (6)$$

$$LST_{min}(NDVI_i) = a' + b'(NDVI_i) \qquad (7)$$

4.3.5. Topographic variables

Topographic variables were derived from the digital elevation model (DEM) with a 30 m spatial resolution by the Shuttle Radar Topography Mission (SRTM), which was downloaded from the US Geological Service website (https://earthexplorer.usgs.gov). Those variables were calculated from the DEM using the QGIS 3.16 software [33] (Table 4).

Table 4. Topographic variables.

Topographic Variable	Equation	Description
Elevation	$Elv = Z(x,y)$	Vertical distance of a point on the earth's surface above sea level [37].
Aspect	$T\theta = arctan\left(\dfrac{-H}{-G}\right)$	North-facing tilt angle of the area [38].
Slope	$s = arctan\left(\sqrt{p^2 + q^2}\right)$	Inclination to the horizontal [37].
Plane curvature	$C_W = 2\dfrac{DH^2 + EG^2 - FGH}{G^2 + H^2}$	Direction of the slope with the highest angle [39].
Wind Exposition Index	$H_L = \dfrac{\sum_{i=1}^{n} \frac{1}{\ln(dLHi)} \cdot tan^{-1}(\frac{dLZi}{dWHi})}{\sum_{i=1}^{n} \frac{1}{n(dLHi)}}$	Calculates the wind effect in all directions [40]

Where: Z, elevation; p and q, are the components of the gradient vector of slope; D, F, G and H were derived according to the equation of Zevenbergen and Thorne [39]; $dWHi$ and $dLHi$ horizontal distance in windward and leeward, $dLZi$ vertical distance to raster cell [40].

4.3.6. Texture Metrics

Texture variables of the LST layer (Table 5) were calculated from a gray level co-occurrence matrix (GLCM). This method results in different variables based on the same raster layer. Each of these variables allows contrasting specific texture properties to highlight the image's heterogeneity [41]. Texture variables were generated for a 3 x 3 kernel, using Rstudio's "glcm" package [42].

Table 5. Texture variables derived from GLCM.

Texture Variables	Equation	Description
Mean	$ME = \sum_{i,j=1}^{Ng} i * P(i,j)$	Mean of the probability values from GLCM. It is directly related to the spectral heterogeneity.
Variance	$SD \sqrt{\sum_{i,j=1}^{Ng} (i-u)^2\ P(i,j)}$	Measure of the global variation in the image. The increase in the values meaning higher levels of spectral heterogeneity.
Homogeneity	$HO = \sum_{i,j=0}^{N-1} i \frac{P_{i,j}}{1+i-j^2}$	Measure of the uniformity of grey-tones in the image.
Contrast	$CO = \sum_{i,j=0}^{N-1} i\,P_{i,j}(i,j)^2$	Quadratic measure of the local variation in the images.
Dissimilarity	$DI = \sum_{i,j=0}^{N-1} i\,P_{i,j}[i-j]$	Linear measure of the local variation in the image.
Entropy	$EN = \sum_{i,j=0}^{N-1} i\,P_{i,j}\left[-ln_i-P_{i,j}\right]$	Measure of the disorder in the image. This measure is inversely related to the second moment.
Second moment	$SM = \sum_{i,j=0}^{N-1} i\,P_{I,J}^2$	Measure of the order in the image. It is related to the energy required for arranging the elements in the system.
Correlation	$CC = \frac{\sum_{i,j} ijP(i,j) - \mu_x\mu_y}{\sigma_x\sigma_y}$	Measure of the linear dependency between neighboring pixels.

Where: P(i,j) = Entries in a normalized gray-tone spatial-dependence matrix; *Ng* = Number of distinct gray levels in the quantized image

4.3.7. Statistical analysis

Alignment of the raster layers was conducted to standardize the spatial resolution and pixel size. This process was the starting point for the statistical analysis. With the zonal statistics plugin of the QGIS 3.16.15 software [33], the SPIFYS data were extracted with a 50-m buffer to obtain information linked to each of the predictor variables (Table 6).

Table 6. Predictor variables

Variable	Resolution (m)	Units
NDVI	30 x 30	-1 to 1
VTCI	30x30	0 to 1
SAVI	30 x 30	-1 to 1
LST	30 x 30	°C
Evapotranspiration	500 x 500	kg m^{-2}
Longitude	30 x 30	DD
Latitude	30 x 30	DD
Mean	30 x 30	-
Variance	30 x 30	-
Homogeneity	30 x 30	-
Contrast	30 x 30	-
Dissimilarity	30 x 30	-
Entropy	30 x 30	-
Second moment	30 x 30	-
Correlation	30 x 30	-
Elevation	30 x 30	meters
Aspect	30 x 30	grades
Slope	30 x 30	grades
Plane curvature	30 x 30	1/100 of z
WEI	30 x 30	5 to-5

Where: NDVI, Normalized Difference Vegetation Index; VTCI, Vegetation Temperature Condition Index; LST, Land Surface Temperature; WEI, Wind Exposition Index.

A Pearson's correlation analysis (r) was used to identify variables most linked to AGB. Lastly, a multicollinearity analysis between variables was conducted using the variance inflation factor (VIF). Variables with a VIF value above 10 were removed, as this means that there is collinearity with some other variable [1,43].

Once variables were selected, a GAM was performed, i.e., a semi-parametric model that allows linear and non-linear responses of the predictor variables based on a dependent variable to be analyzed. GAM models have been successfully used to

analyze AGB values and forest structure with data from remote sensing [25,26]. GAM regression was conducted in RStudio with the "mgcv" package [44,45].

The deviance explained values and the Akaike information criterion (AIC) were obtained, which analyzes the relevance and fit of a model based on complexity; a lower AIC value means a better fit in the model [46]. In addition, a prediction map was made using the layerstack of the previously selected predictor variables as input.

The coefficient of determination (R2) and the root-mean-square error (RMSE) were estimated using Equations (8) and (9), where y_i is the AGB value observed in the field, $\hat{y}_i$ is the value estimated by the model, $\bar{y}_i$ the average AGB, n the number of observations and p the number of model parameters. R2 and RMSE data allowed the goodness of fit of evaluation models to be quantified:

$$R^2 = 1 - \frac{\sum_{i=1}^{n}(y_i\hat{y}_i)^2}{\sum_{i=1}^{n}(y_i\bar{y}_i)^2} \tag{8}$$

$$RMSE = \sqrt{\frac{\sum_{i=1}^{n}(y_i\hat{y}_i)^2}{n-p}} \tag{9}$$

Likewise, a verification of the model was carried out, using an independent field dataset (n = 50), in order to evaluate the AGB predicted from the model values.

4.4. Results

Pearson's correlation analysis showed that AGB had a negative relationship with LST, which was stronger in spring (r = −0.58). As for NDVI and VTCI, a positive relationship was observed, which was also stronger in spring (r = 0.63 and r = 0.32) (Figure 2). ET showed a weak positive relationship, although it becomes slightly stronger in winter (r = 0.43). Regarding the texture variables, the mean and variance variables showed the highest positive correlation. Lastly, the topographic variables with the highest AGB correlation (Figure 3) were altitude (r = −0.12), slope (r = 0.10) and curvature (r = 0.10). The GAM model was built with the highest AGB correlation (positive or negative) variables.

Most predictor variables and AGB showed a non-linear relationship. The variables GLCM_mean, longitude, latitude, LST, VTCI, NDVI, ET, were significant (p < 0.001), and explained between 10.6% and 48.1% of the total variance (Table 7). In addition, four interactions between two variables were tested. All tested interactions were significant (p < 0.001), with percentages of deviance explained ranging from 33% to 36.6% (Table 8). Three out of these interactions were considered as potential GAM components.
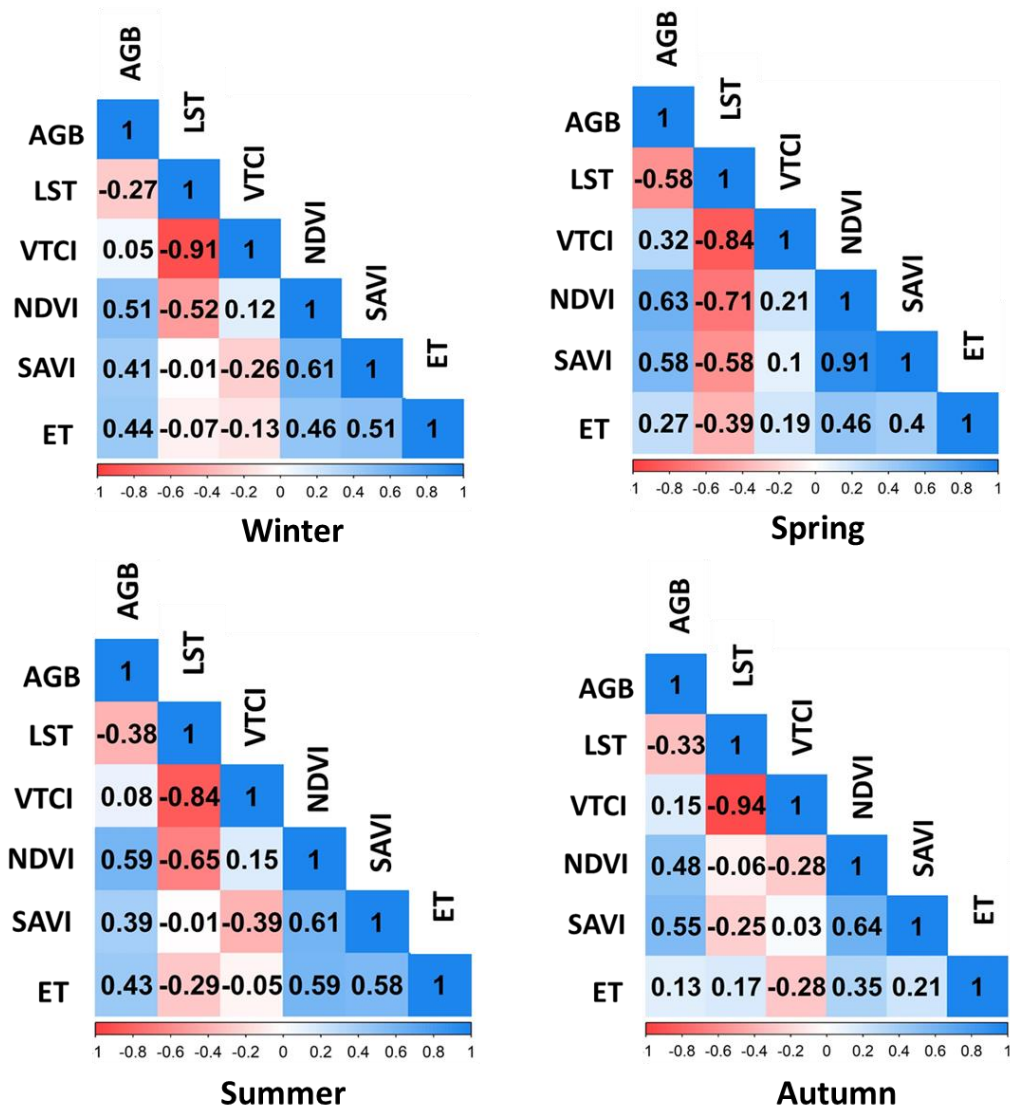
Figure 2. Pearson's correlation between predictor spectral variables and above-ground biomass (AGB) in different seasons of the year. LST, Land Surface Temperature (°C); VTCI, Vegetation Temperature Condition Index; NDVI, Normalized Difference Vegetation Index; SAVI, Soil-adjusted vegetation index; ET, evapotranspiration (kg m^{-2}).
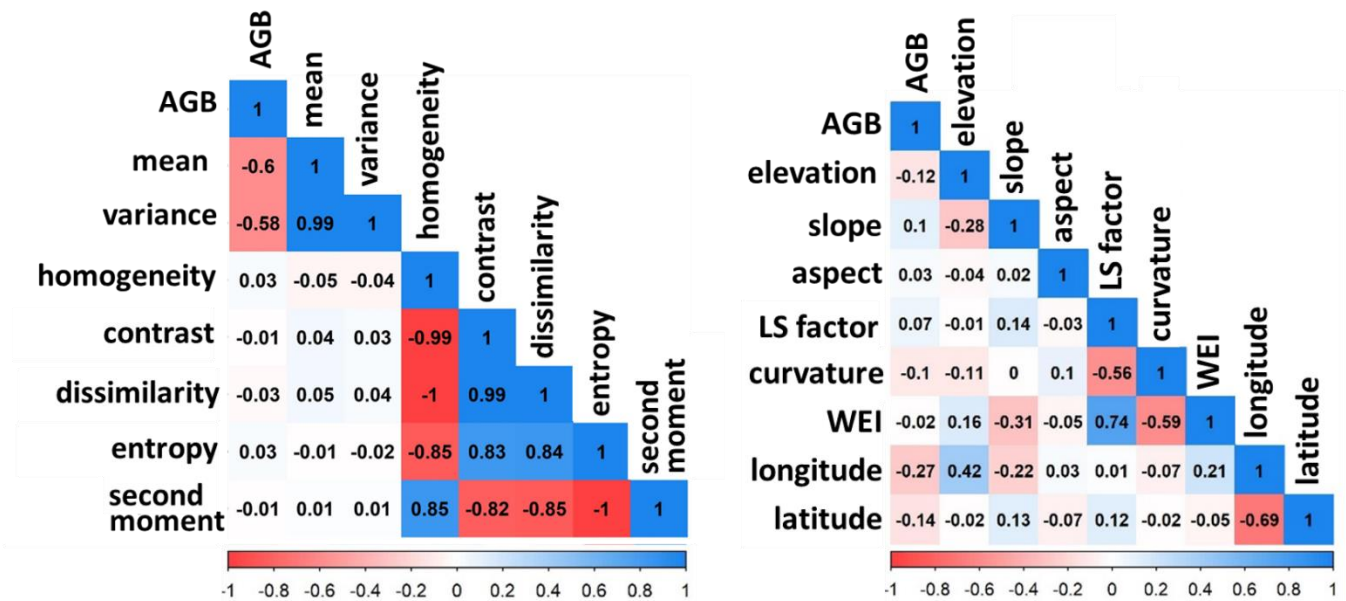
Figure 3. Pearson's correlation between predictor texture of Grey-Level Co-Occurrence Matrix, topographic, and spatial variables and above- ground biomass (AGB), these variables do not change throughout the year. WEI, Wind Exposition Index; AGB (Mg ha^{-1}), elevation (m), slope(°), longitude(DD), latitude(DD).

Table 7. Individual effects of variables on above ground biomass (AGB) in GAM models.

Variable	edf	Residual_df	Deviance explained	Adjusted R^2	p-value
NDVI	3.08	3.99	48.1 %	0.469	<0.001
LST	6.32	8.04	38.9 %	0.384	<0.001
GLCM_mean	2.73	3.46	34.9 %	0.342	<0.001
SAVI	1.38	1.67	34.0 %	0.336	<0.001
GLCM_variance	1.86	2.36	34.0 %	0.335	<0.001
Lon	6.50	7.62	24.3 %	0.223	<0.001
Lat	8.13	8.77	21.8 %	0.192	<0.001
ET	1.00	1.00	12.5 %	0.113	<0.001
VTCI	9.29	11.05	10.6 %	0.101	<0.001
Curvature	1.95	2.52	3.30 %	0.021	0.125
Elevation	1.93	2.45	2.78 %	0.020	0.057
Slope	2.81	3.54	1.60 %	0.012	0.045

Lon, longitude (decimal degress); Lat, latitude (decimal degress); LST, Land Surface Temperature (°C); VTCI, Vegetation Temperature Condition Index; NDVI, Normalized Difference Vegetation Index; SAVI, Soil-adjusted vegetation index; ET, evapotranspiration (kg m^{-2}); GLCM, Grey-Level Co-Occurrence Matrix; Slope (°); Elevation (m).

Table 8. Interactions of significant variables on AGB in GAMs.

Interaction terms	Edf	Residual_df	Deviance explained	R^2	p-value
LST-Elevation	2.87	3.52	36.6%	0.39	<0.001
LST-ET	9.85	13.21	36%	0.35	<0.001
Lon-Lat	11.94	15.58	33%	0.30	<0.001
LST-Slope	4.27	5.83	30.5%	0.27	<0.001

Lon, longitude (DD); Lat, latitude (DD); LST, Land Surface Temperature (°C); ET, evapotranspiration (kg·m^{-2}); Slope (°); Elevation (m).

4.4.1. Model optimization

Variables and interactions were added to the model, and the deviance explained, RMSE and AIC value were evaluated to determine whether adding a variable improved a model's performance. From the six models tested, model six showed a higher explanatory rate (61.0%) with lower RMSE and AIC (28.33 Mg ha-1 and 1994.34) (Table 9).

Table 9. Analysis of deviation in a forward selection regression process in six above-ground biomass (AGB) models.

No	Model Structure	Deviance explained	AIC	RMSE
1	AGB = s(lon,lat) + s(LST) + s(VTCI) + s(ET) + s(Elevation) + s(slope) + s(GLCM_mean)	53.7%	2005.72	30.88
2	AGB = s(lon,lat) + s(NDVI) + s(Elevation) + s(slope) + s(GLCM_mean)	56.8%	2005.72	30.01
3	AGB = s(lon,lat) + s(VTCI) + s(NDVI) + s(ET) + s(Elevation) + s(slope) + s(GLCM_mean)	56.8%	1998.27	29.81
4	AGB = s(lon,lat) + s(NDVI)) + s(ET) + s(Elevation) + s(slope) + s(GLCM_mean)	56.3%	1995.56	29.80
5	AGB = s(lon,lat) + s(LST) + s(VTCI) + s(NDVI) + s(ET)+ s(Elevation) + s(slope) + s(GLCM_mean)	60.2%	1996.01	29.41
6	AGB = s(lon,lat) + s(LST,ET) + s(LST, Elevation) + s(VTCI) + s(NDVI) + s(slope) + s(GLCM_mean)	61.0%	1994.34	28.33

Lon, longitude (DD) Lat, latitude (DD); LST, Land Surface Temperature (°C); VTCI, Vegetation Temperature Condition Index; NDVI, Normalized Difference Vegetation Index; ET, evapotranspiration (kg·m^{-2}); GLCM, Grey-Level Co-Occurrence Matrix; Slope (°); Elevation (m).

The graphs of each variable against AGB show that VTCI has an increasing linear relationship. On the other hand, GLCM_mean had a decreasing linear relationship, while NDVI and Slope showed an initially increasing relationship and

tended to decrease as AGB increased (Figure 4 a–d). The "Longitude, Latitude" interaction showed that areas with increased ABG are linked to western and southern Durango's forests. Meanwhile, the amount of AGB increases in areas with lower LST and ET. Finally, the "LST, DEM" interaction showed a positive relationship with AGB in areas with lower temperature and lower elevation (Figure 5).
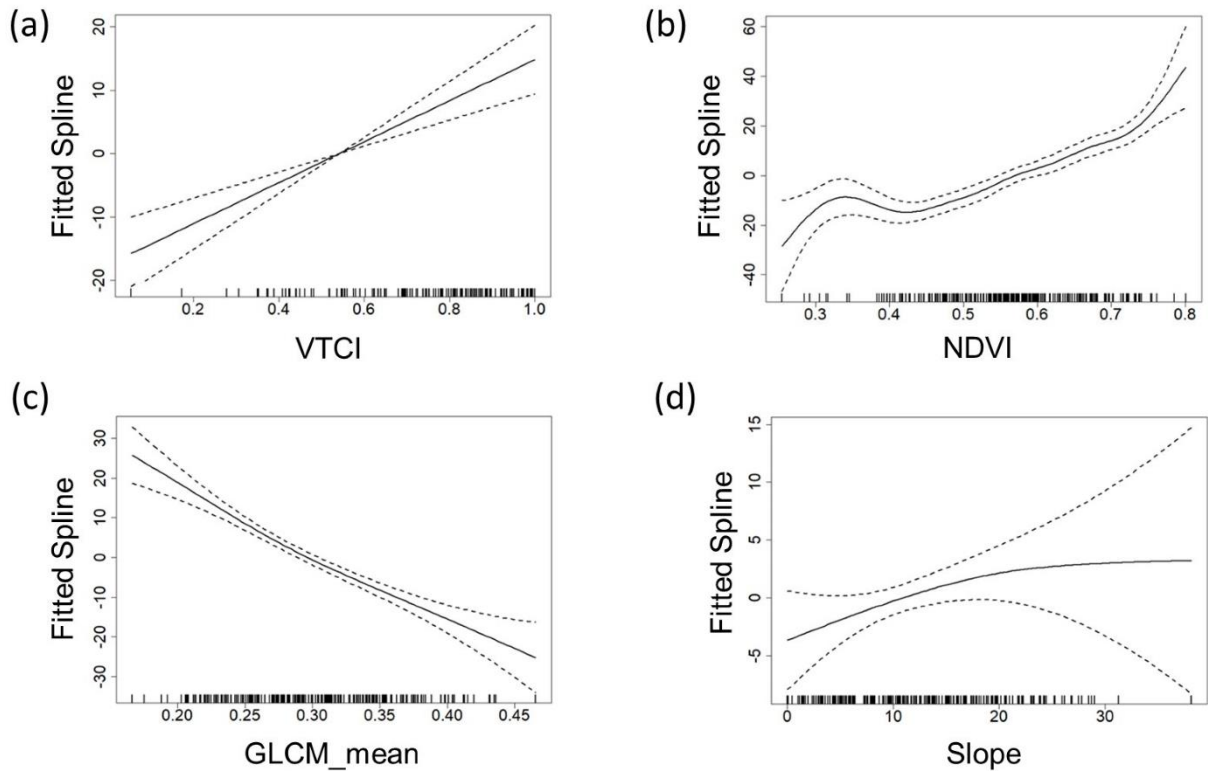

Figure 4. Explanatory variables with significant contribution to the respective binomial response variables. Each plot shows the relationship of the fitted function to the response and scaled to zero. The plots include approximate 95% pointwise. VTCI, Vegetation Temperature Condition In-dex; NDVI, Normalized Difference Vegetation Index; GLCM_mean, mean of Grey-Level Co-Occurrence Matrix
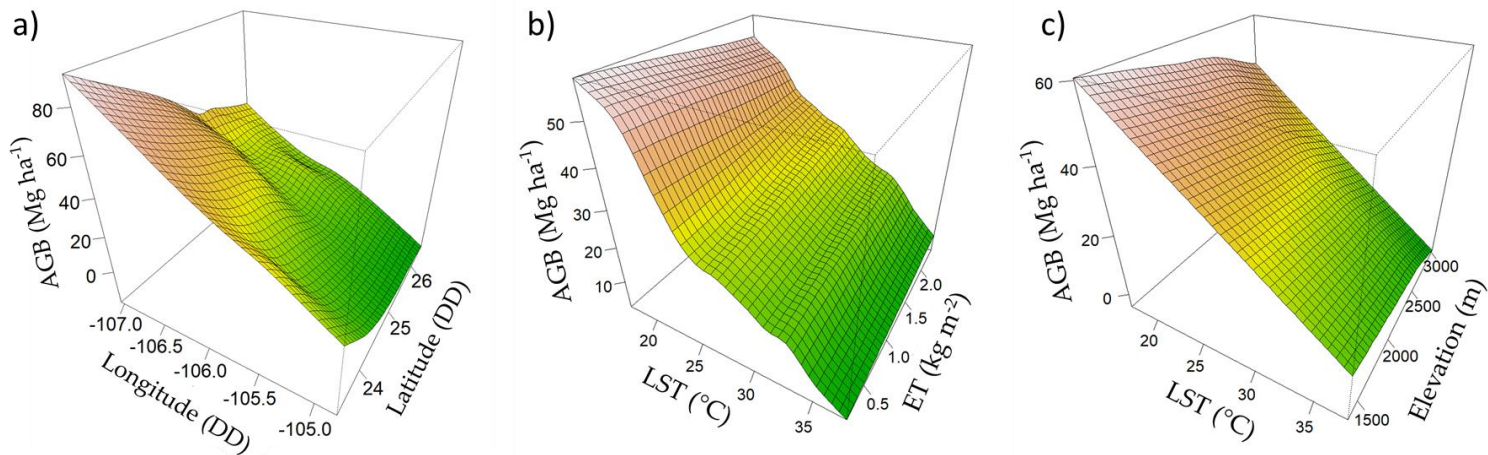
Figure 5. Responses of AGB to the interaction of two variables. a) Latitude and Longitude, b) Land surface temperature (LST) and evapotranspiration (ET), and c) Land surface temperature (LST) and Elevation.

Model diagnostic plots (Figure 6) generally help to understand the model performance. The QQ plot (Figure 6a) shows a normal distribution slightly skewed to the right with long tails, while the residual plot (Figure 6b) confirms independence of the residuals with a slight increase in error variability as the AGB amount increases. The residual distribution plot shows a marked tendency to a normal distribution (Figure 6c), and the overlay plot of the model's response data and fitted values indicate a moderate model efficiency (Figure 6d). Lastly, an AGB prediction map was generated by applying the selected model (Figure 7).
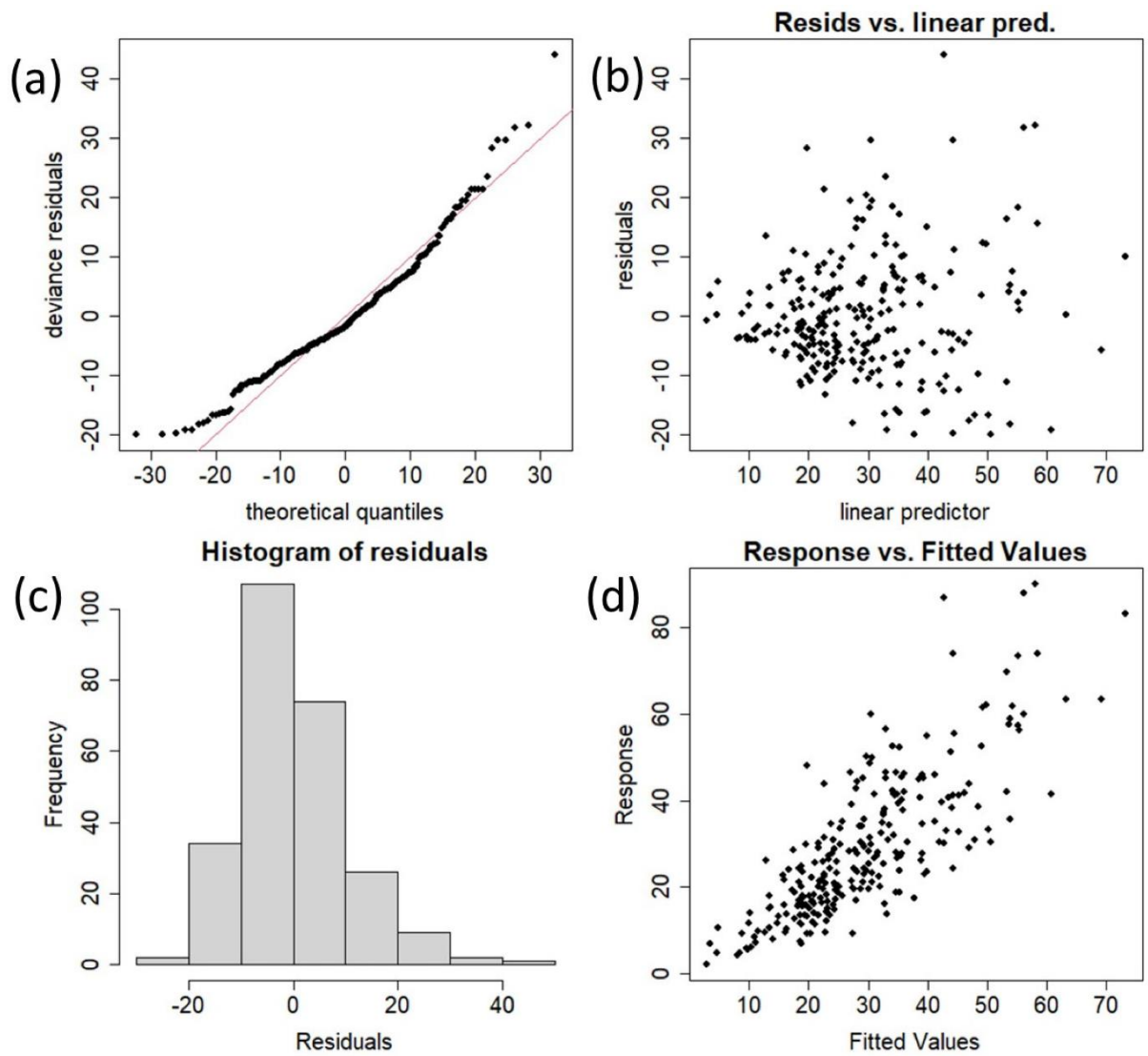
Figure 6. Diagnostic plots of generalized additive model (model six, see Table 9). a) Q-Q plot, b) residual plot, c) density plot of residuals, d) fitted values plotted against response variables.
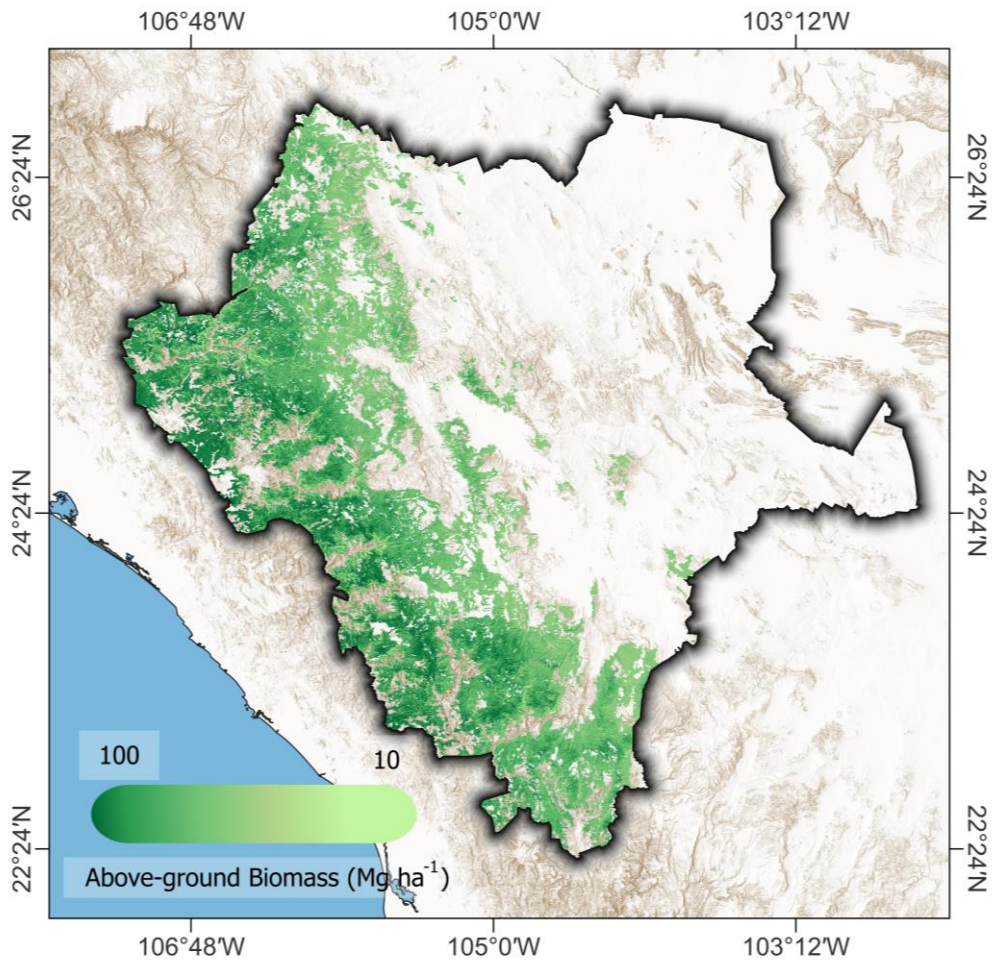
Figure 7. Predicted above-ground biomass (Mg ha−1) in the temperate forest of Durango, Mexico generated from model six (Table 9).

Finally, Table 10 shows the descriptive statistics and adjustment statistics of the verification of the GAM model through the application of the model to 50 AGB data derived from SPIFyS independent of the dataset used to generate the GAM model.

Table 10. Independent verification of the general model to estimate AGB (Mg ha^{-1})

Estimated AGB	Num. of Observations	Min	Max	Mean	SD	R2	RMSE
GAM calibration	318	2.05	92.33	30.82	18.00	0.61	28.33
Independent verification	50	4.79	83.25	27.23	18.15	0.58	31.21

Where: Min = minimum value; Max = maximum value; Mean = mean value; SD = Standard deviation

4.5. Discussion

Interactions between biological and environmental aspects often have complex behaviors (i.e., different from linear), so a model's predictive capacity depends largely on the flexibility to identify non-linear relationships [47]. GAM models are capable of identifying linear and non-linear relationships. Smoothing terms allow for the adjusting of unusual variance patterns that a linear model would not detect, making it possible to visualize and add the contribution of each variable to the plugins [48]. For this paper, GAM modeling was useful to estimate the AGB amount in the temperate forests of Durango, Mexico.

A correlation analysis allowed selecting predictive variables that were subsequently entered into the GAM model. One of the main challenges faced by spatial models is parsimony, [49,50] i.e., models with the least number of predictors, which in turn achieve reasonable estimates. In this paper, a model with moderate precision was developed; however, the number of variables (nine) allows the estimation process to be simpler.

Our observed negative relationship with LST seems to support previous observations that LST tends to increase in degraded forest ecosystems or ecosystems with forest loss [51]. For example, Özkan et al. [52], in a study conducted in forests in Turkey, found that areas with tree cover showed a decrease of 1.14 °C

compared to surfaces with herbaceous vegetation. Because forest structure parameters, such as canopy density, are closely related to the AGB amount [53], so an LST–AGB relationship could be expected.

Teofano et al. [54] analyzed the relation of AGB with indexes vegetation of a forest plantation; they figured out that this relation changes through the year and it is related with the phenostage, the growth stage that shows the weakest relation. Likewise, our results showed that the AGB–LST relationship had variations from the phenological changes of the plant community throughout the year. The AGB–LST relationship becomes stronger in spring, which could be explained by higher temperatures and less precipitation this season, resulting in a more marked contrast between the temperature of the bare soil or with herbaceous vegetation and areas with high forest density [51].

NDVI is the most widely used spectral index for vegetation analysis. It is a plant vigor proxy that measures photosynthetic activity [55]. Our results support the AGB–NDVI relationship described in different studies [9,13,56]. Although the variable with the highest deviance explained percentage was NDVI, the addition of variables such as LST and VTCI improved the model efficiency, so they could be considered as potential variables to be included in AGB models [17].

While VTCI describes regional drought conditions, this index was created considering LST changes that occur in vegetation, due to stomatal closure caused by drought stress [24,57]. Forest ecosystems with lower density or under fragmentation processes are more susceptible to drought stress [58]. The water stress is highly correlated with AGB due to less water availability and is related with populations with lower rates of ABG increase [59]. Furthermore, drought stress events have a negative impact on biomass, as they usually cause massive tree mortality, and favor conditions that can result in forest fires [60].

Several studies have used GLCM features as variables of parametric and non-parametric models [10,61,62,63]. Iqbal et al. [62] assess GLCM variables to classify different types of crops; they concluded that GLCM features improved by 13.65% the

accuracy of the analysis. In the present study, of the GLCM texture variables of the temperature layer, only GLCM-mean was selected, as this variable managed to highlight the heterogeneity in the raster layer and in turn improved the predictive capacity of the dependent variable (AGB).

The Longitude–Latitude interaction was deemed as an influential variable for the productivity of an ecosystem. These spatial variables greatly favor the site's climatic characteristics (e.g., solar incidence, wind currents, humidity) that determine the photosynthetic and plant respiration processes [21,64,65,66]. Our observed lower biomass in northern latitudes agrees with the findings of Gillman et al. [65], who observed that a negative relationship of latitude with Net Primary Productivity on a global scale. In addition, a higher biomass concentration is observed in the extreme west of Durango state, near the Pacific Ocean, a transition zone with tropical deciduous forest [67,68].

The ET–LST interaction showed that, in areas with lower evapotranspiration and temperature, a greater AGB amount is found. Forest cover largely regulates local temperature through the release of water vapor (transpiration), energy and energy exchange between the canopy surface and the atmosphere [69]. ET is deemed as one of the most important LST-shaping mechanisms [70]. Although higher ET rates would be expected in more productive ecosystems, some papers mention that this relationship changes throughout the year; for example, Strilesky et al. [71] analyzed the relationship between biomass and ET in a forest ecosystem, finding that a greater biomass amount does not lead to higher ET levels throughout the year, since forest ecosystems with higher biomass show lower ET in dry months. Our observed stronger relationship with spring water stress indicators seem to support those seasonal variations in the relationships between ET and AGB.

The elevation and LST relationship allowed identifying a greater amount of AGB in areas with medium elevation (1500–2000 m). The middle zone of mountainous ecosystems has a greater amount of precipitation and therefore a higher environmental humidity [72], which results in a temperature decrease. For example,

Liu et al. [72] observed that the middle zone of a mountainous ecosystem in China had a forest structure with a denser canopy and a higher carbon sequestration capacity. In addition, the increase in elevation has a negative relationship with the amount of biomass, as the increase in altitude is related to the decrease in soil water content [64,73]. The decrease in biomass at the upper altitude threshold is explained by the species-energy theory, which indicates that, in more extreme conditions, species tend to reduce their growing seasons length and have slower metabolic processes, as observed in stands with lower AGB [66,74]. This research focused on temperate forest; however, in future research it would be interesting to analyze these relationships for other types of vegetation with a model such as the one developed in this document. This would allow more potential uses of LST and ET to be identified in the monitoring of forest resources.

4.6. Conclusions

The results of the current study showed that the use of GAM models could be adequate for AGB estimation from remote sensed temperature, water stress and other variables in temperate forests of Durango, Mexico. Variables such as LST, ET and VTCI combined with topographic and texture parameters were shown to be useful to understand change processes in terms of ABG productivity and quantity in temperate forests. AGB and LST showed a negative and variable correlation throughout the year. This relationship was clearer in spring (r = −0.58). This seems to indicate that the LST data has greater predictive potential for AGB in seasons when there is less precipitation and higher temperature, resulting in a greater contrast between higher and lower AGB plots.

In future studies, it would be useful to analyze the potential of satellite data available from previous decades to understand AGB dynamics across space and time in temperate forests such as the ones at the state of Durango, Mexico.

4.7. References

1. Jiang, F.; Kutia, M.; Ma, K.; Chen, S.; Long, J.; Sun, H. Estimating the Aboveground Biomass of Coniferous Forest in Northeast China Using Spectral Variables, Land

Surface Temperature and Soil Moisture. *Science of the Total Environment* **2021**, *785*, doi:10.1016/j.scitotenv.2021.147335.

2. Temesgen, H.; Affleck, D.; Poudel, K.; Gray, A.; Sessions, J. A Review of the Challenges and Opportunities in Estimating above Ground Forest Biomass Using Tree-Level Models. *Scand J For Res* **2015**, *30*, 326–335, doi:10.1080/02827581.2015.1012114.

3. Watson, R.T.; Noble, I.R.; Bolin, B.; Ravindranath, N.H.; Verardo, D.J.; Dokken, D.J. *Land Use, Land-Use Change and Forestry*; Cambridge University Press, 2000;

4. Pantaleo, Y. Tropical Reinforest above Ground Biomass and Carbon Stock Estimation for Upper and Lower Canopies Using Terrestrial Laser Scanner and Canopy Height Model from Unmanned Aerial Vehicle (UAV) Imagery in Ayer-Hitam, Malaysia, University of Twente, 2017.

5. Kumar, L.; Mutanga, O. Remote Sensing of Above-Ground Biomass. *Remote Sens (Basel)* **2017**, *9*, doi:10.3390/rs9090935.

6. Holl, K.D.; Zahawi, R.A. Factors Explaining Variability in Woody Above-Ground Biomass Accumulation in Restored Tropical Forest. *For Ecol Manage* **2014**, *319*, 36–43, doi:https://doi.org/10.1016/j.foreco.2014.01.024.

7. Ravindranath, N.H.; Ostwald, M. Carbon Pools and Measurement Frequency for Carbon Inventory. In *Carbon Inventory Methods Handbook for Greenhouse Gas Inventory, Carbon Mitigation and Roundwood Production Projects*; Springer Netherlands: Dordrecht, 2008; pp. 31–44 ISBN 978-1-4020-6547-7.

8. Rodríguez-Veiga, P.; Wheeler, J.; Louis, V.; Tansey, K.; Balzter, H. Quantifying Forest Biomass Carbon Stocks From Space. *Current Forestry Reports* **2017**, *3*, 1–18.

9. Zhu, X.; Liu, D. Improving Forest Aboveground Biomass Estimation Using Seasonal Landsat NDVI Time-Series. *ISPRS Journal of Photogrammetry and Remote Sensing* **2015**, *102*, 222–231, doi:https://doi.org/10.1016/j.isprsjprs.2014.08.014.

10. López-Serrano, P.M.; Cárdenas Domínguez, J.L.; Corral-Rivas, J.J.; Jiménez, E.; López-Sánchez, C.A.; Vega-Nieva, D.J. Modeling of Aboveground Biomass with Landsat 8 OLI and Machine Learning in Temperate Forests. *Forests* **2020**, *11*, doi:10.3390/f11010011.

11. Zeng, Y.; Hao, D.; Huete, A.; Dechant, B.; Berry, J.; Chen, J.M.; Joiner, J.; Frankenberg, C.; Bond-Lamberty, B.; Ryu, Y.; et al. Optical Vegetation Indices for Monitoring Terrestrial Ecosystems Globally. *Nat Rev Earth Environ* **2022**, *3*, 477–493, doi:10.1038/s43017-022-00298-5.

12. Meneses-Tovar, C.L. NDVI as Indicator of Degradation. *Unasylva* **2011**, *62*, 39–46.

13. Vaglio Laurin, G.; Pirotti, F.; Callegari, M.; Chen, Q.; Cuozzo, G.; Lingua, E.; Notarnicola, C.; Papale, D. Potential of ALOS2 and NDVI to Estimate Forest Above-Ground Biomass, and Comparison with Lidar-Derived Estimates. *Remote Sens (Basel)* **2016**, *9*, 18, doi:10.3390/rs9010018.

14. Günlü, A.; Ercanli, I.; Başkent, E.Z.; Çakı, G. Estimating Aboveground Biomass Using Landsat TM Imagery: A Case Study of Anatolian Crimean Pine Forests in Turkey. *Ann For Res* **2014**, *57*, 289–298.

15. Kelsey, K.; Neff, J. Estimates of Aboveground Biomass from Texture Analysis of Landsat Imagery. *Remote Sens (Basel)* **2014**, *6*, 6407–6422, doi:10.3390/rs6076407.

16. García-Santos, V.; Cuxart, J.; Martínez-Villagrasa, D.; Jiménez, M.A.; Simó, G. Comparison of Three Methods for Estimating Land Surface Temperature from

Landsat 8-TIRS Sensor Data. *Remote Sens (Basel)* **2018**, *10*, doi:10.3390/rs10091450.

17. van Leeuwen, T.T.; Frank, A.J.; Jin, Y.; Smyth, P.; Goulden, M.L.; van der Werf, G.R.; Randerson, J.T. Optimal Use of Land Surface Temperature Data to Detect Changes in Tropical Forest Cover. *J Geophys Res Biogeosci* **2011**, *116*, doi:10.1029/2010JG001488.

18. Pongratz, J.; Bounoua, L.; DeFries, R.S.; Morton, D.C.; Anderson, L.O.; Mauser, W.; Klink, C.A. The Impact of Land Cover Change on Surface Energy and Water Balance in Mato Grosso, Brazil. *Earth Interact* **2006**, *10*, 1–17, doi:10.1175/EI176.1.

19. Rosas-Chavoya, M.; López-Serrano, P.M.; Vega-Nieva, D.J.; Wehenkel, C.A.; Hernández-Díaz, J.C. Application of Land Surface Temperature from Landsat Series to Monitor and Analyze Forest Ecosystems: A Bibliometric Analysis. *For Syst* **2022**, *31*, doi:10.5424/fs/2022313-19539.

20. Jaramillo, F.; Cory, N.; Arheimer, B.; Laudon, H.; van der Velde, Y.; Hasper, T.B.; Teutschbein, C.; Uddling, J. Dominant Effect of Increasing Forest Biomass on Evapotranspiration: Interpretations of Movement in Budyko Space. *Hydrol Earth Syst Sci* **2018**, *22*, 567–580, doi:10.5194/hess-22-567-2018.

21. Ali, A.; Lin, S.-L.; He, J.-K.; Kong, F.-M.; Yu, J.-H.; Jiang, H.-S. Elucidating Space, Climate, Edaphic, and Biodiversity Effects on Aboveground Biomass in Tropical Forests. *Land Degrad Dev* **2019**, *30*, 918–927, doi:https://doi.org/10.1002/ldr.3278.

22. Mu, Q.; Heinsch, F.A.; Zhao, M.; Running, S.W. Development of a Global Evapotranspiration Algorithm Based on MODIS and Global Meteorology Data. *Remote Sens Environ* **2007**, *111*, 519–536, doi:10.1016/j.rse.2007.04.015.

23. Nguyen, H.; Wheeler, M.C.; Otkin, J.A.; Cowan, T.; Frost, A.; Stone, R. Using the Evaporative Stress Index to Monitor Flash Drought in Australia. *Environmental Research Letters* **2019**, *14*, 64016, doi:10.1088/1748-9326/ab2103.

24. Wang, P.; Li, X.; Gong, J.; Song, C. Vegetation Temperature Condition Index and Its Application for Drought Monitoring. In Proceedings of the IGARSS 2001. Scanning the Present and Resolving the Future. Proceedings. IEEE 2001 International Geoscience and Remote Sensing Symposium (Cat. No.01CH37217); 2001; Vol. 1, pp. 141–143 vol.1.

25. Soriano-Luna, M.D. los Á.; Ángeles-Pérez, G.; Guevara, M.; Birdsey, R.; Pan, Y.; Vaquera-Huerta, H.; Valdez-Lazalde, J.R.; Johnson, K.D.; Vargas, R. Determinants of Above-Ground Biomass and Its Spatial Variability in a Temperate Forest Managed for Timber Production. *Forests* **2018**, *9*, doi:10.3390/f9080490.

26. Mikeladze, G.; Gavashelishvili, A.; Akobia, I.; Metreveli, V. Estimation of Forest Cover Change Using Sentinel-2 Multi-Spectral Imagery in Georgia (the Caucasus). *IForest* **2020**, 329–335, doi:10.3832/ifor3386-013.

27. Novo-Fernández, A.; Franks, S.; Wehenkel, C.; López-Serrano, P.M.; Molinier, M.; López-Sánchez, C.A. Landsat Time Series Analysis for Temperate Forest Cover Change Detection in the Sierra Madre Occidental, Durango, Mexico. *International Journal of Applied Earth Observation and Geoinformation* **2018**, *73*, 230–244, doi:10.1016/j.jag.2018.06.015.

28. Corral-Rivas, J.J.; Vargas-Larreta, B.; Wehenkel, C.; Aguirre-Calderón, O.A.; Crecente- Campo, F. *Guía Para El Establecimiento, Seguimiento y Evaluación de*

Sitios Permanentes de Monitoreo En Paisajes Productivos Forestales; CONAFOR, 2013;

29. Vargas-Larreta, B.; López-Sánchez, C.A.; Corral-Rivas, J.J.; López-Martínez, J.O.; Aguirre-Calderón, C.G.; Álvarez-González, J.G. Allometric Equations for Estimating Biomass and Carbon Stocks in the Temperate Forests of North-Western Mexico. *Forests* **2017**, *8*, doi:10.3390/f8080269.

30. U.S. Geological Survey. Earth Resources Observation and Science (EROS) Center Science Processing Architecture (ESPA) On Demand Interface (Version 5.4) Available online: https://www.usgs.gov/media/files/eros-science-processing-architecture-demand-interface-user-guide (accessed on 16 September 2022).

31. Mu, Q.; Zhao, M.; Running, S.W. Improvements to a MODIS Global Terrestrial Evapotranspiration Algorithm. *Remote Sens Environ* **2011**, *115*, 1781–1800, doi:https://doi.org/10.1016/j.rse.2011.02.019.

32. Parastatidis, D.; Mitraka, Z.; Chrysoulakis, N.; Abrams, M. Online Global Land Surface Temperature Estimation from Landsat. *Remote Sens (Basel)* **2017**, *9*, doi:10.3390/rs9121208.

33. QGIS Development Team QGIS Geographic Information System. Open Source Geospatial 2021.

34. Rosas-Chavoya, M.; Gallardo-Salazar, J.L.; López-Serrano, P.M.; Alcántara-Concepción, P.C.; León-Miranda, A.K. QGIS a Constantly Growing Free and Open-Source Geospatial Software Contributing to Scientific Development. *Cuadernos de Investigación Geográfica* **2022**, *48*, 197–213, doi:10.18172/cig.5143.

35. Sobrino, J.A.; Raissouni, N.; Li, Z.-L. A Comparative Study of Land Surface Emissivity Retrieval from NOAA Data. *Remote Sens Environ* **2001**, *75*, 256–266, doi:https://doi.org/10.1016/S0034-4257(00)00171-1.

36. Rouse, J.H.; Haas, R.H.; Schell, J.A.; Deering, D.W. Monitoring Vegetation Systems in the Great Plains with ERTS. In *third Earth Resources Technology Satellite- 1 Syposium* ; Freden, S.C., Mercanti, E.P., Becker, M., Eds.; NASA: Washington DC, 1974; Vol. Volume I.

37. Oliver, M.A.; Webster, R. Kriging: A Method of Interpolation for Geographical Information Systems. *International Journal of Geographical Information Systems* **1990**, *4*, 313–332, doi:10.1080/02693799008941549.

38. Horn, B.K.P. Hill Shading and the Reflectance Map. *Proceedings of the IEEE* **1981**, *69*, 14–47, doi:10.1109/PROC.1981.11918.

39. Zevenbergen, L.W.; Thorne, C.R. Quantitative Analysis of Land Surface Topography. *Earth Surf Process Landf* **1987**, *12*, 47–56, doi:https://doi.org/10.1002/esp.3290120107.

40. Böhner, J.; Antonić, O. Chapter 8 Land-Surface Parameters Specific to Topo-Climatology. In *Geomorphometry*; Hengl, T., Reuter, H.I., Eds.; Developments in Soil Science; Elsevier, 2009; Vol. 33, pp. 195–226.

41. Rahimi, E.; Barghjelveh, S.; Dong, P. Quantifying How Urban Landscape Heterogeneity Affects Land Surface Temperature at Multiple Scales. *J ecology environ* **2021**, *45*.

42. Zvoleff, A. Package "Glcm" 2020.

43. Chen, W.; Zhang, S.; Li, R.; Shahabi, H. Performance Evaluation of the GIS-Based Data Mining Techniques of Best-First Decision Tree, Random Forest, and Naïve

Bayes Tree for Landslide Susceptibility Modeling. *Science of The Total Environment* **2018**, *644*, 1006–1018, doi:10.1016/j.scitotenv.2018.06.389.

44. R Core Team R: A Language and Environment for Statistical Computing 2021.
45. Wood, N.S. *Generalized Additive Models*; 2nd edition.; Chapman and Hall/CRC: New York, 2017;
46. Terrer, C.; Phillips, R.P.; Hungate, B.A.; Rosende, J.; Pett-Ridge, J.; Craig, M.E.; van Groenigen, K.J.; Keenan, T.F.; Sulman, B.N.; Stocker, B.D.; et al. A Trade-off between Plant and Soil Carbon Storage under Elevated CO2. *Nature* **2021**, *591*, 599–603, doi:10.1038/s41586-021-03306-8.
47. Levine, J.; de Valpine, P.; Battles, J. Generalized Additive Models Reveal Among-Stand Variation in Live Tree Biomass Equations. *Canadian Journal of Forest Research* **2021**, *51*, 546–564, doi:10.1139/cjfr-2020-0219.
48. Frescino, T.S.; Edwards, T.C.; Moisen, G.G. Modeling Spatially Explicit Forest Structural Attributes Using Generalized Additive Models. *Journal of Vegetation Science* **2001**, *12*, 15, doi:10.2307/3236670.
49. Latifi, H.; Fassnacht, F.; Koch, B. Forest Structure Modeling with Combined Airborne Hyperspectral and LiDAR Data. *Remote Sens Environ* **2012**, *121*, 10–25, doi:10.1016/j.rse.2012.01.015.
50. Toledo, R.M.; Santos, R.F.; Baeten, L.; Perring, M.P.; Verheyen, K. Soil Properties and Neighbouring Forest Cover Affect Above-Ground Biomass and Functional Composition during Tropical Forest Restoration. *Appl Veg Sci* **2018**, *21*, 179–189, doi:10.1111/avsc.12363.
51. Hasnat, G.N.T. A Time Series Analysis of Forest Cover and Land Surface Temperature Change Over Dudpukuria-Dhopachari Wildlife Sanctuary Using Landsat Imagery. *Frontiers in Forests and Global Change* **2021**, *4*, doi:10.3389/ffgc.2021.687988.
52. Özkan, U.; Gökbulak, F. Effect of Vegetation Change from Forest to Herbaceous Vegetation Cover on Soil Moisture and Temperature Regimes and Soil Water Chemistry. *Catena (Amst)* **2017**, *149*, 158–166, doi:10.1016/j.catena.2016.09.017.
53. Alrutz, M.; Gómez Díaz, J.A.; Schneidewind, U.; Krömer, T.; Kreft, H. Forest Structural Parameters and Aboveground Biomass in Old-Growth and Secondary Forests along an Elevational Gradient in Mexico. Bot. Sci. 2021, 100, 67–85.
54. Theofanous, N.; Chrysafis, I.; Mallinis, G.; Domakinis, C.; Verde, N.; Siahalou, S. Aboveground Biomass Estimation in Short Rotation Forest Plantations in Northern Greece Using ESA's Sentinel Medium-High Resolution Multispectral and Radar Imaging Missions. Forests 2021, 12, 902.
55. Huang, S.; Tang, L.; Hupy, J.P.; Wang, Y.; Shao, G. A Commentary Review on the Use of Normalized Difference Vegetation Index (NDVI) in the Era of Popular Remote Sensing. J. For. Res. 2021, 32, 1–6.
56. Wang, Y.; Shen, X.; Jiang, M.; Tong, S.; Lu, X. Spatiotemporal Change of Aboveground Biomass and Its Response to Climate Change in Marshes of the Tibetan Plateau. Int. J. Appl. Earth Obs. Geoinf. 2021, 102, 102385.
57. Damavandi, A.A.; Rahimi, M.; Yazdani, M.R.; Noroozi, A.A. Assessment of Drought Severity Using Vegetation Temperature Condition Index (VTCI) and Terra/MODIS Satellite Data in Rangelands of Markazi Province, Iran. J. Rangel. Sci. 2016, 6, 33–41.

58. Negret, B.S.; Pérez, F.; Markesteijn, L.; Castillo, M.J.; Armesto, J.J. Diverging Drought-Tolerance Strategies Explain Tree Species Distribution along a Fog-Dependent Moisture Gradient in a Temperate Rain Forest. Oecologia 2013, 173, 625–635.

59. Hernández-Stefanoni, J.L.; Castillo-Santiago, M.Á.; Mas, J.F.; Wheeler, C.E.; Andres-Mauricio, J.; Tun-Dzul, F.; George-Chacón, S.P.; Reyes-Palomeque, G.; Castellanos-Basto, B.; Vaca, R.; et al. Improving Aboveground Biomass Maps of Tropical Dry Forests by Integrating LiDAR, ALOS PALSAR, Climate and Field Data. Carbon Balance Manag. 2020, 15, 15.

60. de Meira Junior, M.S.; Pinto, J.R.R.; Ramos, N.O.; Miguel, E.P.; de Oliveira Gaspar, R.; Phillips, O.L. The Impact of Long Dry Periods on the Aboveground Biomass in a Tropical Forest: 20 Years of Monitoring. Carbon Balance Manag. 2020, 15, 12.

61. Blanco, A.C.; Babaan, J.B.; Escoto, J.E.; Alcantara, C.K. Modelling of Land Surface Temperature Using Gray Level Co-Occurrence Matrix and Random Forest Regression. Int. Arch. Photogramm. Remote Sens. Spat. Inf. Sci. 2020, XLIII-B3-2020, 23–28.

62. Iqbal, N.; Mumtaz, R.; Shafi, U.; Zaidi, S.M.H. Gray Level Co-Occurrence Matrix (GLCM) Texture Based Crop Classification Using Low Altitude Remote Sensing Platforms. PeerJ Comput. Sci. 2021, 7, e536.

63. Ciobotaru, A.-M.; Andronache, I.; Ahammer, H.; Radulovic, M.; Peptenatu, D.; Pintilii, R.-D.; Drăghici, C.-C.; Marin, M.; Carboni, D.; Mariotti, G.; et al. Application of Fractal and Gray-Level Co-Occurrence Matrix Indices to Assess the Forest Dynamics in the Curvature Carpathians—Romania. Sustainability 2019, 11, 6927.

64. Cairns, M.A.; Brown, S.; Helmer, E.H.; Baumgardner, G.A. Root Biomass Allocation in the World's Upland Forests. Oecologia 1997, 111, 1–11. [Google Scholar] [CrossRef] [PubMed]

65. Gillman, L.N.; Wright, S.D.; Cusens, J.; McBride, P.D.; Malhi, Y.; Whittaker, R.J. Latitude, Productivity and Species Richness. Glob. Ecol. Biogeogr. 2015, 24, 107–117.

66. Ullah, F.; Gilani, H.; Sanaei, A.; Hussain, K.; Ali, A. Stand Structure Determines Aboveground Biomass across Temperate Forest Types and Species Mixture along a Local-Scale Elevational Gradient. For. Ecol. Manag. 2021, 486, 118984.

67. Zhu, K.; Zhang, J.; Niu, S.; Chu, C.; Luo, Y. Limits to Growth of Forest Biomass Carbon Sink under Climate Change. Nat. Commun. 2018, 9, 2709.

68. González-Elizondo, M.S.; González-Elizondo, M.; Tena-Flores, J.A.; Ruacho-González, L.; López-Enríquez, I.L. Vegetación de La Sierra Madre Occidental, México: Una Síntesis. Acta Bot. Mex. 2012, 100, 351–403.

69. Ma, W.; Jia, G.; Zhang, A. Multiple Satellite-Based Analysis Reveals Complex Climate Effects of Temperate Forests and Related Energy Budget. J. Geophys. Res. Atmos. 2017, 122, 3806–3820.

70. Gibbard, S.; Caldeira, K.; Bala, G.; Phillips, T.J.; Wickett, M. Climate Effects of Global Land Cover Change. Geophys. Res. Lett. 2005, 32, L23705.

71. Strilesky, S.L.; Humphreys, E.R. A Comparison of the Net Ecosystem Exchange of Carbon Dioxide and Evapotranspiration for Treed and Open Portions of a Temperate Peatland. Agric. For. Meteorol. 2012, 153, 45–53.

72. Liu, L.; Wang, Z.; Wang, Y.; Zhang, Y.; Shen, J.; Qin, D.; Li, S. Trade-off Analyses of Multiple Mountain Ecosystem Services along Elevation, Vegetation Cover and Precipitation Gradients: A Case Study in the Taihang Mountains. Ecol. Indic. 2019, 103, 94–104.
73. Galicia, L.; López-Blanco, J.; Zarco-Arista, A.E.; Filips, V.; García-Oliva, F. The Relationship between Solar Radiation Interception and Soil Water Content in a Tropical Deciduous Forest in Mexico. CATENA 1999, 36, 153–164.
74. Wright, D.H. Species-Energy Theory: An Extension of Species-Area Theory. Oikos 1983, 41, 496.

CAPÍTULO 5   CONCLUSIONES GENERALES

La información de Temperatura superficial (TS) estimada a partir de información satelital para el monitoreo y análisis de recursos forestales demostró ser útil para el análisis especifico de los bosques templados del estado de Durango.

El uso de TS es un tema en desarrollo, que ha mostrado múltiples aplicaciones en el análisis de recursos naturales, específicamente en monitoreo forestal, análisis de cambio de uso de suelo y procesos biofísicos asociados al cambio climático, como el estrés hídrico. Se observa que es un área de oportunidad para continuar desarrollando.

Uno de los usos de la información de TS es su potencial para el análisis de factores térmicos en ecosistemas montañosos, en particular el gradiente térmico (*temperature lapse rate*), esto debido a que las condiciones de inaccesibilidad y la vulnerabilidad de ante el cambio climático de estos ecosistemas los hacen propicios para aplicar técnicas en el análisis termal utilizando sensores remotos.

Así mismo, la vegetación asociada a ecosistemas montañosos del estado de Durango puede analizarse mediante información térmica. Por lo que, se desarrolló un método para estimar Biomasa aérea utilizando datos de TS y evapotranspiración. Este modelo permitió estimar con precisión moderada la biomasa acumulada en los bosques templados del estado de Durango. Así mismo, se identificó que en la primavera la información de TS tiene mayor correlación con la Biomasa aérea arbórea, en comparación con las otras estaciones del año.

RECOMENDACIONES PARA FUTURAS INVESTIGACIONES

En próximas investigaciones se sugiere incorporar al análisis con imágenes térmicas de alta resolución: drones con sensor termal. Así mismo se sugiere incorporar al análisis información multitemporal que permita identificar zonas con riesgo a incendios o con características que sugieran el mejor uso de suelo.

Mediante la incorporación de sensores de tipo LiDAR será posible identificar características que se encuentren por debajo del dosel superior, lo que será relevante para comprender mejor la estructura de los bosques de Durango.